Localising Discrete Points in 3D Space using Stereo Pairs of Digital Slot-scanning X-rays

Susan M Wynne

Submitted to the Faculty of Health Sciences at the University of Cape Town in partial fulfilment of the requirements for the degree of Master of Science in Biomedical Engineering.

Cape Town

December, 2006

Declaration

I, SUSAN MARGARET WYNNE, hereby declare that the work on which this thesis is based is my original work (except where acknowledgements indicate otherwise) and that neither the whole nor any part of it has been, is being or is to be submitted for any other degree in this or any other University.

I empower the University to reproduce for the purpose of research, either the whole or part of the contents of this thesis in any manner.

Signature

Date

Abstract

Obtaining three-dimensional information about the human body through the use of X-ray stereophotogrammetry provides medical professionals with more information on which to accurately plan, assess or implement procedures. Such information has been used in previous studies in order to assess the micro-motion of hip-joint prostheses, scoliosis treatment effectiveness and brachytherapy seed implantation positioning.

The main objective of this study was to assess the feasibility of using the Statscan low dose X-ray scanner at the Groote Schuur Hospital, Cape Town for the localisation of discrete points using X-ray stereophotogrammetry. The X-ray source and detector bank of the scanner are mounted on a C-arm that travels horizontally to produce X-ray images. The X-ray beam is fan-shaped as opposed to a conical shaped beam often used in conventional radiography, which results in magnification of objects in X-ray images in one dimension only.

To find a suitable stereophotogrammetric technique, traditional and newly developed methods were explored. The most suitable method for the three-dimensional localisation of points in Statscan images was established to be one previously developed for computed tomography scan projected radiographs (surviews), which have similar geometrical properties to Statscan images. Using information gathered from previous studies, a calibration frame with radio-opaque markers was designed and constructed specifically for use with Statscan. The three dimensional marker positions were measured using a line-of-sight photogrammetric technique and a marker location routine was written in Matlab to locate the marker centroids on the X-ray images.

Experiments were performed to establish the reconstruction errors and characteristics of the Statscan set-up using different control point configurations and various X-ray scanning angles. In addition, reconstruction accuracies when using both extrapolation and interpolation were assessed.

It has been demonstrated that stereophotogrammetry with the Statscan scanner would be suitable for applications where errors above 1 mm and lower than 2 mm can be tolerated, such as cephalometry, brachytherapy planning and assessment of the spine.

Acknowledgements

This research would not have been possible without the support and contribution of many people. All those who were involved are warmly thanked for their valuable input and expertise in their various fields.

My sincere thanks goes to my project supervisors and mentors, Prof C L Vaughan and Dr T S Douglas, who provided me with support, motivation and guidance throughout this project and the field of Biomedical Engineering.

Ms G Bowie, Chief Radiographer at the Groote Schuur Hospital, for her assistance in obtaining the initial Statscan X-ray test data.

Mr M C Briers, Postgraduate Student, Geomatics and Surveying Department, UCT, for his assistance in calibrating the calibration frame.

Mr J Markus, Biomedical Workshop Artisan, University of Cape Town, for his assistance in the construction of the calibration frame.

Dr E Meintjes, Senior Lecturer and Scientific Officer, Medical Imaging Research Unit, UCT, for her assistance in the theory of stereophotogrammetry.

Mr D Moore and Ms R Campbell, Researchers at the Sports Science Institute, for their assistance in obtaining 3D information with the Vicon measurement system.

Ms V Sanders and Mr S Steiner, Researchers, University of Cape Town, for their assistance in taking Statscan X-ray images.

Mr D Tabakin, Sport Science Institute, for the measurement of the calibration frame using the Vicon Motion System.

African Medical Imaging (Pty) Ltd for financial support in 2000 – 2001.

My parents, Margaret and David Wynne, my sister, Heather Wynne and my husband, Iwan van Wyk, for their encouragement and patience during the course of this project.

Table of Contents

List of Figures

List of Tables

Abbreviations

ACL	Anterior Cruciate Ligament
CCD	Charge Coupled Device
CT	Computed Tomography
DICOM	Digital Communication format for Medical use
DLT	Direct Linear Transformation
DPI	Dots Per Inch
FCP	Fiducial and Control Plane
GSH	Groote Schuur Hospital
ILUT	Input Look-up Table
lp/mm	Line pairs per millimetre
Matlab	"Matrix Laboratory" programming and computing tool
MDLT	Modified Direct Linear Transform
MeV	Mega electron Volts (1 X 10^6 eV)
MRI	Magnetic Resonance Imaging
NAC	National Accelerator Centre
ROI	Region of Interest
RSA	Roentgen Stereophotogrammetric Analysis
RSA-CMS®	Radio Stereometric Analysis - Clinical Measurement Solution
SD	Standard Deviation
SPG	Stereophotogrammetry
SPR	Scan Projected Radiography
THR	Total Hip Replacement
µSv	Micro-Sieverts

Chapter 1 : Introduction

1.1 Locating Points in Three Dimensions

There are many areas in engineering and medicine where locating discrete points in three-dimensional space is extremely valuable. Three-dimensional imaging techniques, such as Computed Tomography (CT) and Magnetic Resonance Imaging (MRI), have become standard medical imaging tools around the world. Stereophotogrammetry is another method of locating points in three dimensions.

Stereophotogrammetry is a method of obtaining spatial data (X, Y and Z point coordinates) of objects from images of the objects using the two-dimensional x, y image coordinates (van Geems, 1997). The stereophotogrammetry technique is widely used in land surveying, where the contours of the land are calculated from overlapping planar images of the land (Judge, 1926; Moffit, 1967; Hallert, 1960). Similar techniques can be used to find three-dimensional information of objects from stereo images.

For medical applications, stereophotogrammetry can be performed using X-ray images to provide the three-dimensional information of internal structures. Finding the spatial coordinates of points from stereo X-rays has been an area of interest since as early as 1897, two years after Roentgen discovered X-rays (Selvik *et al.*, 1983).

In early studies, the X-ray images were viewed using stereoscopes and three-dimensional localisation was done visually (Judge, 1926; Adams, 1981). An early stereogram of a gunshot wound in the foot is shown in Figure 1.1. When viewed through a stereoscope, the position of the buckshot in relation to the foot structures can be seen (Judge, 1926).

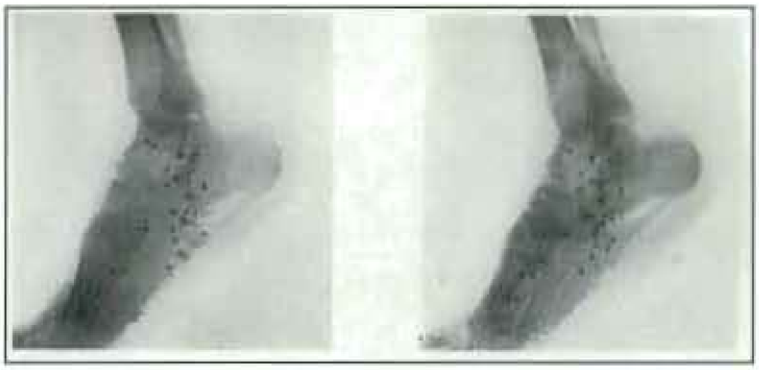

Figure 1.1 An early 1900's X-ray stereogram of a gunshot wound in the foot (Judge, 1926)

As computer technology advanced and more studies were done using stereo-photogrammetry based on photographs, a number of techniques were developed to locate three-dimensional coordinates of points from stereo X-rays. Most of the early development in this area was done in the field of orthopaedics with the development of Roentgen Stereo-photogrammetric Analysis (RSA). RSA is used to assess the relative motion of the skeletal system, for example the hip joint, using implanted markers (Djerf *et al.*, 1987; Selvik *et al.*, 1983). X-ray stereo-photogrammetric studies have since extended into a multitude of different fields including radiation oncology for radiation therapy positioning (Lam and Ten Haken, 1991; Gall *et al.*, 1993), the assessment of prosthesis stability and migration (Djerf *et al.*, 1987; Valstar *et al.*, 2002), the evaluation of spinal disorders (Aubin *et al.*, 1997; Petit *et al.*, 1998; Benameur *et al.*, 2003), source localisation in brachytherapy[1] (Li *et al.*, 1996; Cai *et al.*, 1997; Bice *et al.*, 1999), craniofacial reconstruction (Baumrind *et al.*, 1983) and cranial growth assessment (Alberius *et al.*, 1990).

The laborious traditional X-ray stereophotogrammetry that required manual marker identification and manual calculation of coordinates prompted the development of more efficient systems through the use of computers. Researchers introduced a level of automation into X-ray stereophotogrammetry by using digitised X-ray films (Adams and Constant, 1988) and digital image processing techniques for marker identification (Ostgaard *et al.*, 1997; Vrooman *et al.*, 1998).

In addition, researchers have performed studies using different types of reconstruction algorithms and calibration frames in order to increase the scope of application of X-ray stereophotogrammetry and to improve the accuracy and efficiency of the method.

Products for use in clinical applications have also become available following X-ray stereo-photogrammetry research, such as the RSA-CMS© (RSA Clinical Measurement Solution) automated measurement software developed in conjunction with Leiden University, The Netherlands (Vrooman *et al.*, 1998) and the Umeå RSA system (Biomedical Innovations AB), developed in conjunction with Lund University, Sweden (Bragdon *et al.*, 2003). Figure 1.2 shows an example of automated RSA software showing knee prostheses with RSA markers identified on a digitised X-ray image.

---

[1] The treatment of cancer through the use of implanted radioactive beads.

Figure 1.2 An example of automated RSA software (DIRSA) showing knee prostheses with RSA markers identified on a digitised X-ray image (RSA-CMS® product brochure, 2005)

1.2 Basic Theory of Stereophotogrammetry

Stereophotogrammetry, also called Biostereometrics in the medical field (Adams, 1981), can be explained using normal human sight, called stereoscopic vision. When looking at an object, each eye has a slightly different view of the object. The brain combines the images from each eye so that we perceive one image.

The brain recognises the difference in the parallactic angles (angles a and b as shown in Figure 1.3) and this difference in the two images allows for depth perception (Moffit, 1967; Kreel, 1981; van Geems, 1997).

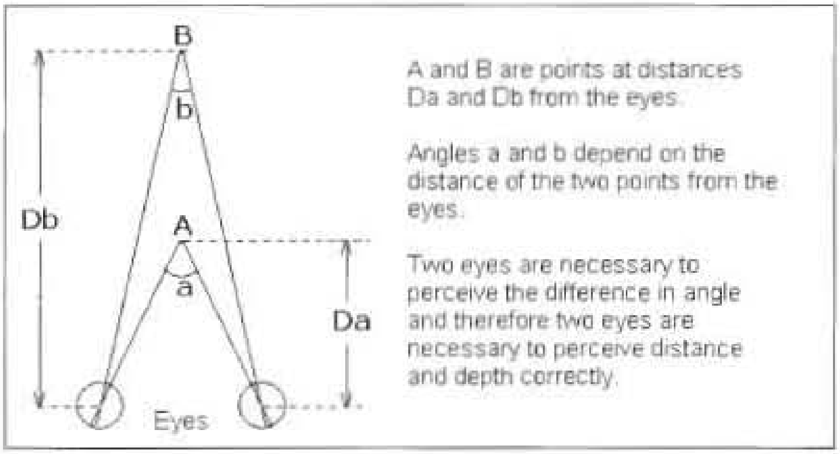

Figure 1.3 The stereopsis of human vision (adapted from Moffit, 1967)

Just as two eyes are required to perceive depth correctly, stereophotogrammetry requires two slightly different images of an object to be able to obtain three-dimensional information (van Geems, 1997).

In conventional stereophotogrammetry, photography is used to obtain two-dimensional images of an object with unknown dimensions, taken from different angles. The three-dimensional position of object points can be found if the relationship between the image views is known. This is determined through calibration using a calibration object which has previously determined, known coordinates. Measurements of corresponding landmarks or markers are then taken from the images and the photogrammetry process is used to transform two-dimensional corresponding points into three-dimensional coordinates (Adams, 1981).

Similarly, X-ray stereophotogrammetry uses two-dimensional X-ray images to locate the coordinates of specific points in three-dimensions. The two-dimensional limitations of conventional X-rays are overcome and accurate three-dimensional measurements of internal structures can be found. This reconstruction can either be done optically by viewing the images through a stereoscope or mathematically (Veress, 1989).

The X-ray machine used in this project is a low dose digital scanner called Statscan[2] (Model LDXADM) developed by De Beers, which can take full-body X-rays in about 13 seconds (Beningfield *et al.*, 2003). An example of a full body X-ray is given in Figure 1.4.

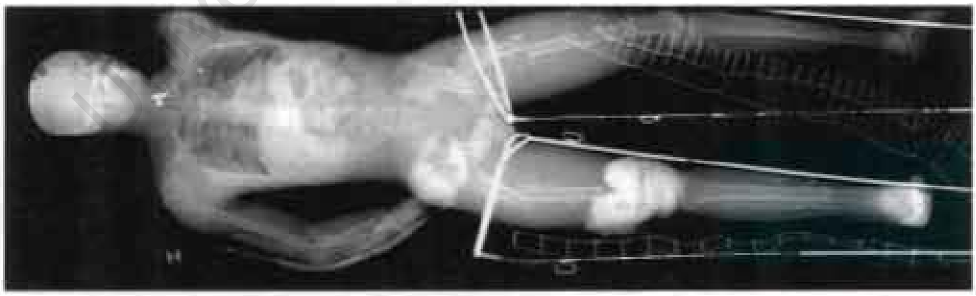

Figure 1.4 An example of a full-body digital Statscan X-ray image of a trauma patient with multiple injuries (Beningfield *et al.*, 2003)

---

[2] Lodox Systems (Pty) Ltd, Sandton, South Africa. http://www.lodox.com

The Statscan X-ray source and detectors are mounted on a rotating C-arm so that images can be taken from angles between 0° and 90° (see Figure 1.5 below). The X-ray source emits a collimated fan-beam of X-rays as the C-arm moves horizontally.

Figure 1.5 Statscan C-arm and patient trolley

The ability to take X-ray images from different angles without moving the object or patient makes Statscan suitable for performing X-ray stereophotogrammetry to locate discrete points. One must bear in mind that a volume could not be found accurately with only two X-ray images because the volume would not be accurately represented with such limited views. Nevertheless, a marker's three-dimensional coordinates can be found since it can be represented as a discrete point and not a volume.

1.3 Objectives of the Study

The objectives of this project were the following:

1.3.1 Explore traditional and recent stereophotogrammetric techniques to calibrate stereo X-ray images for the three-dimensional reconstruction of image points.

1.3.2 Investigate mathematical methods for the three-dimensional reconstruction of image points.

1.3.3 Illustrate the feasibility of using stereophotogrammetric techniques on images produced by a low dose digital X-ray imaging system called Statscan.

1.3.4 Determine the optimum configuration for performing stereophotogrammetry and determine the reconstruction errors of the method.

1.3.5 Determine clinical applications for which the stereophotogrammetry method would be suitable.

1.3.6 Provide conclusions and recommendations for further studies.

1.4 Scope and Limitations

The project is limited to experiments using Statscan digital X-ray images that were obtained from the Groote Schuur Hospital (GSH) Trauma Unit machine.

1.5 Sources of Information

Through the course of this project members of various University departments were consulted for assistance and advice. These included members of the Department of Biomedical Engineering, Digital Image Processing group in the Department of Electrical Engineering, and the Geomatics Department. In addition, specialists from the Trauma Unit at Groote Schuur Hospital and De Beers were also consulted. The individuals involved have been acknowledged in the relevant section of this report.

1.6 Overview

Chapter 2 provides a review of the relevant literature where the methods and applications of previous X-ray stereophotogrammetry studies are discussed.

Chapter 3 provides a description of the project materials and methods. The materials include the Statscan digital X-ray scanner and the computer hardware and software. The method includes a detailed description of the transformation algorithm, the calibration frame design and digital image processing used in the three dimensional reconstruction of discrete points. Chapter 4 describes the experiments performed and the results obtained. The results are evaluated and compared to the literature in Chapter 5.

Finally, conclusions are drawn and recommendations are made in Chapters 6 and 7.

Chapter 2 : Reconstruction Methods and Applications in X-Ray Stereophotogrammetry

A selection of three-dimensional reconstruction methods, chosen based on their relevance to X-ray and biomedical applications, were studied in order to determine which method would be most appropriate for use with Statscan images. There are a few obvious differences between conventional and X-ray stereophotogrammetry since X-ray images have different characteristics to photographic images. X-ray images are generated by projecting X-rays from a focal point in a generating tube, through an object to be imaged and onto a film (Slama *et al.*, 1980), or in the digital case, on to detectors.

The X-ray image can thus be described as a shadow of the object corresponding to its density (Veress, 1989). The X-ray focal point depends on the dimensions of the X-ray source, which has a finite size. However, the effective focal point is described as a point to allow the use of central projection, where any point in three dimensional space lies on a straight line between the projected point on an image plane and the source. Figure 2.1 depicts an X-ray set-up showing the effective focal point. In the mathematical description of image generation, and in practice, it is assumed that the X-ray stereophotogrammetry is based on perfect central projection, and therefore no corrections are made for focal point length (Veress, 1989; Slama *et al.*, 1980).

Image distortion can be explained by Figure 2.1 since it is clear that the image of the object will be larger than the real size of the object (Slama *et al.*, 1980). The amount of image distortion depends on the position of the object between the focal point and the X-ray film or detectors.

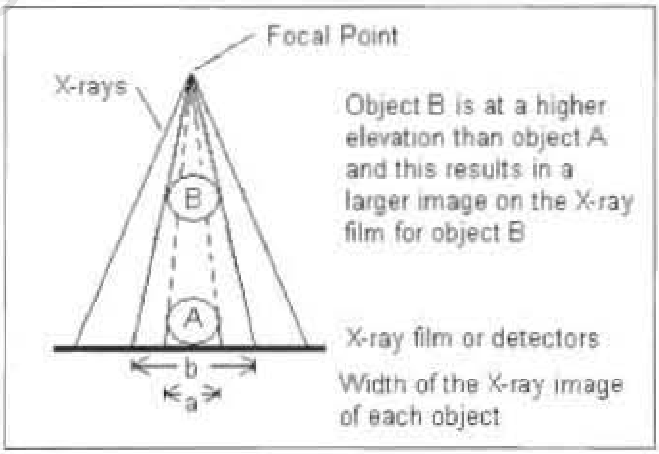

Figure 2.1 A typical X-ray set-up illustrating the effective focal point and the image distortion phenomenon (adapted from Slama *et al.*, 1989)

Conventional X-ray machines typically use a conical X-ray beam to generate the images which would result in even distortion around the object. The Statscan machine used in this study makes use of a fan-beam for slot scanning which brings about image distortion in one direction only (see Figure 2.2).

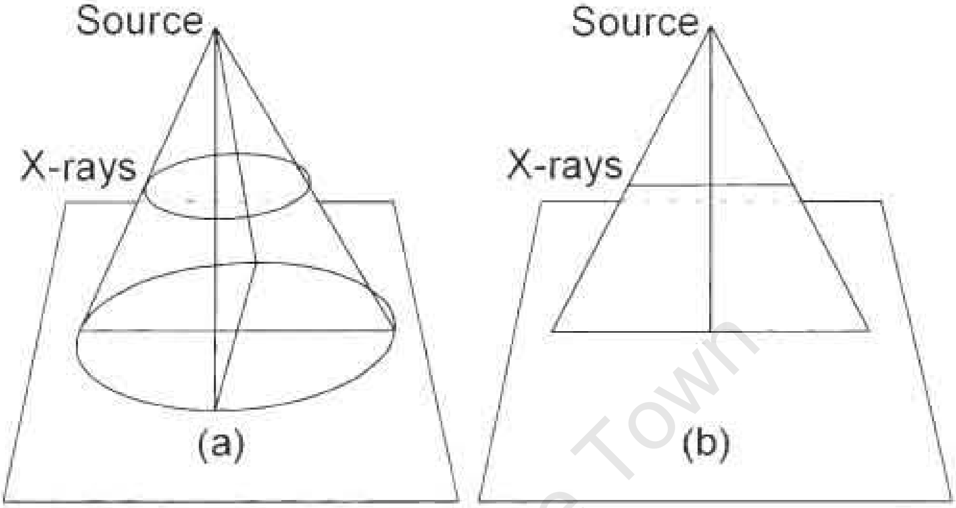

Figure 2.2 Illustration of the imaging geometry of (a) 3D conventional X-ray cone, and (b) Statscan or computed tomography 2D X-ray fan-beam

The distortion in one direction can be clearly seen by comparing Statscan X-ray images of identical ball-bearings at different elevations from the X-ray detectors (see Figure 2.3).

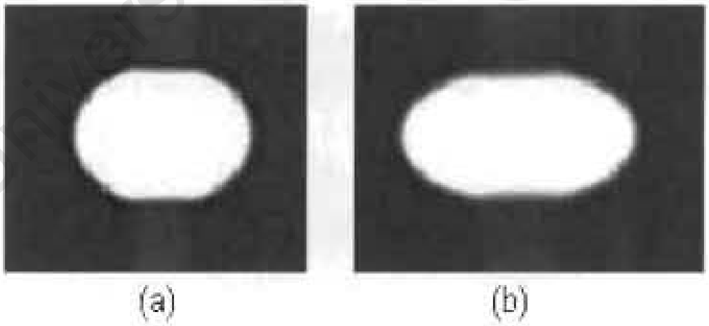

Figure 2.3 Two Statscan images showing the distortion of spherical ball bearings of the same size depending on the distance from the X-ray detectors: (a) The ball-bearing closer to the detector, (b) The ball bearing further away from the detectors. The distortion is most prominent in the image x-direction

One factor that usually needs to be taken into consideration is the influence of the X-ray film on the quality of the image (Veress, 1989). This factor does not affect this project since the X-ray images obtained are digital images. Another factor is the penumbra effect, also called image degradation, which creates a soft edge on objects being X-rayed, and is due to the geometry of the X-ray machine and the finite focal point length (Veress 1989; Slama *et al.*, 1980). This effect is described in more detail in Section 3.4.1. The penumbra effect is considered negligible particularly because the image object is bigger than the actual object, and therefore it is said to have no effect on measurements taken from an X-ray image, as any measurement must take magnification into account (Slama *et al.*, 1980; Veress, 1989).

When taking stereo-images, it is of vital importance that the object or patient is not moved with respect to the calibration object between scans. If the patient moves, errors will be introduced that will destroy the ability to perform three-dimensional transformations correctly (Slama *et al.*, 1980; Veress, 1989).

2.1 Roentgen Stereophotogrammetric Analysis (RSA)

Roentgen Stereophotogrammetric Analysis (RSA)[3] was developed by Goran Selvik in 1974 (Selvik, 1989) in order to have a method of analysing orthopaedic treatments such as prosthetic implants non-invasively through medical imaging. Using RSA, the three-dimensional coordinates of radio-opaque points can be found from two-dimensional X-ray images. This method is sometimes referred to as a fiducial and control plane (FCP) technique due to the use of two planes bordering the object for the calibration (Choo and Oxland, 2003). Based on the numerous Swedish biomechanical studies that have been conducted using this method, it can be concluded that this method is considered to be the gold-standard of X-ray stereophotogrammetry in the field of orthopaedics in Sweden and other Scandinavian countries.

The RSA method as described by Selvik (1989) can be summarised as follows:

- Radio-opaque markers (object markers) are inserted into an object (e.g. prosthetic hip joint).
- The object with a calibration frame is radiographically examined from different angles. The frame has several calibration markers with known coordinates that are restricted to fiducial and control planes (FCPs) to provide a fixed standard of

---

[3] RSA is sometimes called Radiostereometric Analysis (Ryd *et al.*, 2000).

reference for comparison. The examination could either be performed in an interpolation or extrapolation configuration.

- Object and calibration markers are identified from the X-ray images. The two-dimensional image coordinates of the calibration markers, together with their pre-determined 3D coordinates, determine the transformations from 2D images to 3D space.

- Object marker locations are calculated in 3D using reconstruction algorithms.

2.1.1 The RSA reconstruction algorithm

The RSA reconstruction method uses the same reconstruction principles as used in conventional stereophotogrammetry except that X-rays are used instead of visible light (Selvik, 1989). Since the X-rays are not deflected in any significant way when passing through an object, a straight-forward mathematical central projection can be used (Selvik, 1989). In the RSA method, the X-rays radiate from the source to form an effective cone-shape. It is important to note that the Statscan scanner does not have this property (see Figure 2.2).

To be able to calculate the three dimensional coordinates of the markers, the measured image coordinates have to be transformed to the fiducial plane (lower plane of the calibration frame). The formulae that provide the relationship between the image coordinates (x', y') and fiducial plane coordinates (x, y) are (Selvik, 1989):

$$x = \frac{a_1 x' + b_1 y' + d_1}{a_4 x' + b_4 y' + 1} \quad (1)$$

$$y = \frac{a_2 x' + b_2 y' + d_2}{a_4 x' + b_4 y' + 1} \quad (2)$$

where:

$a_1, b_1, d_1, a_2, b_2, d_2, a_4, b_4$	projective transformation parameters
x, y	calibration marker fiducial plane co-ordinates
x', y'	corresponding marker image co-ordinates

A calibration plane with fiducial (calibration) markers in known positions (x, y) is used together with the image coordinates of the markers (x', y') to solve for the eight unknown transformation parameters in these equations and this determines the central projection. Typically nine fiducial markers are used; therefore the system is over-determined and the eight parameters can be found by the least squares method (Selvik, 1989).

Each ray, *R* is a straight line given by the formula:

$$R = P_i + k(P_i - P_i') \tag{3}$$

Where:

P_i	i^{th} control point
P_i'	the i^{th} control point's projection to the fiducial plane
k	a real value (for any real value of *k*, *R* would be a point on the line)

Another plane with control markers is required to determine the X-ray source focus. These two planes are fixed together to form the rigid calibration frame or cage that is described in the next section in more detail.

2.1.2 The RSA calibration

The calibration frame provides key information about the transformation from two to three dimensions. The calibration frames or cages described in the literature were typically designed specifically for the required application. For example, in some cases, the study required the patients to be in a fully weight bearing position within the calibration frame (Kiss, 1996; Alfaro-Adrian *et al.*, 1999), while others required the patients to be in supine and then erect positions (Önsten *et al.*, 1995; Johnsson, 1999). These requirements dictated which type of calibration frame was used. However, regardless of the application, the fundamentals of the calibration frame remain the same. A radiolucent frame with radio-opaque calibration markers (control and fiducial markers) at known positions on fiducial and control planes is required (Selvik, 1989). The fiducial plane is the plane closest to the radiographic film to define the three-dimensional coordinate system. The points on the fiducial plane are typically distributed symmetrically and cover the area of interest. The control plane is the plane further away from the radiographic film and is used to determine the position of the Roentgen foci (Valstar, 2002). The points on the control plane are typically distributed evenly in lines however it is not necessary for these points to cover the volume of interest.

The RSA transformation algorithm requires the markers to be on mathematical planes; therefore the calibration frame has to be made from flat material to reduce errors. In the earlier studies reviewed, the calibration frames were made from a type of acrylic plastic, e.g. Plexiglass, although this material is not perfectly flat (Kärrholm *et al.*, 1989; Ryd *et al.*, 1986). In further support of the use of Plexiglass for use in a calibration frame, the refraction of X-rays through a thin Plexiglass plate is said to be completely negligible (Veress, 1989). In his 1989 paper, Selvik mentions using mirror glass to make the calibration frames in future because of possible warping of the Plexiglass, however no other study that was reviewed mentioned the use of this material. Since 2001, a carbon calibration box has been used in several studies (Kaptein *et al.*, 2003; Kaptein *et al.*, 2005; Kaptein *et al.*, 2006; Valstar *et al.*, 2005).

The calibration (fiducial) markers used in previous RSA studies were all radio-opaque metal (stainless steel or tantalum) balls. They were typically 0.5 mm (Selvik, 1989), 0.8 mm (Selvik, 1989; Önsten *et al.*, 1995; Johnsson *et al.*, 1999; Alfaro-Adrian *et al.*, 1999) or 1 mm (Kiss *et al.*, 1996; Valstar *et al.*, 2001) in diameter and some were mounted in specially machined indentations in the plexiglass (Selvik, 1989).

In order for the frame to be effective, the three-dimensional coordinates of the calibration markers must be known. In Selvik's study, the measurement of the markers was a long process using a rectangular coordinatograph (Selvik, 1989).

For in vivo studies, tantalum object markers were often used because the bony landmarks were not distinctive enough for accurate identification (Kärrholm *et al.*, 1989; Önsten *et al.*, 1995; Valstar *et al.*, 2001). The tantalum markers are favoured by researchers doing in vivo work since tantalum is unaffected by body fluids (corrosion resistant) and causes no adverse effects in tissue, while still having a high atomic number so that it can be easily identified on X-ray images (Aronson, 1985). Tantalum is also attenuated more than titanium, the material commonly used for prosthetic hips, and therefore it is suitable for reference markers (Wang *et al.*, 1996). In some studies, stainless steel marker balls were used (Kiss *et al.*, 1996). The markers were typically 0.8 mm (Johnsson *et al.*, 1999; Alfaro-Adrián, 1999) or 1 mm (Djerf *et al.*, 1987; Kiss *et al.*, 1996; Nelissen *et al.*, 1998) in diameter. Usually between 3 and 9 balls were used (Kärrholm *et al.*, 1989; Önsten *et al.*, 1995).

2.1.3 Accuracy of RSA

The accuracy of RSA has been shown to vary depending on the way the study was set up. A summary of RSA accuracies in previous studies is given in Table 2.1.

Table 2.1 Accuracies of a selection of previous RSA studies and their separation angles

Authors	**Reported RSA Accuracies**	**Separation Angle**	**RSA Research Details**
Ryd *et al.* (1986)	0.2 mm (translation) ; 0.4° (total rotations)	90°	Analysis of the micromotion between implanted markers in the tibia and tibial component of the noncemented Freeman-Samuelson knee prostheses in gonarthrosis[4] patients.
Djerf *et al.* (1987)	0.30, 0.33, 1.42 mm (dx, dy, dz)	30°	Analysis of micromotion between the prosthetic stem and femur after total hip replacement (THR)
Kärrholm *et al.* (1989)	Not assessed	90°	Evaluation of chronic anterolateral instability of the knee
Kiss *et al.* (1996)	0.25 – 0.5 mm; 0.2 – 0.8°	60°	Analysis of the migration of cemented Hinek femoral components after THR. Stainless steel markers were implanted into the bone. Simultaneous patient and calibration frame exposures.
Vrooman *et al.* (1998)	0.11mm; 0.24° (automated) 0.13 mm; 0.27° (manual)	< 45° (assumed from set-up schematic)	Comparing the accuracy of automated RSA marker identification and a manual procedure using a phantom and in vivo studies for the micromotion of knee prostheses.
Johnsson *et al.* (1999)	0.3, 0.6, 0.7 mm (transverse, vertical, saggital)	40°	Evaluation of intervertebral stability by transpedicular bone screw systems in posterolateral lumbar spine fusion. Metallic markers were implanted into the bone. Simultaneous patient and calibration frame exposures.
Önsten *et al.* (1995)	Not assessed	90° assumed	Evaluation of the migration of the Charnley stem in rheumatoid arthritis and osteoarthritis
Alfaro-Adrian *et al.* (1999)	Prosthesis Tip: 0.35, 0.28, 0.28 mm (transverse, vertical, saggital)	60°	Establishing where migration occurs when using the Charnley Elite and Exeter hip replacement femoral stems. Tantalum markers were implanted into the bone and prostheses.

---

[4] Gonarthrosis is a disorder of the knee joint, generally involving early joint surface damage of any kind.

Accuracy could either be determined from the standard deviation of a series of measurements or by using a test object (Kiss *et al.*, 1996). The original study found an RSA accuracy of 0.03 – 0.05 mm for translations and 0.2° for rotations (Selvik, 1989). One must bear in mind that the accuracies cannot be compared directly since slight differences in apparatus and approach may affect the overall accuracy of the study. One such variable is the separation angle, the angle between the X-ray beams at their point of intersection, also called the X-ray tube convergence angle. The studies reviewed used a separation angle of between 30° (Djerf *et al.*, 1987) and 90° (Ryd *et al.*, 1986).

The studies of Yuan and Ryd (2000) have shown that a higher marker reconstruction accuracy can be obtained using an interpolation cage (object markers inside the calibration volume) as opposed to extrapolation (object markers outside the calibration volume). This result agrees with the camera photogrammetry field research findings that have shown large extrapolation errors when markers outside a calibration volume are reconstructed (Wood and Marshall, 1986; Gazzani, 1993; Yuan and Ryd, 2000). Certain applications require unrestricted space, e.g. gait analysis, and therefore extrapolation is still used even though it has been shown to be less accurate (Wood and Marshall, 1986; Choo and Oxland, 2003). In addition, an improvement in accuracy is reported when greater numbers of control points are used, although accuracy improvement approaches an asymptote when the number of control points exceeds twenty-one (Yuan and Ryd, 2000).

Since RSA has been used for several decades, various improvements have been made that have resulted in a more user friendly and less time consuming approach. In the early literature, the X-ray films were measured by cartographers and microcomputers were used to calculate the 3D coordinates (Ryd *et al.*, 1986; Kärrholm *et al.*, 1989). As technology progressed, the X-ray images could be digitised using a electromagnetic digitising tablet (Kiss *et al.*, 1996) or CCD camera linked to a computer (Wang *et al.*, 1996) so that image processing could be used to automate the marker identification process. In the most recent literature, digital X-ray images and image processing techniques were used to perform the RSA (Vrooman *et al.*, 1998; RSA Biomedical Website, 2006).

2.2 Direct Linear Transformation (DLT)

2.2.1 Overview

Abdel-Aziz and Karara (1971) originally developed the Direct Linear Transformation (DLT), which represents a projective transformation between the object space and the image plane and allows spatial coordinate reconstruction from two-dimensional images (Adams, 1981). The DLT algorithm is frequently used for three dimensional reconstruction of points from calibrated two-dimensional images in camera and video photogrammetry applications (Chen *et al.*, 1994; Ras *et al.*, 1996; Meintjes *et al.*, 2002; Douglas *et al.*, 2003). Like the RSA method, the DLT plays a significant role in biomechanics for reconstruction in stereo-photogrammetric systems (Challis and Kerwin, 1992; Hinrichs and McLean, 1995; Kofman, *et al.*, 1998). Choo and Oxland (2003) presented a comparison between the DLT method and the fiducial control plane (RSA) method and concluded that DLT analysis could be used to enhance the accuracy of traditional extrapolation sterophotogrammetry.

2.2.2 DLT Algorithm

During calibration, the DLT equations are used to calculate eleven transformation parameters (B_1 – B_{11}) for each image. These parameters describe the relationship between two and three dimensions. Using these parameters and the image coordinates of unknown points, the spatial coordinates of the unknown points can be found.

Figure 2.4 below illustrates the 'co-linearity condition'. This means that since a standard X-ray image is formed by the projection of an object on the image plane, a point on an object, M, and its corresponding point on an image, P, and the projection centre node, X-ray source S are in a straight line (collinear). This intuitive condition is very important as it leads to the development of vector relationships that allow us to define the eleven DLT parameters. These parameters are in fact a description of the relationship between the object space reference frame and the image plane reference frame (Mitton *et al.*, 2000; Kwon website, 2006).

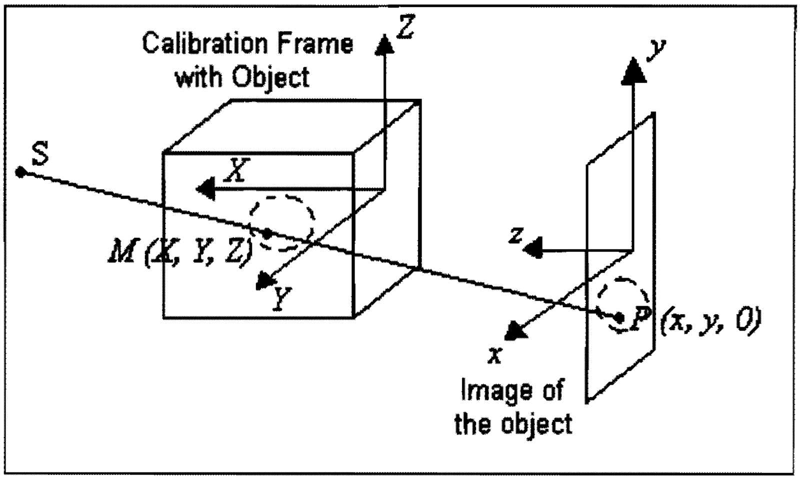

Figure 2.4 The object space and image plane can be related by using the co-linearity assumption and vector algebra (Adapted from Mitton *et al.*, 2000)

The DLT uses equations (4) and (5) to describe the relationship between the two dimensional images and three dimensional co-ordinate system (Abdel-Aziz and Karara, 1971):

$$x = \frac{B_1X + B_2Y + B_3Z + B_4}{B_9X + B_{10}Y + B_{11}Z + 1} \qquad (4)$$

$$y = \frac{B_5X + B_6Y + B_7Z + B_8}{B_9X + B_{10}Y + B_{11}Z + 1} \qquad (5)$$

where:

X, Y, Z	3D calibration frame marker coordinates
x, y	2D calibration frame marker coordinates on the image
$B_1 - B_{11}$	Eleven projective transformation parameters describing the relationship between 2D images and 3D coordinate system

When at least six control points are known, the least squares method can be used to determine the eleven parameters since the parameters will be overdetermined (Abdel-Aziz and Karara, 1971).

Marzan and Karara (1975) show that equations (4) and (5) can be altered to partially correct for non-linear systematic errors and random errors introduced due to lens distortion and digitisation of the X-ray images (Wood and Marshall, 1986; Gazzani, 1993).

The DLT differs from the RSA method in that it does not assume separate planar calibration markers, instead it uses all the markers simultaneously to calculate the calibration parameters (Abdel-Aziz and Karara, 1971; Choo and Oxland, 2003). The advantages, listed by Challis and Kerwin (1992), of the DLT are that (a) the optical axes of the cameras do not need to intersect; (b) the camera positions can be arbitrary; (c) only two camera images are required; and (d) additional cameras can be accommodated. These advantages are also valid for the RSA reconstruction algorithm.

2.2.3 The DLT calibration frame

As with the calibration for the RSA method, the DLT calibration frame depends on the intended application, as well as whether the DLT will be performed using extrapolation or interpolation. A few examples of calibration frames discussed in the literature are described here.

In order to assess the 3D structure of the human spine by radiographic DLT interpolation, André *et al.* (1994) used a calibration frame made from three parallel equidistant acrylic plates, each plate having 21 steel balls (calibration markers) embedded in the acrylic. The steel balls were 0.7 mm in diameter and the coordinates of the calibration markers were measured using a vertical vernier (André *et al.*, 1994). In another lumbar spine study, Plamondon and Gagnon (1991) describe a calibration frame (30 cm x 30 cm x 20 cm) using 153 metallic balls 1 mm in diameter, however only 30 of these balls were used for calibration purposes at any one time. In this study, the calibration frame was rotated instead of the X-ray source.

Wood and Marshall (1986) performed a DLT study in extrapolation using conventional cameras to assess a sprinter's stride. The large calibration cage was made from square aluminium tubing (3.5 m x 2.5 m x 1.5 m) with forty three calibration markers painted onto the structure. Close-range photogrammetric techniques were used to calibrate the coordinates of each marker to an accuracy (mean error over X, Y and Z) better than ±1 mm. In another conventional camera DLT study of stride, Hatze (1988) also used a large calibration frame (0.4 m x 2 m x 2 m) with thirty 40 mm square markers.

To assess the accuracy of the DLT method and its sensitivity to number of control points and control point distribution in conventional stereophotogrammetry, Chen *et al.* (1994) used a rectangular (2.10 m x 1.35 m x 1.00 m) calibration frame with 32 control markers

(3M retroreflective tape). Each marker was 3.16 cm in diameter and the marker locations were established with a transit theodolite to an accuracy of 0.5 mm.

In a conventional cinematography study to compare the accuracy of the DLT with and without extrapolation, Hinrichs and McLean (1995) used large spherical markers (3 cm diameter) that were hung on strings from a ceiling (4 markers on each of the 27 strings). The positions of the markers were found using triangulation, sliding callipers and a transit theodolite to an accuracy of 0.5 mm.

In a study to determine the effect of control point configuration on DLT reconstruction accuracy, Challis and Kerwin (1992) evaluated results using a 1.0 m x 0.6 m x 1.0 m calibration frame that incorporated five different configurations. By selecting specific points, the frame was changed from one where control points encompassed the whole volume of interest ("Christmas tree" configuration) to where control points were distributed around the outside of the volume of interest. The markers were fifty 42 mm diameter spheres that were centrally drilled to fit on steel tubing. The markers were colour coded according to the different configurations. Since this was a camera photogrammetry study, there was no concern regarding the X-ray characteristics of the material. The marker locations were determined using a laser-based surveying system to an accuracy of ± 0.8mm.

In order to compare the RSA and DLT reconstruction techniques, Choo and Oxland (2003) used several different calibration cages, one for extrapolation and several interpolation cages. The reference markers used were 3 mm in diameter.

2.2.4 The DLT calibration process

In order to solve for the eleven DLT parameters (see equations 4 and 5) of each X-ray source position, a minimum of twelve equations is needed. This means that we need at least six control points with known X, Y and Z coordinates in very good 3D spatial distribution, along with the corresponding (x, y) image coordinates of those points (Chen, 1994; Mitton *et al.*, 2000), since each control point provides two equations. The system is then overdetermined since there are more equations than unknowns. To compute the DLT parameters, a linear least squares method could be used (Hatze, 1988). The method of least squares is a common method for solving overdetermined systems of equations (Zill and Cullen, 1992).

The two sets of eleven DLT parameters, one set for position 1 or left X-ray source position (B_{L1} – B_{L11}) and one set for position 2 or right X-ray source position (B_{R1} - B_{R11}), are used together with the image points from the left image (x_L, y_L) and the right image (x_R, y_R) to calculate the 3D coordinates of a point (X,Y,Z) within the calibrated volume. Once the transformation parameters have been obtained, the X-ray source-detector configurations must not be disturbed to ensure that no further errors are introduced.

2.2.5 Accuracy of the DLT

Like the RSA method, the DLT accuracy reported in journal papers varies. One must also bear in mind that the axes (X, Y, Z) used are often labelled differently in each study. It must also be noted that the apparent accuracy given when points that were used in the development of the transformation parameters (control points) are reconstructed can be misleading. True reconstruction accuracy should be assessed by the reconstruction of non-control (test) points (Challis and Kerwin, 1992). Transformation errors from a selection of previous DLT studies are summarised in Table 2.2.

Table 2.2 Three dimensional error of a selection of previous DLT studies. σ = standard deviation; RMS = root mean square.

Author	Transformation Error	Separation Angle(s)	Application
Andre (1994)	15.0 mm (using vertebral landmarks) 1.0 mm (using implanted steel ball markers.)	30°	Vertical stereo-radiography for the clinical 3D reconstruction of the spine.
Wood and Marshall (1986)	5.7 mm (best result from all experiments)	45° and 90°	Conventional camera stereo-photogrammetry using extrapolation to assess a sprinter's stride. Control points have been reconstructed.
Hatze (1988)	4.7 – 5.2 mm (mean RMS errors for 30 - 7 control points using DLT)	59°	Conventional camera stereo-photogrammetry comparing the DLT and a modified DLT using reconstruction of control points
Dansereau and Stokes (1988)	0.72 mm (σ of measurement errors)	20°	The development of a method to measure the 3D shape of the rib cage to provide descriptive data and to study symmetry in the normal population.
Plamondon and Gagnon (1991)	0. 2 mm (mean accuracy, each axis)	15° - 90° (in intervals of 15°), 105° and 120°	Assessing the effect of configuration of data acquisition on the accuracy of stereo-radiographic system for an application in lumbar spine motion studies.

Author	Transformation Error	Separation Angle(s)	Application
Chen *et al.* (1994)	6 – 7 mm (resultant errors)	35°	Conventional camera stereo-photogrammetry studying the effect of number and distribution of control points.
Hinrichs and McLean (1995)	mean = 0.61 mm, σ = 0.14 mm; extrapolation: mean = 6.01 mm, σ =1.42 mm	90°	Conventional cinematography using the standard DLT and extrapolation DLT.
Stefansic *et al.* (2000)	0.7 ± 0.2 mm (11 control points used)	N/A (mapping is from 3D to single 2D image)	Mapping 3D patient space to laparoscopic (endoscopic) image space using the DLT and in minimally invasive hepatic surgery. Different numbers of control points were assessed.
Choo and Oxland (2003)	0.33 mm (control point calculation in simulations) 0.23 mm (test point reconstruction in phantom study)	20°	A study showing improved RSA accuracy when including DLT and balanced marker distribution.
Challis and Kerwin (1992)	4.3 – 5.5 mm RMS error for non-control points (11 control points)	85°	Study of the DLT accuracy for the reconstruction of control points and test points with different control point quantities and configurations.

André *et al.*, 1994 reports three dimensional error (differences between the measured and reconstructed marker coordinates) of under 1.0 mm when using steel balls as markers. The error increased to as much as 15.0 mm when using vertebral landmarks since they were not as clearly visible on the X-ray images (André *et al.*, 1994), see Table 2.2. This highlights the importance of accurate identification of the markers on the X-ray images. The calibration marker coordinates should also be measured with a high degree of accuracy in order to reduce the reconstruction errors (André *et al.*, 1994).

Wood and Marshal (1986) investigated the accuracy of the DLT-extrapolation method in a conventional camera stereophotogrammetric assessment employing several different experiment configurations. It was found that there are significant reconstruction errors when using extrapolation. The best results were achieved in the experiment with the highest number of control points (30) and the greatest distance:base ratio[5] between camera positions. The average RMS error for this best situation was 5.7 mm.

---

[5] This ratio describes the orientation of the cameras and is interpreted to correspond to the separation angle discussed in similar studies.

As in RSA, an improvement in accuracy is observed when increased numbers of control points are used for the DLT, however this improvement has been shown to be limited when more than 16 control points are used (Chen *et al.*, 1994): the resultant mean absolute error and resultant standard deviations were 14.6 mm and 19.5 mm when eight control points were used, 6.6 mm and 3.0 mm when sixteen control points were used, and 7.1 mm and 3.4 mm when twenty-four control points were used. The Chen *et al.* (1994) study also reinforces the importance of using well-distributed control points around the volume, especially when few control points are used and emphasises that extrapolation should be avoided where possible.

Hinrichs and McLean (1995) also compared the accuracy of the standard DLT and extrapolated DLT and the results agreed with Wood and Marshal (1986) and Chen *et al.* (1994) in that higher errors are to be expected when using extrapolation.

The study by Plamondon and Gagnon (1991) addressed whether the configuration of data acquisition in radiography has an effect on the accuracy of three-dimensional reconstruction using the DLT. The accuracy of 3D reconstruction was found by reconstructing twenty known points on the calibration frame that were not used in the generation of transformation parameters. The error was taken as the absolute difference between the calculated coordinate and the measured coordinate value. The results showed that as the separation angle was increased, the accuracy in the Z-axis (defined as the axis between the film and the X-ray source for one exposure) increased. The mean accuracy for each axis (X, Y, Z) was less than 0.2 mm for all stereograms and the maximum error was 0.39 mm in the Z direction when a separation angle of 30° was used.

The modified DLT (MDLT) was developed by Hatze (1988) in an attempt to improve the accuracy of the three-dimensional object space reconstruction. Linear and non-linear algorithms were presented however there are certain conditions that must be satisfied since the MDLT reduces the number of DLT parameters needed. The linear algorithm requires at least 15 evenly distributed control points, and the non-linear algorithm requires more than 30 evenly distributed control points (Hatze, 1988).

The MDLT makes use of the fact that the eleven parameters of the standard DLT are made up of only ten independent unknown parameters. The MDLT works to eliminate the redundant parameter by expressing one parameter in terms of the others.

The MDLT has only ten parameters since it assumes that the x and y axes in the image space are perpendicular. With the MDLT, theoretically only 5 known control points are needed, but an increased number increases reliability with the increased redundancy. A reconstruction accuracy of 0.733 mm RMS mean error was reported when reconstructing control points in the original study using the non-linear MDLT (Hatze, 1988).

In a computer simulation, Gazzani (1993) compared the extrapolation DLT method to a method he called CESNO (Collinearity Equation Solution by Numerical Optimisation), which is similar to the MDLT, for an application in conventional camera stereophotogrammetry. The separation angle of the simulated cameras was 60°. The minimum number of control points for reasonable accuracy when using the linear DLT was given as 12 control points, while between 12 and 16 control points are needed when using the MDLT / CESNO.

2.3 A Two-Dimensional Projective Transformation Method

2.3.1 Overview

Adams (1981) published a method for three dimensional localisation of image points in stereo X-ray images using three-dimensional projective transformation algorithms. The proposed system did away with the requirement to perform the studies under ideal conditions so that stereophotogrammetry could be performed with the use of apparatus normally available in a clinical environment (Adams, 1981).

Based on the Adams method, van Geems *et al.*, (1995) devised a two-dimensional projective transformation resembling the DLT for the calculation of three-dimensional computed tomography (CT) coordinates of image points from CT scan projection radiographs (SPRs). A variety of names have been given to SPRs including: ScoutView^{TM}, Pilot Scan^{TM}, Surview^{TM}, Topogram^{TM}, Scanoscope^{TM}, Scanogram, radiographic mode and localizer image (Medcyclopaedia website, 2006).

An SPR is a series of image lines obtained along the body's vertical axis in a CT system (the Z axis) to make up one image. The X-ray beam producing each image line projects outwards in the XY-plane, where the X direction is along the body's anterior-posterior axis and the Y direction is along the body's lateral axis, similarly to the Statscan X-ray beam. This method was initially applied to anterior-posterior and lateral SPR views (van Geems, 1996).

The equations used relate SPR coordinates to CT slice coordinates. The x-coordinates of a point in two two-dimensional SPR lines determine the X- and Y coordinates of the corresponding point in the three-dimensional CT image. The y-coordinate of the SPR is linearly related to the Z-coordinate in the CT image.

2.3.2 The Projective Transformation Algorithm

The algorithm details can be found in Section 3.2 since this method was used with Statscan images to locate the three-dimensional coordinates of markers.

2.3.3 Calibration for the Projective Transformation

Van Geems (1997) made use of 16 well distributed control markers with known three dimensional coordinates for calibration. The method requires a minimum of six control markers. The coordinates were measured using a metrograph[6] with a measuring resolution of 0.1 mm on each axis.

2.3.4 Accuracy using the Projective Transformation

The accuracy of the study performed by van Geems (1997) is given by the mean error and the standard deviation of the difference between reconstructed points using the SPR and actual CT slice coordinates as shown in Table 2.3.

Table 2.3 Comparison of CT slice coordinates and those calculated from the SPRs

	dX	**dY**	**dZ**
Mean Error (mm)	-0.9	0.3	1.4
Standard Deviation (mm)	0.5	0.5	0.6

For comparison, the study by Aubin *et al.* (1997) reported an accuracy for CT-scan 3D reconstructions being approximately 1.1 ± 0.8 mm. The accuracy of the X and Y coordinates were therefore within the typical accuracy of a CT scanner.

---

[6] Instrument for line-of-sight three dimensional measuring

2.4 The Non-stereo Corresponding Point Method (NSCP)

2.4.1 Overview

This method, presented by Mitton *et al.* (2000), shows an improvement on the DLT procedure for three-dimensional reconstruction of X-ray images of dry cervical vertebrae. The method uses two-dimensional points identified in one X-ray image only, deformable meshes with simulated springs and the principle that any non-stereo corresponding point belongs to a line joining the X-ray source and the projection of the point in one view. This has been called the non-stereo corresponding point (NSCP) method. A validation of the NSCP three-dimensional reconstruction technique for lumbar vertebrae was performed by Mitulescu *et al.* (2001) by comparing four techniques: direct measurement, CT scan, the DLT and the NSCP method.

In addition to the corresponding points, this method also makes use of points that are not clearly defined on a stereo-pair of images and could therefore be employed when anatomical landmarks are reconstructed. This may be useful since the studies of both Dansereau (1988) and André (1994) mention that it is difficult to identify corresponding points when using anatomical landmarks.

2.4.2 The NSCP algorithm

The NSCP algorithm method consists of first performing the DLT (Abdel-Aziz and Karara, 1971; Marzan and Karara, 1975) in order to reconstruct the corresponding points on two X-ray images. The NSCP technique is then used to reconstruct the non-corresponding points (Mitton *et al.*, 2000). If a point is clear on one image, but not clear on the other, the only information that can be used for reconstruction is that the 3D position is on a straight line (named the constraint line) between the X-ray source and the single 2D image point. To enable reconstruction of this point, assumptions need to be made about the geometry of the object to be reconstructed (Mitton *et al.*, 2000). A generic object is defined using the constraint lines and 3D points obtained from the DLT as geometrical constraints. The position of the non-stereo corresponding point on the constraint line is found by elastically deforming the generic object while respecting the defined geometrical boundaries. In order to get the mesh as close as possible to the generic object, deformation energy is calculated using Hooke's law (Mitton *et al.*, 2000):

$$E = \sum_{k=1}^{m} \frac{1}{2} K \left(l_k - l_{0k} \right)^2 \qquad (6)$$

where:

l_{0k}	initial length of the k^{th} spring in the generic object
l_k	actual length of the k^{th} spring in the generic object
K	the spring constant (stiffness)

2.4.3 Accuracy of the NSCP method

The NSCP reconstruction technique has reported mean errors of 1.1 mm with a maximum error of 7.8 mm compared to direct measurements (Mitulescu *et al.*, 2001). The drawback of this method is that the generic object has to be well defined based on previous knowledge about the object to be radiographed.

2.5 Image Marker Identification used in Previous Studies

Accurate identification of the two-dimensional coordinates from a pair of stereo X-ray images is vital to ensure good reconstruction of the three dimensional point position. This section reviews the literature on the use of digital image processing of X-ray images, with a focus on marker centroid[7] identification.

2.5.1 Identifying the two-dimensional marker positions

One of the challenges in X-ray stereophotogrammetry is the identification of markers on the X-ray images since the marker positions may be distorted and it could be difficult to identify the corresponding points on two separate images (Nyström *et al.*, 1994). In a conventional camera stereophotogrammetry study, van der Vlugt (1991) investigated a marker matching technique to match the appearance of an object on one image with it's appearance on another two images, however this approach was not used in the final program since some markers appeared on two, but not three images. Instead, a combination of automatic and computer aided manual techniques were used to identify the markers on each image (van der Vlugt, 1991).

---

[7] Centre of gravity of an object

User intervention, together with careful calibration frame design was required in most studies to simplify the identification of the stereo-pairs. The user had to be familiar with the calibration frame and marker numbering in order to identify the same marker on each image since the markers were first identified by means of a mouse and cursor (Ostgaard *et al.*, 1997).

Vrooman *et al.* (1998) used pixel thresholding and Sobel digital edge enhancement followed by a circle finding technique on raw digitised X-ray images (150 dpi, 8-bit resolution) in order to identify the markers in an RSA study on total knee prosthesis micromotion. The different types of markers, which were labelled prosthetic, bone and calibration markers, had different diameters and could therefore easily be identified by altering the diameter used in the circle finding algorithm. The technique relied on the known distribution and pattern of the calibration markers in order to label them correctly. The bone and prostheses markers were then matched using projection lines. The program allowed for the marker labelling to be checked and corrected by the user if it was incorrect.

2.5.2 Locating the Marker Centroid

Prior to using digital means to locate the marker centroid in RSA studies, the location was typically done using a measuring table (Ostgaard *et al.*, 1997). Ostgaard *et al.* (1997), assessed the accuracy and reproducibility of marker centroid positions using digital image processing algorithms and digitised X-rays with a resolution of 600 dpi and 256 grey levels. A 30 X 30 pixel area around the marker, which was identified by the user using a mouse and cursor, was used as a region of interest. The image was first smoothed using an averaging filter and then the region of interest was binarised using the threshold values determined by the mean of the minimum and maximum grey-scale values. The edge of the marker was detected by contour analysis; using the edge of the marker, the centre was found by a linear approximation of the circle equation (Ostgaard *et al.*, 1997).

Using a computer and digitised images proved advantageous in that it was easier to identify the markers on the PC monitor; however, a disadvantage was that the digitisation of the films limited the resolution (Ostgaard *et al.*, 1997). This is not a problem in the current study since the X-ray images are already digital and the user has an option of high or low resolution when scanning.

Wang *et al.* (1996) provided an optimised method for locating reference markers on orthopaedic X-ray images. This was for the purpose of performing RSA effectively and with high accuracy. The reference markers were implanted during surgery. X-ray films were digitised and non-linear image processing algorithms based on mathematical morphology, e.g. erosion and dilation, were used to find the markers. For the marker centre, a grey-scale weighting function was used.

In a conventional camera stereophotogrammetry study, van der Vlugt (1991) used a threshold technique to convert the images to binary images in order to separate the markers from the background. The technique converts all the pixel intensity values above a suitable threshold value to 225 (white) and all below to 0 (black). The program used an input look up table (ILUT) and user inspection to threshold the image (van der Vlugt, 1991). Using the thresholded image and edge detection, the edges of the markers were identified. Using this information and the original grey image to ensure that all information was used, a weighted centre of gravity method was used to determine the marker centres. If the marker area was found to be larger or smaller than a preset value, then it was discarded as a non-marker (van der Vlugt, 1991).

In another conventional camera stereophotogrammetry study, Rogus *et al.* (1999) designed a system to reduce patient positioning errors for radiation therapy. The standard thresholding and centroid calculations that were employed did not include size, shape or location constraints such as that used by van der Vlugt (1991), and therefore any non-marker reflective objects had to be covered to prevent the false identification of such objects as markers (Rogus *et al.*, 1999). The markers were often seen as ovals since the camera viewed the circular markers from an angle (Rogus *et al.*, 1999).

Lam *et al.* (1993) developed algorithms to automatically locate markers on digitised X-ray images for use in radiation therapy patient positioning. The first algorithm was used to locate marker positions on a pair of X-ray images by linear filtering where image features with a circular component were enhanced and those without were suppressed. Grey scale thresholding was then performed where non-marker features were suppressed to form a binary image and finally, potential marker regions that were too large or too small to be markers were rejected (Lam *et al.*, 1993).

The second algorithm located marker positions on a pair of X-ray images by comparing them to a reference pair obtained in the first patient examination. By exploiting information from the reference images such as marker shape, size, contrast and locations, marker identification could be done automatically and the algorithm only needed to search small regions around the reference marker position (Lam *et al.*, 1993).

Vrooman *et al.* (1998) fitted a paraboloid to the grey scale value of the markers in order to find the centroid.

More advanced digital methods of calculating the two-dimensional marker position using mathematical models have been described by Börlin 1997 and Börlin et al., 2002; however, these are not investigated in detail in this project.

2.6 X-Ray Stereophotogrammetric Applications

This section reviews applications of X-ray stereophotogrammetry in the field of medicine. A summary of the use of photogrammetry in medicine, not specific to X-ray photogrammetry can be found in the literature by Mitchell and Newton (2002).

2.6.1 Migration Assessment

RSA is widely used in the field of orthopaedics and biomechanics, especially in the assessment of the migration of prosthetics and joint stability since the method allows the rotations and translations of skeletal segment movements to be determined (Selvik, 1989). The technique can measure the migration and rotation of prostheses relative to bone in tenths of millimetres and degrees (Kiss *et al.,* 1996).

Conventional X-rays can detect a certain degree of micromotion of prostheses, but are limited to measurements of the acetabular region and can only measure in one plane (Nilsson and Kärrholm, 1996). Routine X-ray images can be used to detect movement of approximately 5 mm (Nilsson and Kärrholm, 1996), which is not sufficient accuracy to assess the success of the surgery since the prosthesis shift that must be detected is much smaller than this.

Much of the literature reviewed involves the analysis of hip prosthesis stability. RSA is used to measure the movement of an implant relative to bone in three dimensions to an acceptable degree of accuracy (Önsten *et al.*, 1995; Nilsson and Kärrholm, 1996; Alfaro-Adrian *et al.*, 1999; Valstar *et al.*, 2002). To enable an assessment of the success of hip replacement surgery, it is advantageous to determine any movements between femur and prosthesis shortly after the operation (Djerf *et al.*, 1987). RSA has the potential to predict implant performance as soon as possible after implantation, which means that the success of a new prosthesis can be analysed without the patient suffering through the usual clinical trial time of 10 years (Kiss *et al.*, 1996). The RSA technique is therefore very important in biomechanics (de Lange *et al.*, 1990).

Roentgen Stereophotogrammetry has also been used in the evaluation of knee arthroplasty since 1979 (Ryd *et al.*, 1986). The stability of the knee following injury has also been assessed using RSA, for example in the study of chronic anterolateral instability of the knee (Kärrholm *et al.*, 1989).

2.6.2 Spinal Assessment and Treatment Planning

Another application of finding points accurately in three dimensions from X-ray images is in the study of scoliosis. Scoliosis is a condition where the spine develops pronounced curvature deformation. The spine therefore twists, as does the rib cage. A spine with scoliosis is shown in Figure 2.5. The characteristic S-shape can be clearly seen from this X-ray.

Figure 2.5 A Statscan image of the spine of a 13 year-old girl with scoliosis

X-ray images are essential in the diagnosis and treatment of scoliosis. When stereophotogrammetry is used, the third dimension can be exploited to aid in spine assessments, visualisation, measurement of the curvature, as well as surgery planning. Using this method the stability and rate of scoliosis progression can also be calculated more effectively (Mitton *et al.*, 2001).

Studies on the effectiveness of scoliosis treatment often use X-ray stereophotogrammetry to evaluate the results (André *et al.*, 1994; Aubin *et al.*, 1997). In a study by Weisz *et al.* (1989) the surface anatomy of the patient's back was also investigated to assess the effect of a brace on the appearance of the back. Berg *et al.* (2002) used three dimensional surface maps to assess changes in scoliotic deformities; however, this study did not include X-ray stereophotogrammetry. Andre *et al.* (1994) used the DLT algorithm for the three-dimensional reconstruction of the human spine. The DLT can be performed on patients in an upright position and is therefore compatible with diagnostic protocols for scoliosis diagnosis (Mitton *et al.*, 2000).

The intervertebral stability of transpedicular fixation lumbar fusion of the spine has been evaluated in previous studies with high accuracy using the RSA method. RSA provides a safe radiographic method for assessing fixation without the intrusive surgery required for fusion exploration (Johnsson *et al.*,1999).

2.6.3 Radiation Oncology

The 3D localisation of points from images has applications in radiation oncology such as brachytherapy, the implantation of radioactive seeds to treat cancer. (Jackson, 1983; Siddon and Chin, 1985; Lam and Ten Haken, 1991). A post-implant evaluation is necessary to evaluate the source placement errors so that the impact on the coverage of the volume of interest can be established (Martel and Narayana, 1998).

The positioning of patients for radiation therapy is another application in the treatment of cancer. Accurate patient positioning in relation to the treatment machine and thus the radiation beam is very important in conformal radiation therapy such as proton therapy because of the small margins used (Rogus *et al.*, 1999). In conformal radiation therapy, the radiation beam is shaped in three-dimensions so that the radiation dose to the target volume is maximised while the dose to the surrounding normal tissue is minimised (Martel and Narayana, 1998).

2.6.4 Cephalometry

The use of X-rays to determine the three dimensional measurements of craniofacial landmarks was first introduced by Broadbent (1931) and a variety of methods have since been developed with applications in the fields of dentistry, orthodontics and maxillofacial surgery (Papadopoulos *et al.*, 2002). It is of photogrammetric interest that in several facial studies, X-ray techniques have been used together with camera photogrammetry (Mitchell and Newton, 2002). There is also scope for the use of X-ray stereophotogrammetry in cranium growth assessments (Alberius *et al.*, 1990).

2.6.5 Additional Applications

Additional applications for X-ray stereophotogrammetry exist, such as assessing fracture stability and joint kinematics, where joint stability can be assessed (Kärrholm *et al.*, 1989) and where the stability of ligaments (e.g. anterior cruciate ligament) is determined. There is also scope for the use of X-ray stereophotogrammetry in computer assisted surgery (Mitton *et al.*, 2000; Valstar *et al.*, 2002). In addition studies have even been done using X-ray stereophotogrammetry for use in minimally invasive hepatic surgery (Stefansic *et al.*, 2000).

Chapter 3 : Materials and Method

3.1 Statscan Materials and Technical Apparatus

3.1.1 The Statscan Digital Scanner

The Statscan digital scanner (see Figure 3.1) is a low dose digital X-ray machine currently used for trauma applications at the Groote Schuur Hospital in Cape Town. The scanner is capable of taking whole body X-ray images in approximately 13 seconds.

Figure 3.1 The Statscan Digital X-ray Scanner with global coordinate system

Statscan performs slot scanning with 12 CCD cameras and produces high-quality digital X-ray images with low radiation exposure, approximately 2 - 72% of the standard conventional dose in trauma applications (Benningfield *et al.*, 2003). The X-ray source and detector banks are mounted on a C-Arm assembly that can be rotated around the patient trolley. This enables anterior-posterior (0°) and lateral (90°) X-ray images to be taken, as well as images at any angle between 0° and 90°. This function is essential in this project since it allows for X-ray images to be taken from different angles without moving the patient or requiring multiple X-ray sources. The trolley is a 26 mm board made of a single piece of low density structural foam surrounded by a carbon fibre skin.

The Statscan axes have been defined as shown in Figure 3.1 in order to be consistent with that of van Geems *et al.*, (1995). With the source-detector at a 0° scanning angle with respect to the patient, the X-axis is vertical, the Z-axis is in the direction of horizontal C-arm travel and the Y-direction is orthogonal to the X-Z plane.

3.1.2 Statscan Digital Radiographs

The digital radiographs are formed from a series of line or slot scans obtained as the C-arm moves across the patient trolley. The fan-beam projects outward from the source in two dimensions on the XY plane. The imaging geometry is therefore similar to the fan-beam of computed tomography (CT) rather than the cone of conventional X-ray imaging as illustrated in Figure 2.2, Section 2.

In fact, in the planning phase of computed tomography, patients often undergo scan projection radiography (see Section 2.3.1) where the position of the X-ray source is kept at a fixed angular position with respect to the plane of patient movement in order to localise the target region. This is effectively what the Statscan scanner achieves.

The Statscan scanner can produce images of an area ranging from 100 mm x 100 mm to a maximum of 680 mm x 1800 mm. These constraints are important when designing the calibration equipment (see Section 3.3.1).

The spatial resolution required can be set before performing an X-ray scan. This can be either 2.78 lp/mm on high resolution, or 1.67 lp/mm on low resolution with 5 x 5 pixel binning. The fundamental pixel size is 60 µm. The image pixels are square. The contrast resolution is 16 000 grey levels. Using the console tools, it is possible to scroll through the grey levels to improve visibility of structures with differing densities (Benningfield *et al.*, 2003). The X-ray images can be saved in the DICOM format, however the Bitmap format was used since it was easier to manipulate in Matlab.

The density of the patient trolley was not taken into account during the image processing of the images since the density was assumed to be constant throughout and the table density made a small and insignificant difference to the images. The total attenuation of X-rays by the table is approximately equivalent to 0.7 mm of aluminium.

3.1.3 The Computer Equipment

A Pentium IV processor was used during this project. The operating system used was Microsoft Windows XP Home. All programming was done in Matlab 6.5[8]. Matlab is very efficient in running matrix calculations and since images are essentially matrices made up of pixels, which have different greyscale or colour values, this program was found to be suitable to perform the processing required.

3.2 Method of X-ray Stereophotogrammetry used with Statscan

The Statscan image acquisition technique is similar to the technique used to obtain scan projection radiographs (SPRs) for computed tomography (see Section 2.3.1); therefore it was reasonable to assume that a stereophotogrammetry technique suitable for SPRs could also be used with Statscan images. The van Geems *et al.* (1995) method of two-dimensional projective transformation for the calculation of three-dimensional CT coordinates of image points from CT scan projection radiographs (SPRs) will be used in this project (see Section 2.3).

3.2.1 Stereophotogrammetry technique suitable for use with SPRs

An important initial observation is that the Statscan Z-coordinate, in the direction of horizontal C-arm movement, is linearly proportional to the image y-coordinate and therefore the measurements (in mm) could be obtained from the image coordinates (in pixels). Since this dimension can easily be derived, we can focus on finding the X and Y coordinates of each "slice".

Using CT terminology one could say that, if calibration markers are known to be on the X-Y plane, only one CT slice is required to produce the three-dimensional CT slice marker co-ordinates. A two-dimensional projective transformation of the x-coordinates from X-ray images taken at different angles would be sufficient in order to find the X, Y coordinates of each "slice". Following this, the three-dimensional coordinates of the markers could be established.

In order to determine the transformation parameters, two Statscan images (effectively SPRs) of the calibration frame must be scanned from different orientations and the

---

[8] The Mathworks, Inc., Natick MA, USA

calibration markers must be able to be identified on the images. The equation for the x-coordinate $x_{k,i}$ of point i on image k is (van Geems *et al.*, 1995):

$$x_{k,i} = \left(h_{k,1} - x_{k,i}.h_{k,4}\right)X_i + \left(h_{k,2} - x_{k,i}.h_{k,5}\right)Y_i + h_{k,3} \qquad (7)$$

where the slice coordinates X_i and Y_i, and the five h parameters ($h_{k,1}$, ..., $h_{k,5}$) relate to image k. The $x_{k,i}$ value can be found by taking measurements from the X-ray image k and points X_i and Y_i are known from the independent calibration of the calibration frame. These points for each X-ray image are substituted into equation (7).

The five unknown *h* parameters remain unsolved, thus requiring five non-collinear calibration markers for a unique solution. If more than five calibration markers are used this would provide an over-determined system and a least squares method can be used to solve for the parameters.

Equation (7) can be written in matrix form for calibration markers $1-n$:

$$A\omega = L \qquad (8)$$

where:

$$A = \begin{bmatrix} X_1 & Y_1 & 1 & -x_{k,1}X_1 & -x_{k,1}Y_1 \\ X_2 & Y_2 & 1 & -x_{k,2}X_2 & -x_{k,2}Y_2 \\ . & . & . & . & . \\ . & . & . & . & . \\ X_n & Y_n & 1 & -x_{k,n}X_n & -x_{k,n}Y_n \end{bmatrix} \quad \omega = \begin{bmatrix} h_{k,1} \\ h_{k,2} \\ h_{k,3} \\ h_{k,4} \\ h_{k,5} \end{bmatrix} \quad L = \begin{bmatrix} x_{k,1} \\ x_{k,2} \\ . \\ . \\ x_n \end{bmatrix}$$

The slice coordinates X_i and Y_i of an unknown marker can now be found by back substitution into equation (7). The coordinate Z_i can be determined from the X-ray image and the slice system. Therefore the three-dimensional coordinates (X_i, Y_i, Z_i) of a point can be found (van Geems *et al.*, 1995).

3.3 Calibration Equipment

3.3.1 The Calibration Frame Design

A calibration frame or cage is a three-dimensional frame with markers of known coordinates usually covering the volume of interest. Challis and Kerwin (1992) established that the use of control points around the outside of the volume of interest is preferred to control points distributed within the volume. The calibration frame is needed to define the laboratory coordinate system and to find the transformation parameters that will allow three dimensional coordinates to be found from two-dimensional image coordinates. Once the volume is calibrated, it will be possible to calculate the spatial coordinates of unknown markers within the specified space with respect to the defined laboratory coordinate space.

The accuracy of the transformation depends on the accuracy of the calibration marker coordinates, and therefore this section of the project was vital. The following had to be considered during the calibration frame design process:

- The frame had to be rigid and stable with the markers firmly attached so that the coordinate measurements remain valid.
- The calibration markers had to cover the outside limits of the volume of interest, as recommended by Challis and Kerwin (1992).
- Theoretically the transformation technique only requires six known calibration markers or control points; however, studies have demonstrated that reconstruction accuracy improves with an increased number of control points with limited improvement when more than 16 control points are used in DLT (Chen *et al.*, 1993). The calibration frame therefore had to have at least 16 control points.

The calibration frame had to be calibrated using a line-of-sight camera stereo-photogrammetry technique; therefore the following characteristics were required to ensure good calibration:

- The markers had to be visible on photographs of the frame taken from many different angles.
- There had to be sufficient contrast between the markers and the frame structure so that the markers can be easily identified on the photographs.
- The frame structure material had to be limited so that as few control frame points as possible were obscured.
- Markers had to be large enough to allow easy identification on the photographs.

In addition, the accuracy of calculating the coordinates of unknown markers depends on the accuracy to which the corresponding coordinates of the markers are located on the X-ray images. This in turn depends on the image quality, resolution, size of calibration markers and level of contrast available on the X-ray images. The calibration frame therefore needed to be optimally designed to enable easy identification of the corresponding markers on the digital X-ray images:

- The frame material had to be radiolucent and the calibration markers had to be radio-opaque to provide sufficient contrast between the frame and markers.
- The arrangement of the markers had to be irregular to prevent overlapping markers on the X-ray images.
- A logical, standardised calibration marker numbering system had to be established as recommended by Kärrholm *et al.* (1989).

The dimensions of the possible scanning area also had to be taken into account when designing the calibration frame. The C-arm of the Statscan machine can only be rotated with the trolley in a raised position and raising the trolley would shrink the maximum scanning volume available; therefore the trolley height was taken into account. With the trolley fully raised, the maximum scanning width was 560 mm (see Figure 3.2).

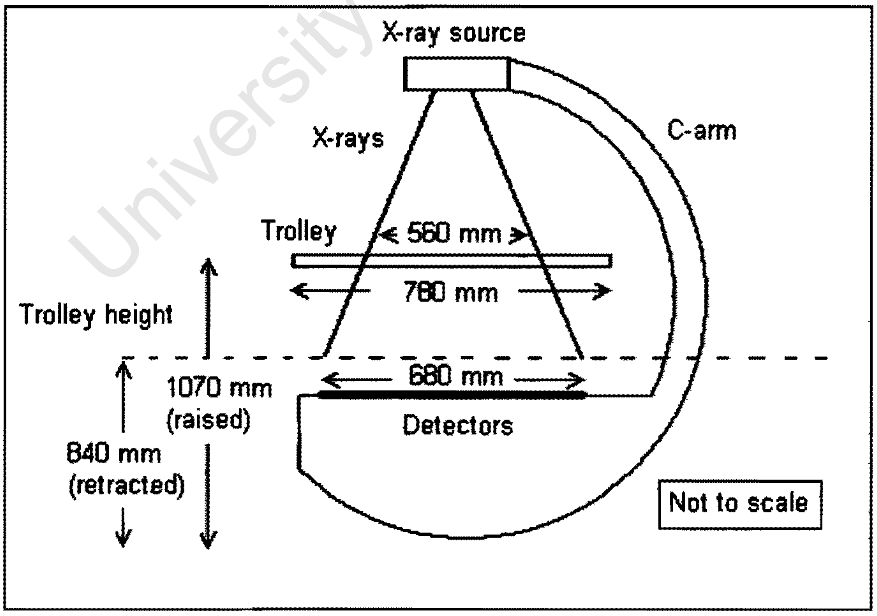

Figure 3.2 The dimensions of the Statscan machine and the height of the trolley limit the imaging space and provide constraints for the design of the calibration frame.

The frame volume had to be big enough to allow experimental objects to be placed within it; however, it also had to be within the scanning volume limits even when the C-arm was at 45° and 90° angles. The frame scanned in the A-P view may not necessarily give an acceptable oblique view due to truncation (see Figure 3.3 below for an illustration).

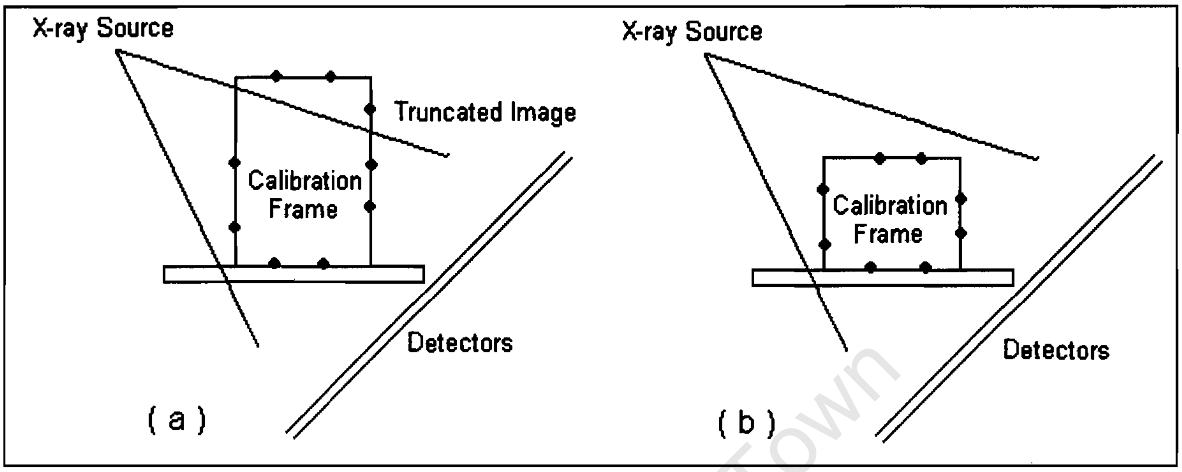

Figure 3.3 (a) Illustrating how an image could be truncated if the frame is outside the X-ray fan-beam. (b) A good image is obtained when the frame is within the X-ray beam.

The early calibration frames for use in X-ray photogrammetry described in the literature review were made from acrylic plastic sheeting since the refraction of X-rays through a thin Plexiglass plate is said to be completely negligible (Veress, 1989); however, during an assessment of different materials for this study it was found that the thickness of the acrylic sheet when placed vertically and viewed from the top made the acrylic radio-opaque and obscured the markers. This effect can be seen in the Statscan image of the phantom (see Figure 3.13), which consists of some Plexiglass columns.

The final calibration frame design was pyramid-shaped in order to cover a large volume while avoiding truncation (base: 30 x 30, height: 28 cm). The frame consisted of fibreglass struts glued into Perspex L-pieces. Fibreglass was identified as a suitable alternative to Plexiglass since it was sufficiently radiolucent. The L-pieces were sufficiently thin so that refraction of X-rays was minimal. These pieces were drilled so that the rods would fit in at the correct angles. The frame base was 300 mm x 300 mm and the height was 280 mm. Twenty-five steel ball bearings 10 mm in diameter were used as markers. Twenty five markers were chosen so that there were enough markers to allow different configurations of control points and test points to be used in the experiments. The large diameter markers were chosen to provide a robust and stable calibration frame that could be easily calibrated using conventional camera stereophotogrammetry. The steel ball bearings were annealed and then centrally drilled by Pro-touch Engineering cc. (Wolraad Street, Maitland) so that they would easily slide onto the fibreglass rods. This technique is similar to that employed by Challis and Kerwin (1992), where the markers were also centrally drilled. An epoxy glue was used to glue both the ball bearings and the rods into place. The frame was then painted black using matt blackboard paint to reduce reflections. This technique was also used by Challis and Kerwin (1992). The ball bearings were painted white using reflective road paint to provide a visual contrast for the conventional photogrammetry calibration. The frame is shown in Figure 3.4 below.

Figure 3.4 The pyramid-shaped calibration frame with twenty-five radio-opaque markers

The twenty-five calibration markers were numbered in a spiral fashion from the bottom to the top to enable easy identification (see Figure 3.5).

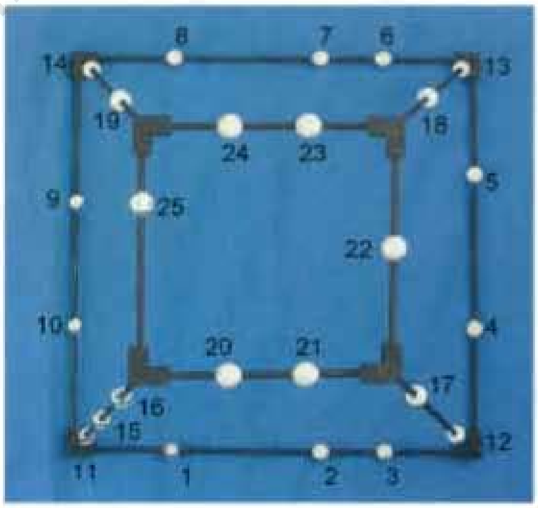

Figure 3.5 The calibration frame viewed from above. The numbers indicate the marker position labels.

Marker number one was chosen to be near the only vertical strut with three markers to enable the user to identify the markers correctly.

3.3.2 The Calibration Frame Survey

The calibration frame was surveyed by conventional close range digital photogrammetry using the Australis software package (Department of Geomatics, University of Melbourne) that performs a least squares bundle adjustment. The Statscan calibration frame along with the Geomatics control frame can be seen in Figure 3.6. The Geomatics control frame is used for camera photogrammetry only and it is therefore simply a metal frame with white retroreflective stickers as markers.

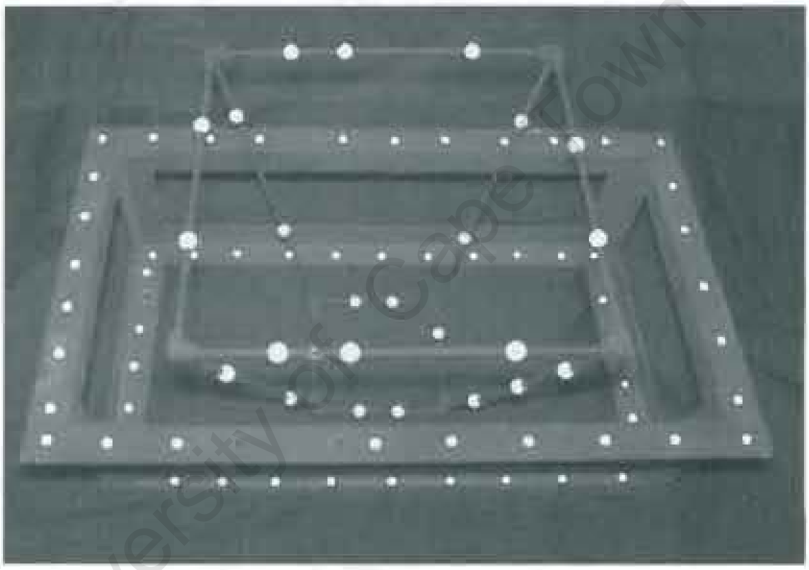

Figure 3.6 One of the calibration images used to measure the three-dimensional position of the markers accurately.

The maximum standard deviations (σ) for the measured marker coordinates were 0.10 mm, 0.12 mm and 0.06 mm, respectively in the X-, Y-, and Z-directions. The mean standard deviations were 0.07 mm, 0.06 mm and 0.04 mm, respectively.

The calibration frame coordinates were changed from the Geomatics frame coordinate system to a calibration frame coordinate system using marker number 11 as the origin. The three-dimensional coordinates and definition of the axes are given in Appendix A.

3.4 Image Marker Centroid Location

3.4.1 Calibration Frame Marker Centroid Location

Discrete point reconstruction accuracy depends on the accuracy of the three-dimensional spatial coordinates of the calibration markers as well as the accuracy of locating the two-dimensional coordinates of the marker centroids on the X-ray images (Adams and Constant, 1988).

Most of the literature reviewed on marker identification used some kind of user interaction to ensure that the markers were labelled correctly (see Section 2.5). The calibration frame markers are large and easily recognisable on the digital X-ray images, which aids in the identification and location of the two-dimensional coordinates. An automatic marker identification routine, such as that developed by Vrooman *et al.* (1998) for RSA was not developed in this project. Instead, user selection of markers followed by automatic marker correction was employed (see Appendix C).

The calibration markers on the digital X-ray images were identified according to the numbering system shown in Figure 3.5. The user was prompted to select the calibration markers in the correct order from 1 to 25. As the user clicks on the marker, a circle is drawn around the point and it is labelled (see Figure 3.7).

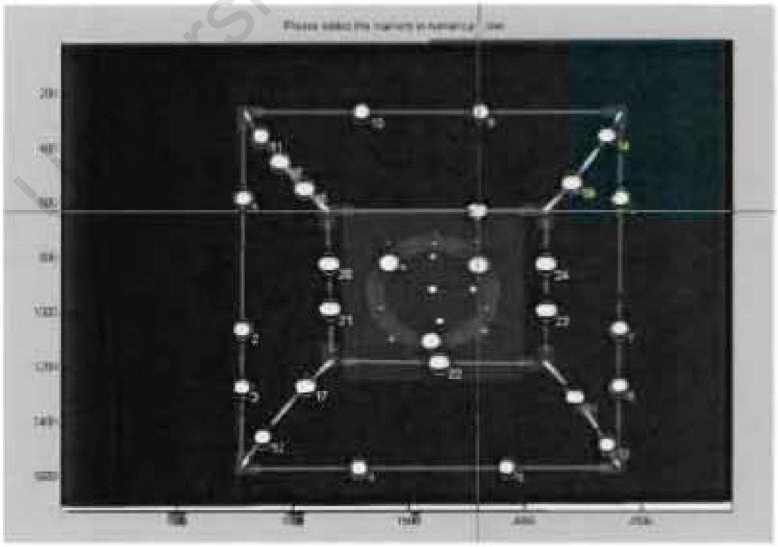

Figure 3.7 An X-ray image of the calibration frame with the phantom object in the centre during marker identification. The Matlab program requires user intervention to select the calibration frame markers in the correct order using the mouse and a cursor. Once selected, the marker is labelled as shown.

The marker centre correction program uses each of the user-selected points as a reference and defines an 80 x 80 pixel region of interest (ROI) around each point. These ROI's are transferred to an empty matrix (black image) of the same size as the original image to remove any non-marker grey or white areas. This approach is similar to that used by van der Vlugt (1991). A threshold pixel value then determined for each ROI by taking the mean of the ROI pixel intensities. For each ROI, the threshold pixel value is used to find the location of pixels with intensities higher than the threshold. The locations of these pixels are given in x and y image coordinates. Taking the mean of the x and then y coordinates gives the centre point of the marker. This value is rounded off to give the nearest pixel value and hence the centre of the marker is given in x and y coordinates.

The marker centroid correction of two markers on a 90° X-ray image is seen in Figure 3.8 where the outer black square is the user-selected point and the central black square is the position found by the algorithm.

Figure 3.8 Examples of marker centre correction on two calibration markers imaged at an angle of 90°

The contrast between the radio-opaque markers (seen as white on X-ray images) and the radiolucent frame (seen as darker shades of grey on X-ray images) is very obvious which makes thresholding a successful method to locate the marker centroid. The program returns a list of marker centroid coordinates for each image for use in reconstruction.

The hole that was drilled through the centre of each ball bearing is noticeable on some of the X-ray images depending on the angle of radiography (see Figure 3.9). This was shown to have negligible effects since the Matlab marker centre correction program was still capable of finding the centre of such markers.

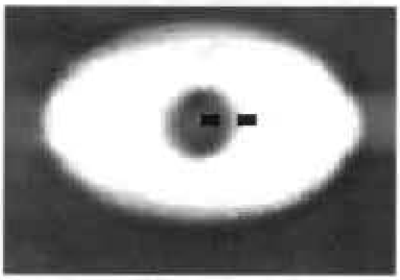

Figure 3.9 A marker imaged at 90° where the hole through the ball-bearing is visible. The outer black square is the user-selected point and the central black square is the position found by the centre correction algorithm.

One shortcoming of the marker centre correction program is that in cases where the markers overlap on X-ray images, the algorithm incorrectly identifies centre points based on the centre of the entire white space (see Figure 3.10). In these cases, the image marker coordinates were estimated manually using the Matlab zoom and pixel coordinate functions.

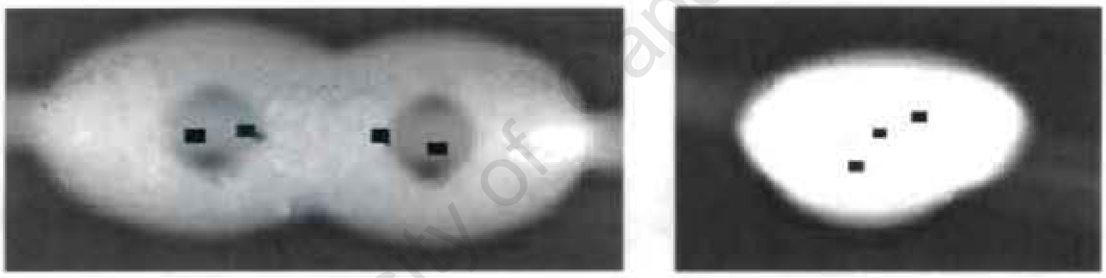

Figure 3.10 Overlapping markers on Statscan images taken at 90°. The outlying black squares are the user-selected points and the "corrected" or more central black squares are the positions found by the algorithm.

In order to gain confidence that the penumbra effect can be ignored in the determination of the centroid (Slama *et al.*, 1980; Veress, 1989), the extent of the penumbra was established for each marker in a random sample of 10 markers from the X-ray images. The markers were at different elevations from the X-ray detectors. By counting the number of pixels in the penumbra region on each side of the marker along a bisecting line, the penumbra was found to be symmetrical for each marker. Figure 3.11 shows the symmetrical penumbra of one such marker. The penumbra symmetry ensures that the centroid calculation will not be affected by the penumbra.

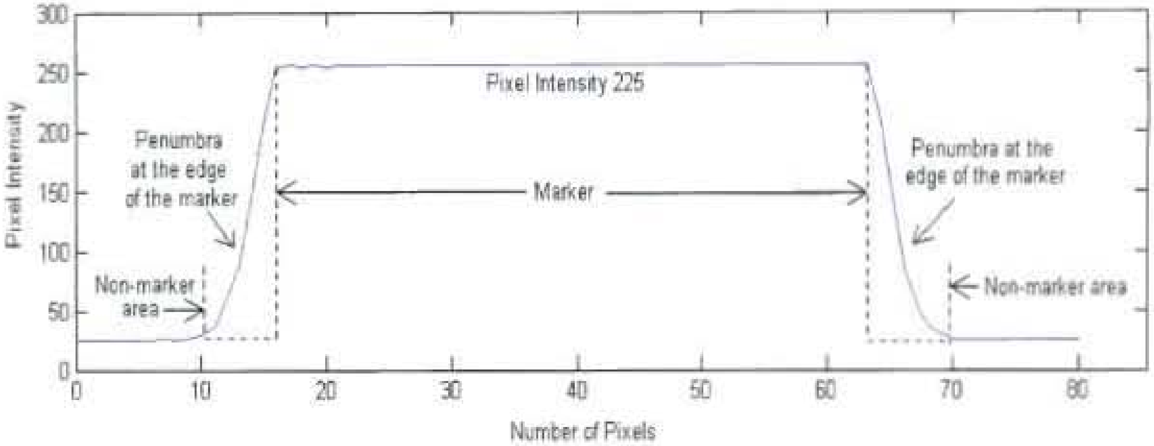

Figure 3.11 The pixel intensity values on opposite edges of a marker showing the symmetrical intensity drop from 225 (marker) to about 30 (non-marker) over 6 pixels.

An experiment was performed to assess the reproducibility of the computer assisted marker centroid location program (see Section 4.1).

3.4.2 Phantom Marker Centroid Location

A Perspex phantom was used for the interpolation experiment (see Section 4.5) where known 3D phantom marker coordinates were compared to the calculated X-, Y- and Z coordinates to establish the accuracy of the reconstruction method in interpolation.

The phantom consists of a Perspex base plate with protruding cylindrical Perspex rods of varying lengths (see Figure 3.12). It has a Perspex ring glued to the top of the three longest and thickest cylinders. Thirteen 1-mm diameter steel balls are embedded in special indentations in the top of the columns and on the ring. The coordinates of the ball bearings were measured using a reflex metrograph during a previous study in the Department of Biomedical Engineering, UCT (see Appendix B for the definition of the axes and the coordinates). The resolution of measurements using a reflex metrograph is typically 0.1 mm for each axis (Adams and Constant, 1988).

The phantom markers were labelled as shown in Figure 3.13. Steel markers were missing from some of the Perspex columns. However, this does not affect the experiments and these locations were simply ignored. Phantom marker number 8 is difficult to see on the 0° image since the Perspex column also shows up as bright white on the X-ray image (see Figure 3.13). The shorter Perspex columns do not pose a problem since the X-ray attenuation is less and the markers can be seen clearly.

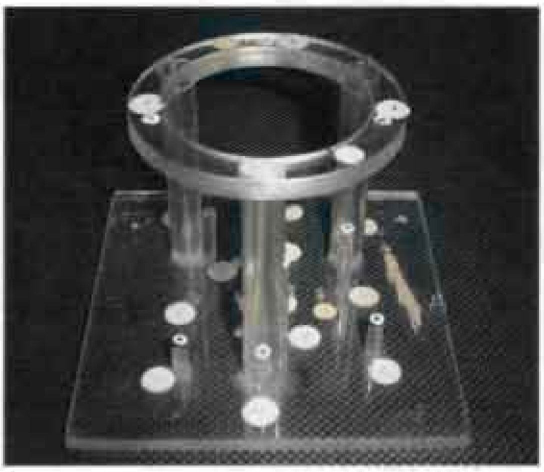

Figure 3.12 The Perspex phantom frame used for experiments involving reconstruction of unknown points using interpolation

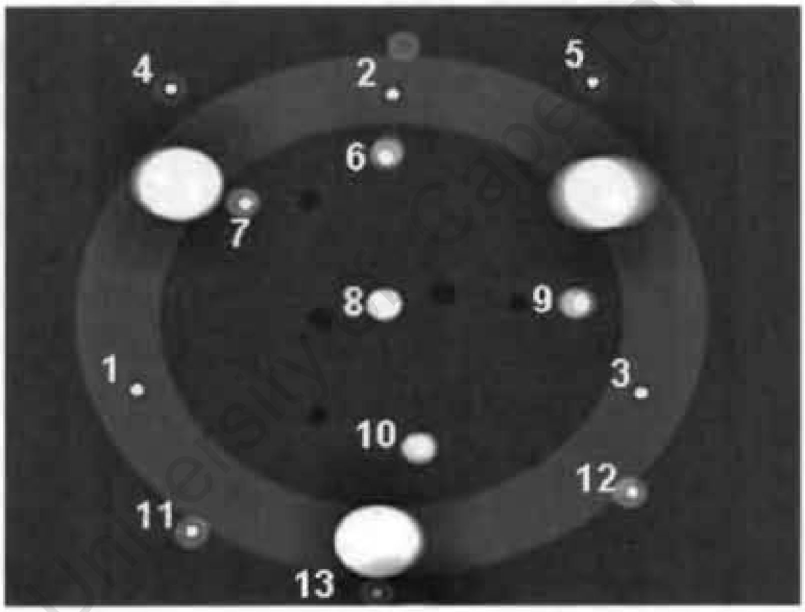

Figure 3.13 An anterior-posterior Statscan X-ray of the ring phantom. Each marker (small white dot) has been labelled for ease of identification. The large white objects are the Perspex columns X-rayed through their length.

The location of the small marker (1 mm) centroids on the X-ray images was done using a slightly different image processing technique to that used for the larger (10 mm) calibration frame markers.

In this program, the user is first required to select a 30 x 30 pixel region of interest using the mouse and cursor for each phantom marker in the correct order (see Figure 3.13). The maximum pixel values are identified within this region of interest (ROI) and the ROI is converted into a binary image where the maximum pixel values with a connectivity of 4 pixels are given a value 1 (white) and the other pixels are changed to 0 (black). The inbuilt Matlab function "imfeature" is then used to find the centre of mass of each white marker region. Based on the visual inspection of 91 selected markers (13 markers in each of the 7 radiographs), the program accurately found the marker centres as long as there were no other interferences such as overlapping markers, markers within the 30 x 30 pixel region of interest or interferences from the radio-opaque Perspex columns (see Figure 3.14).

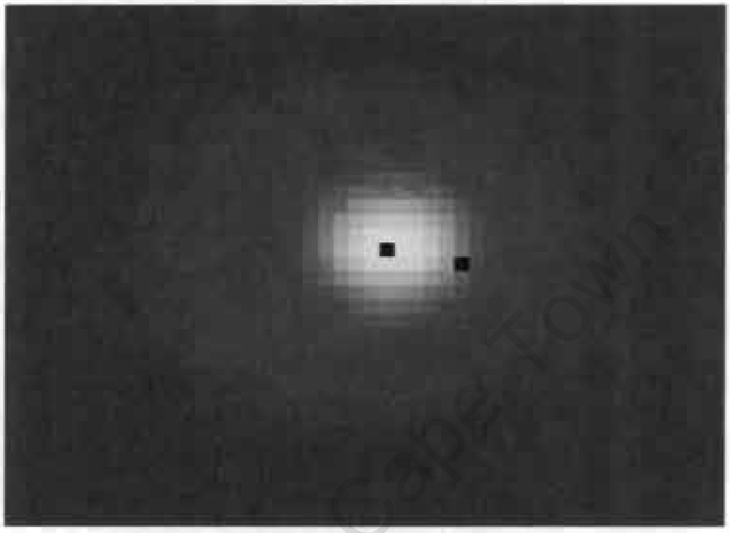

Figure 3.14 The marker centre correction of a 1 mm steel marker embedded in a Perspex rod. The outer black square is the user selected point and the central square is the corrected centre.

3.5 Reconstruction Software

Computer programs written in Matlab were used to perform the three dimensional reconstruction as described by van Geems (1997) (see Appendix C). The known three-dimensional coordinates of the control points were used as inputs as well as the corresponding two dimensional coordinates of the same points and the two-dimensional coordinates of the test points. The program uses functions to generate the required matrix given by the algorithm in Section 3.2.1.

The output of the program is a matrix containing the calculated marker coordinates. The program compares these calculated coordinates to the known coordinates and provides the X, Y and Z errors for each point.

Chapter 4 : Experiments and Results

To establish proof of concept for the use of Statscan for X-ray stereophotogrammetry, several experiments were performed. Two sets of images (image-sets A and B) were taken of the control frame for use in these experiments. They were obtained at different times (March and August 2006 respectively) using the Groote Schuur Hospital Trauma Unit Statscan X-ray machine.

Both image-sets consisted of seven X-ray images where each image was taken at a different scanning angle (0°, 15°, 30°, 45°, 60°, 75°, and 90°). These X-ray images were paired to form 21 combinations at six different separation angles (see Figure 4.1). The separation angle is the angle between the X-ray beams at their point of intersection and is therefore the angle through which the C-arm was moved to obtain the pair of X-ray images.

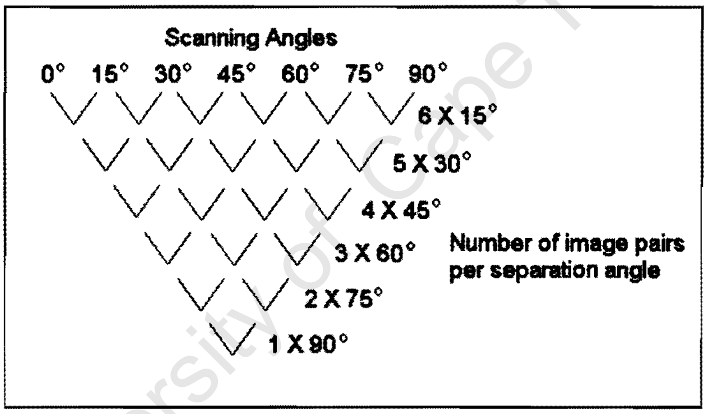

Figure 4.1 Explanation of how the images taken at seven different scanning angles are paired to form 21 combinations at six separation angles

In image-sets A and B, the majority of marker centres were located using the centre correction program (see Section 3.4.1). In cases where the markers overlapped one another (see Figure 3.10) or were too close to the edge of the X-ray image, the marker centres were located manually (see Table 4.1).

Table 4.1 Manually corrected markers in image-sets A and B

C-Arm Angle	**Manually corrected markers in Image-set A**	**Manually corrected markers in Image-set B**
45°	None	8, 6, 16, 17
75°	16, 18, 19, 20, 24, 21, 23	16, 17, 18, 19
90°	4, 5, 9, 11, 14	4, 5, 9, 10, 11, 14, 22

In image-set B, with the C-arm at 60° and 75°, markers 23 and 24 were truncated and so were not present on the X-ray images. With the C-arm angle at 90° (scanning laterally), markers 20 and 21 were truncated (see marker labelling in Figure 3.5). This problem was not experienced when image-set A was obtained, and so this truncation is possibly due to slight changes in the operating table set-up between scanning image-sets A and B. These four markers have been excluded from all the experiments.

The method of establishing the accuracy of point reconstruction varies among researchers depending on the information available (Challis and Kerwin, 1992). Some researchers compared calculated distances with measured distances (Adams and Constant, 1988), while others compared calculated point coordinates with measured coordinates (Wood and Marshal, 1986; Plamondon and Gagnon, 1991; Challis and Kerwin, 1992). The comparison of distances is mainly used when the object coordinate systems and calibration frame coordinate systems differ. In the Statscan experiments, marker coordinates were compared to measured coordinates except in phantom point reconstruction (see Section 4.5), where the marker distances from an origin marker to other markers were compared with measured distances.

The following experiments were performed to assess the suitability of Statscan for X-ray stereophotogrammerty:

1) The reproducibility of locating two-dimensional marker centroids using two images taken at 0° and 90° from image-set B.
2) The reconstruction of control points (points on the calibration frame that were used in determining the transformation parameters) using image-sets A and B.
3) The reconstruction of test points (non-control points on the calibration frame) using image-set B only.
4) The reconstruction of test points (non-control points on the calibration frame) using extrapolation and image-set B only.
5) The reconstruction of phantom test points that lie within the control point volume using interpolation and image-set B only.

4.1 Reproducibility of the 2D marker centroid location

The reproducibility of the manual marker selection and the marker centroid correction program was tested by assessing the marker selection results of three independent operators. Each operator selected the 15 markers on the image-set B, 0° and 90° images three times according to the numbering given in Figure 3.5, with the exception of markers numbered 4, 5, 9, 10, 11, 14, 20 and 21. These markers were excluded because they overlapped on the 90° image and gave obviously incorrect results when using the marker centroid correction program. The results are given as the mean standard deviations of the x and y image coordinates for the sets of manually selected and corrected markers.

To establish the effect of the marker centroid identification on the three dimensional reconstruction, the nine sets of two dimensional marker coordinates obtained from manual marker selection and the centroid correction program as described above were used to reconstruct the 15 control points. The results are given as the mean standard deviations of the nine sets of X-, Y- and Z-coordinates for each identification technique.

4.1.1 Results: Reproducibility of 2D marker centroid selection and correction

The mean standard deviations for the manual selection of the 15 markers (nine sets per image) were 0.46 and 0.45 pixels (0° image), 0.31 and 0.25 pixels (90° image) and 0.39 and 0.35 pixels (0° and 90°) for x and y respectively. The image resolution is approximately 0.2 mm per pixel, so the mean standard deviations for x and y image coordinates when manually selected can be given as 0.08 mm and 0.07 mm respectively (see Table 4.2).

The mean standard deviations of the x and y image coordinates for the nine corrected marker selections were 0.42 and 0.09 pixels (0° image) and 0.53 and 0.09 pixels (90° image) in the image x and y directions respectively. In the 0° scanning angle, the image x axis corresponds to the Statscan Y axis and the image y axis corresponds to the Statscan Z axis (direction of travel). The total mean standard deviations for 0° and 90° images are 0.47 and 0.09 pixels (approximately 0.09 mm and 0.02 mm) in the x and y directions respectively (see Table 4.2). It was noted that both the x and y errors were generally greater for markers that were further from the X-ray detectors, than for those closer to the detectors (see Table D.1, Appendix D).

Table 4.2 The mean standard deviations for the 2D coordinates of the markers identified manually and using the marker correction program

	x (pixels)	y (pixels)	x (mm)	y (mm)
Manual marker centroid identification	0.39	0.35	0.08	0.07
Marker centroid correction program identification	0.47	0.09	0.09	0.02

The mean standard deviations for the 3D reconstruction of the nine sets of 15 markers were 0.05 mm, 0.07 mm, 0.05 mm for X, Y and Z-coordinates respectively when using the manually selected 2D coordinates, and 0.07 mm, 0.06 mm and 0.02 mm for X, Y and Z-coordinates respectively when using the corrected marker coordinates (see Table 4.3).

Table 4.3 The mean standard deviations for the reconstruction of 3D coordinates of the markers identified manually and using the marker correction program

	X (mm)	Y (mm)	Z (mm)
Manual marker centroid identification	0.05	0.07	0.05
Marker centroid correction program identification	0.07	0.06	0.02

The X direction manual marker centroid identification gives a lower standard deviation than the marker centroids correction program. The marker centroids correction program should be optimised to at least be an improvement on the manual method.

4.2 Reconstruction of control points

The reconstruction of points that are used in the calculation of the transformation parameters (control points) does not fully test the reconstruction accuracy of this method, although it does provide information about the accuracy of the mathematical technique and any unaccounted for aspects of the reconstruction, e.g. noise (Challis and Kerwin, 1992). The reconstruction of control points has previously been used as a measure of accuracy by Wood and Marshal (1986) and Hatze (1988). In this experiment, the reconstruction of two independent image-sets (image-sets A and B) was used to assess the repeatability of the method.

The three dimensional reconstruction results are used to test repeatability instead of merely comparing the marker centroids from the X-ray stereo-pairs (Wang *et al.*, 1996) since the positioning of the calibration frame in the Y-Z plane may differ between image-sets, resulting in possible reconstruction repeatability errors.

Image-sets A and B are X-ray images of the control frame that were taken using source-detector assembly scanning angles with respect to the scanned object in intervals of 15° from 0° to 90°. These intervals were also used by Plamondon and Gagnon (1991) in their DLT study. The X-ray images were paired to form 21 combinations at six different separation angles (see Figure 4.1).

4.2.1 Description of the control point sets for control point reconstruction

Sets of 21, 16, 11 and 7 calibration frame markers were chosen as control points and these same points were reconstructed in each case. Each set consisted of four different control marker positions evenly arranged around the frame, except the case of 21 markers, where only one set was used (see Table 4.4). Even distribution was chosen in an attempt to reduce errors that could be introduced by grouped control points (Chen *et al.*, 1993). However, it should be noted that there are fewer available control points at the top of the frame than around the base due to the pyramid style design. The four different marker configurations were chosen to provide assurance that the results were not dependent on one specific control point configuration (Chen *et al.*, 1993).

Table 4.4 The marker sets used to test the transformation by reconstruction of control points

Control point configuration	Markers used as control points and test points
21	1,2,3,4,5,6,7,8,9,10,11,12,13,14,15,16,17,18,19,22,25
16	1,3,4,5,6,8,9,11,12,13,14,15,17,19,22,25
	1,2,4,5,7,9,10,11,13,14,16,17,18,19,22,25
	1,2,3,4,5,6,8,10,11,12,14,15,17,18,19,25
	1,2,3,4,5,7,9,11,12,13,14,16,17,18,19,22
11	1,3,4,6,9,12,13,14,15,22,25
	1,2,5,7,11,14,16,17,19,22,25
	2,4,6,8,10,14,15,17,18,19,25
	3,5,7,9,11,12,13,14,16,19,22
7	1,6,9,12,14,22,25
	1,5,7,11,16,22,25
	2,6,10,14,17,19,25
	3,5,7,12,16,19,22

4.2.2 Results of control point reconstruction

The transformation error is expressed as the mean absolute difference between the known three-dimensional coordinates, as measured by the Australis system (see Section 3.3.2), and the calculated coordinates of each marker. The mean absolute errors (e_X, e_Y, e_Z) were calculated as shown below for each stereo-pair to allow analysis of the effect of the separation angle.

$$e_X = \frac{1}{n}\sum_{i=1}^{n}\left|X_{mi} - X_{ci}\right| \qquad (9)$$

$$e_Y = \frac{1}{n}\sum_{i=1}^{n}\left|Y_{mi} - Y_{ci}\right| \qquad (10)$$

$$e_Z = \frac{1}{n}\sum_{i=1}^{n}\left|Z_{mi} - Z_{ci}\right| \qquad (11)$$

where:

n	number of points for each series (i.e. 21, 16 x 4, 11 x 4, 7 x 4)
X_{mi}, Y_{mi}, Z_{mi}	3D coordinates of the points measured by the Australis system
X_{ci}, Y_{ci}, Z_{ci}	3D coordinates calculated using the transformation parameters

The program uses linear fitting on the two stereo X-ray images to obtain two reconstructed Z-coordinates for each marker since the object Z-coordinate has a linear relationship with the image y coordinate. The Z-coordinate (Z_{ci}) is taken as the mean of the two reconstructed Z-coordinates for each marker. The resultant error (e_{Res}) was calculated as shown in equations 12 and 13.

$$e_{\mathrm{Res}} = \frac{1}{n}\sum e_i \qquad (12)$$

where: $$e_i = \sqrt{(X_{mi} - X_{ci})^2 + (Y_{mi} - Y_{ci})^2 + (Z_{mi} - Z_{ci})^2} \qquad (13)$$

In addition to the mean absolute errors, the maximum absolute errors were also calculated for the X, Y and Z coordinates and are given in Table D.2 and D.3 in Appendix D.

The results reported in the graphs average across the control point sets as well as across the different angles. The results from the reconstruction of image-set A control point sets (see Figure 4.2 and Table D.2, Appendix D) show that the mean absolute X- and Y-errors decrease with increasing separation angles. The resultant mean absolute errors also decrease with decreasing numbers of control points. The greatest resultant error was found when using the highest number of control points (21) and the smallest separation angle (15°), whereas the smallest resultant error was found when using the lowest number of control points (7) and the greatest separation angle (90°).

Comparing the X and Y errors, the Y- coordinate mean absolute error was generally found to be higher than that of the X- coordinate. The mean absolute X-errors and maximum absolute X-errors for 21, 16, 11 and 7 control points were lowest when the maximum separation angle (90°) was used, whereas the mean absolute Y-errors were found to stabilise at 30° for 11, 16, and 21 control points and at 75° for 7 control points. The maximum absolute Y-errors were lowest when large separation angles were used (90° for 21, 16 and 11 control points, 75° for 7 control points).

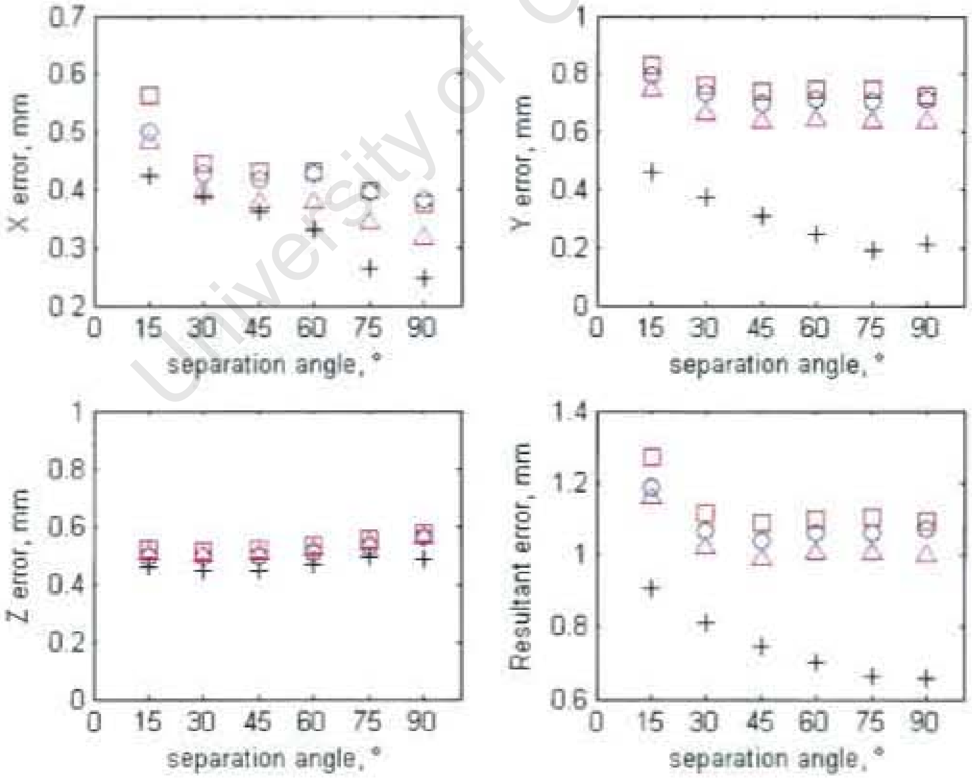

Figure 4.2 Image-set A - Mean absolute X-, Y-, Z- and resultant errors for the reconstruction of control point sets 21 (□); 16 (○); 11(Δ); 7(+) control points.

It is clear from Figure 4.2 that the mean absolute Z-error is fairly constant across all separation angles for all control point sets. There is a very slight upward trend in the error as the separation angle is increased.

The results of the image-set B control point reconstructions (see Figure 4.3 and Table D.3, Appendix D) show similar characteristics to those of image-set A. The resultant mean absolute errors decrease with increasing separation angles. The resultant mean absolute errors also decrease with decreasing numbers of control points. Like image-set A, the greatest resultant error is found when using the highest number of control points (21) and the smallest separation angle (15°) and the smallest resultant error is found when using the lowest number of control points (7) and the greatest separation angle (90°).

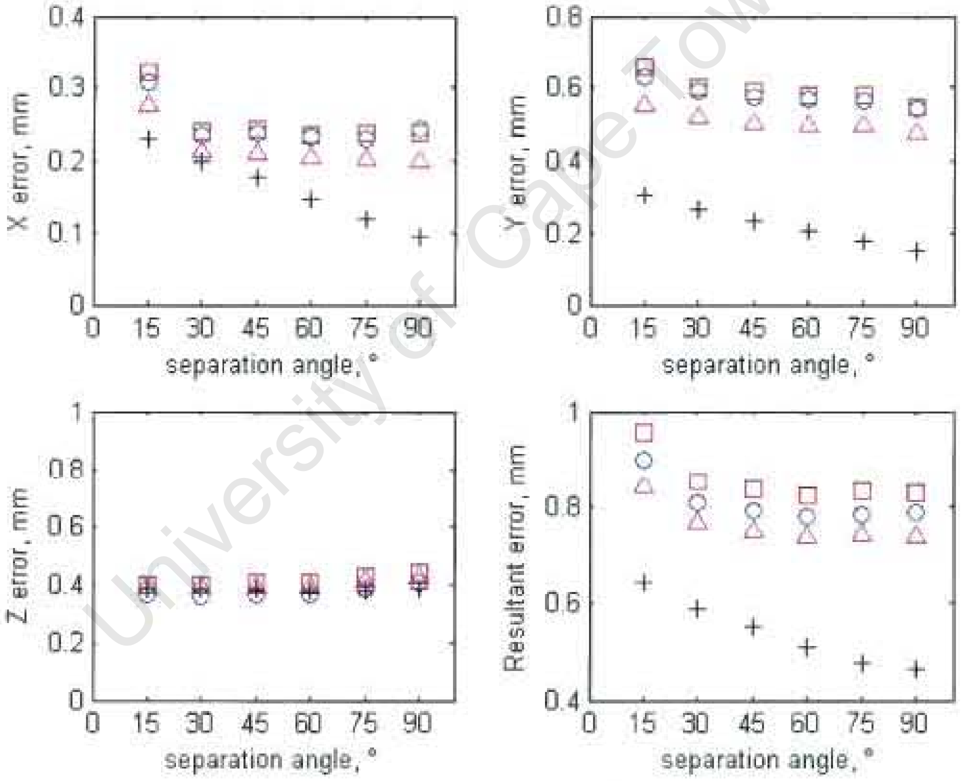

Figure 4.3 Image-set B - Mean absolute X-, Y-, Z- and resultant errors for the reconstruction of control point sets, 21 (□); 16 (○); 11 (Δ); 7 (+) control points.

Similarly to the image-set A results, the mean absolute errors were larger in the Y-direction than in the X- direction.

In agreement with image-set A, the image-set B results showed that the mean absolute Z-error was quite constant across all separation angles for all control point sets. There was a very slight upward trend in the error as the separation angle increased.

Although the error trends for image-sets A and B were consistent, the error magnitudes differed between the two image-sets. In all cases, lower mean absolute errors were recorded for Image-set B than image-set A. The mean differences between the mean absolute X-, Y- and Z errors of image-set A and B were 0.18 mm, 0.14 mm and 0.12 mm respectively. Image-set B was obtained a few months after image-set A and the differences in error could be attributed to improvements in the Statscan image reconstruction software. The differences in mean absolute error and maximum absolute error between image-sets A and B are tabulated in Table D.4 in Appendix D for completeness. Image-set B was chosen to be used for the rest of the experiments since it yielded better overall accuracy than image-set A.

To summarise, in this experiment we have seen that when points that were used in the derivation of transformation parameters (control points) were reconstructed, the lowest mean absolute errors were observed when using the lowest number of control points and the largest separation angle. The low error when using large separation angles is in agreement with the literature and the low error when few control points are used can be explained by the "over-fitting" of the DLT equations to the few control points. The observed accuracy can therefore not be taken as a true representation of unknown point reconstruction.

4.3 Reconstruction of test points using calibration frame markers

In this experiment, the reconstruction of non-control point calibration frame markers (test points) was used to test the accuracy of locating unknown points. These non-control points were not used in establishing the transformation parameters. This approach of reconstructing non-control point calibration markers has been used by several researchers in the past to establish the true accuracy of reconstructing unknown points (Challis and Kerwin, 1992; Plamondon and Gagnon, 1991; Chen *et al.*, 1994). Image-set B was used in this experiment.

4.3.1 Description of the control point sets for test point reconstruction

The same sets of 16, 11 and 7 calibration frame markers as in Section 4.2 were chosen as control points, but instead of reconstructing these same points, five different points were reconstructed (see Table 4.5).

The points were well-distributed around the calibration frame. The evaluation using 21 control markers was not repeated here since there would not have been sufficient non-control markers to act as test points.

Table 4.5 Marker sets used to test the unknown point transformations

Control point configuration	Markers used as control points	Markers used as test points for testing the unknown set
16 – configuration 1	1,3,4,5,6,8,9,11,12,13,14,15,17,19,22,25	2,7,10,16,18
16 – configuration 2	1,2,4,5,7,9,10,11,13,14,16,17,18,19,22,25	3,6,8,12,15
16 – configuration 3	1,2,3,4,5,6,8,10,11,12,14,15,17,18,19,25	7,9,13,16,22
16 – configuration 4	1,2,3,4,5,7,9,11,12,13,14,16,17,18,19,22	6,8,10,15,25
11 – configuration 1	1,3,4,6,9,12,13,14,15,22,25	2,7,10,16,18
11 – configuration 2	1,2,5,7,11,14,16,17,19,22,25	3,6,8,12,15
11 – configuration 3	2,4,6,8,10,14,15,17,18,19,25	7,9,13,16,22
11 – configuration 4	3,5,7,9,11,12,13,14,16,19,22	6,8,10,15,25
7 – configuration 1	1,6,9,12,14,22,25	2,7,10,16,18
7 – configuration 2	1,5,7,11,16,22,25	3,6,8,12,15
7 – configuration 3	2,6,10,14,17,19,25	7,9,13,16,22
7 – configuration 4	3,5,7,12,16,19,22	6,8,10,15,25

4.3.2 Results of test point reconstruction

The error was once again calculated as the difference between the known three-dimensional coordinates, as measured by the Australis system (see Section 3.3.2), and the reconstructed coordinates of each test point. The mean absolute errors and maximum absolute errors for X, Y and Z were calculated for each stereo-pair to allow analysis of the effect of the separation angle on accuracy. The resultant error was calculated as shown by equations 12 and 13 in Section 4.2.2.

The results reported in the graphs average across the control point sets as well as across the different angles. The results from the reconstruction of the five image-set B test points (see Figure 4.4 and Table D.5 in Appendix D) showed that the resultant mean absolute errors tended to decrease with increasing separation angles. This was also observed in the reconstruction of control points (see Section 4.2). However, in contrast to the reconstruction of control points, when test points were reconstructed, the resultant mean absolute errors tended to increase with decreasing numbers of control points.

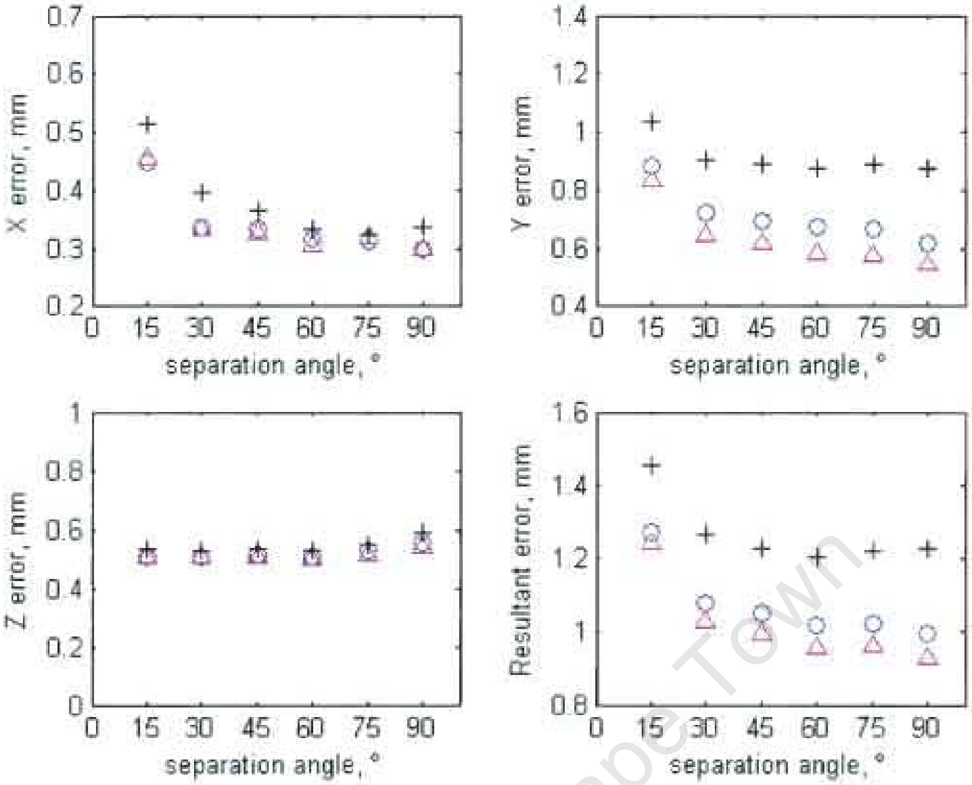

Figure 4.4 Mean absolute X-, Y-, Z- and resultant errors for the reconstruction of five unknown test points when using 16 (○); 11(Δ) and 7(+) control points.

The greatest resultant error was found when using the smallest number of control points (7) and the smallest separation angle (15°). The smallest resultant error was found when using the greatest separation angle (90°), however, contrary to expectations; the highest number of control points (16) did not yield the smallest error. Instead, the smallest error was found when using 11 control points.

Comparing the X and Y errors, the Y- coordinate mean absolute error was generally found to be higher than that of the X- coordinate. This finding corresponds to that of control point reconstruction.

The mean absolute errors and standard deviations for the Z coordinates were consistent across all separation angles and control point configurations used, however, as with the reconstruction of control points (see Section 4.2), we noticed a very slight upward trend towards the 90° separation angle.

To establish how sensitive the reconstruction of test points was to the control point and test point configuration, the mean absolute X-, Y- and Z errors were compared for the reconstruction of test points using 16 control points in the four different configurations (defined in Table 4.5). The configurations are different well-distributed arrangements of control and test points around the frame.

It is clear from Figure 4.5 that the configuration of control points and test points influenced the reconstruction of test points.

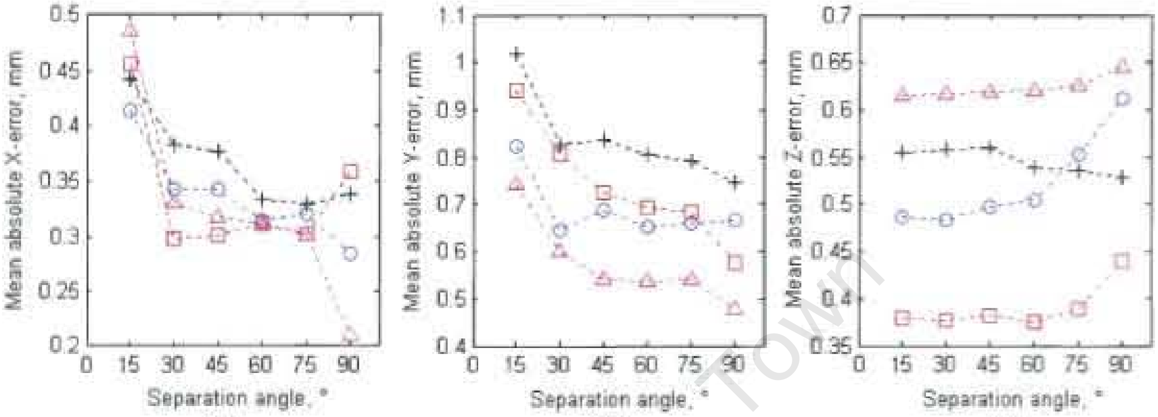

(a) (b) (c)

Figure 4.5 The mean absolute (a) X-, (b) Y- and (c) Z errors for the reconstruction of 5 test points using 16 control points in different configurations; configuration 1 (□), configuration 2 (○), configuration 3 (Δ), configuration 4 (+) (Configurations defined in Table 4.5).

Through experimentation we have shown that separation angles affected the reconstruction of test points, although we have not yet established whether the scanning angle at which the stereo-images were taken in relation to the object affected the results. To study this effect, the mean absolute X, Y and Z errors for reconstruction of the five test points using 16 control points in configuration 1 with six different stereo-images (separation angles of 15° each) were plotted (see Figure 4.6). The results show that the orientation of the X-ray source with respect to the calibration frame had an effect on reconstruction accuracy. The highest errors were observed in the Y-direction when the higher C-arm scanning angles were used, whereas the X-direction errors decreased beyond 15°-30° C-arm scanning angles. The Z-direction errors increased with increasing scanning angle.

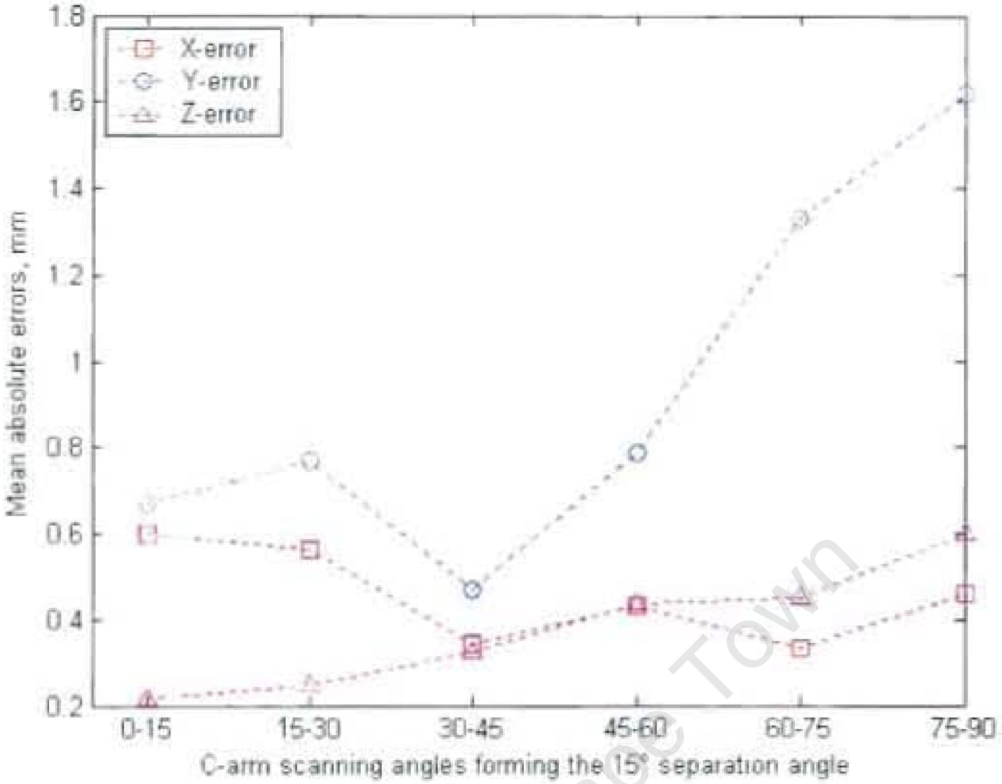

Figure 4.6 An illustration of the effect on the C-arm scanning angles that form the separation angle of 15° on X (□), Y (o) and Z (Δ) mean absolute errors when reconstructing 5 test points using 16 control points in configuration 1.

To summarise, the best performance was observed when 11 control points and a large separation angle (90°) were used to reconstruct the five well-distributed test points. In contrast to the control point reconstruction (see Section 4.2), using 7 control points resulted in the highest errors. The reconstruction of test points provides a more realistic assessment of reconstruction accuracy than the reconstruction of control points since over-fitting of equations to the few points (over-parameterisation) is not experienced. This experiment also showed that the separation angle, scanning angle and control point configuration plays a role in the reconstruction of well-distributed test points.

4.4 Reconstruction of test points using extrapolation

Extrapolation is the location of unknown points outside the space that is defined by the control points. By evaluating the errors in locating such points, we can draw conclusions about the limitations of the use of the Statscan machine for applications where the points to be located are not within the control space.

4.4.1 Description of the control point sets for extrapolation

In order to evaluate extrapolation in the direction of each axis, four sets of 11 control points were selected for each direction. Five unknown test markers were selected in the direction of the extrapolation (see Table 4.6). Two of the four sets extrapolate in the positive axis direction and two extrapolate in the negative axis direction. Image-set B was used in this experiment, where X-ray images of the control frame were taken using different source-detector assembly scanning angles with respect to the scanned object in intervals of 15° from 0° to 90°.

Table 4.6 Marker sets used to assess the transformation for use in extrapolation.

Control point configuration	Markers used as control points	Markers used as test points for testing the unknown set
X-extrapolation-1	1,2, 3,4,7,8,9,10,11,12,13	16,17,19,22,25
X-extrapolation-2	1,2,3,4,5,6,8,9,10,11,14	15,16,17,18,22
X-extrapolation-3	11,12,13,14,15,16,17,18,19,22,25	1,3,5,7,9
X-extrapolation-4	11,12,13,14,15,16,17,18,19,22,25	2,4,6,8,10
Y-extrapolation-1	5,6,7,8,9,13,14,18,19,22,25	1,3,11,12,17
Y-extrapolation-2	5,6,7,8,9,10,13,14,18,19,25	1,2,15,16,17
Y-extrapolation-3	1,2,3,4,10,11,12,15,16,17,22	5,9,13,14,18
Y-extrapolation-4	1,2,4,10,11,12,15,16,17,22,25	6,14,13,18,19
Z-extrapolation-1	1,2,8,9,10,11,14,15,16,19,25	4,5,12,17,22
Z-extrapolation-2	1,8,7,9,10,11,14,15,16,19,25	5,13,17,18,22
Z-extrapolation-3	2,3,4,5,6,7,12,13,17,18,22	9,11,14,15,25
Z-extrapolation-4	2,3,4,5,6,7,12,13,17,18,22	10,15,16,19,25

4.4.2 Results of point reconstruction using extrapolation

Extrapolation results were obtained by reconstructing the four different sets of test points using the corresponding control points as shown in Table 4.6. The error is calculated as the difference between the known three-dimensional coordinates, as measured by the Australis system (see Section 3.3.2), and the reconstructed coordinates of each test point.

The mean absolute errors of the X-, Y-, and Z coordinates were calculated for extrapolation in the X-, Y- and Z directions for each stereo-pair to allow analysis of the effect of the separation angle on accuracy (see Figure 4.7). The resultant for each extrapolation direction was found as shown in equations 12 and 13 in Section 4.2.2.

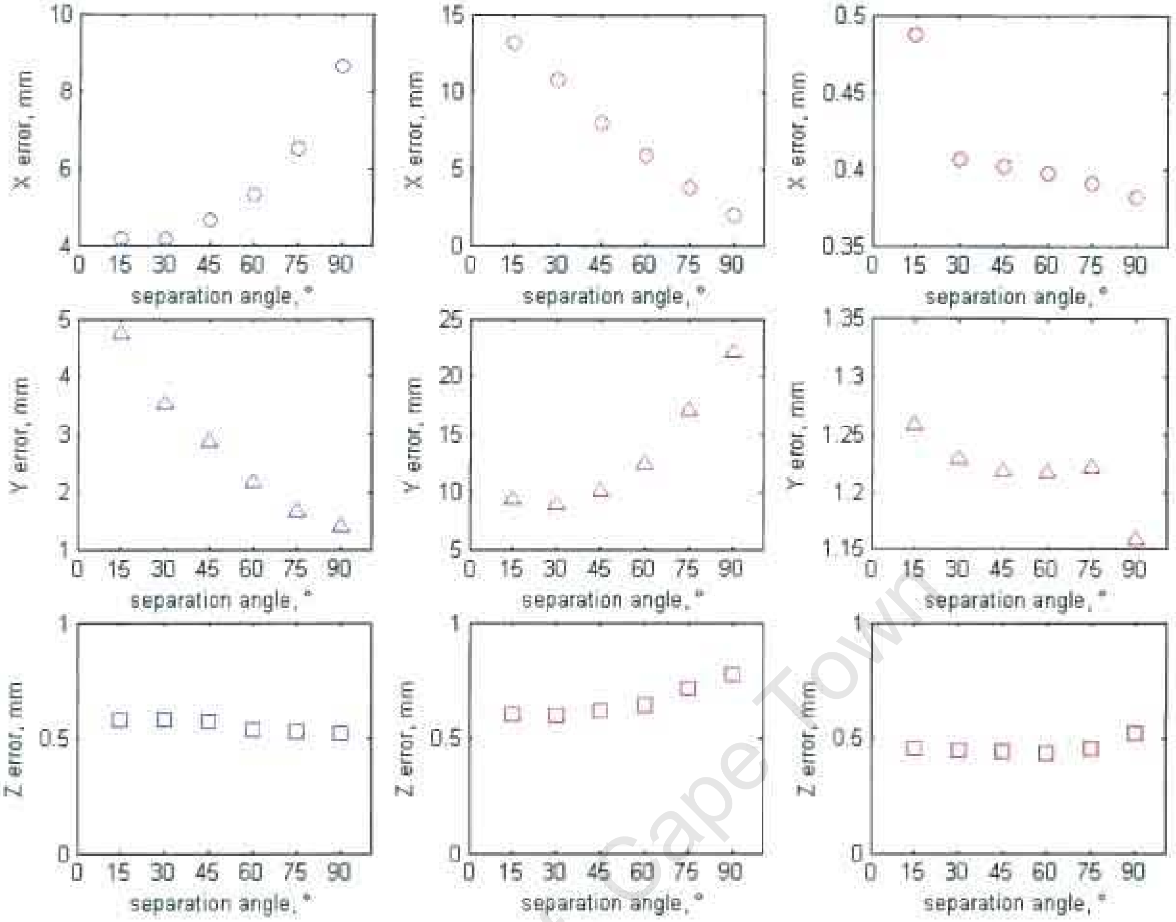

(a) (b) (c)

Figure 4.7 The mean absolute errors for the reconstruction of X (o), Y (Δ) and Z (□) coordinates of five test points when extrapolating in the (a) X, (b) Y, and (c) Z directions.

When extrapolating in the X-direction, the largest error was found at a 90° separation angle in the X coordinate and when extrapolating in the Y direction, the largest error was found at a 90° separation angle in the Y coordinate. It is also shown that the X-error increases with increasing separation angle when extrapolating in the X-direction and the Y-error increases with increasing separation angle when extrapolating in the Y-direction.

As expected, the Z-direction extrapolation yielded decreasing X and Y errors as the separation angle increased. This is the same as when there is no extrapolation. The magnitudes of the X and Y errors are also similar to those shown in the reconstruction of test points (see in Figure 4.4).

The Z-error is fairly constant and below 1 mm across all separation angles for all directions of extrapolation.

The resultant errors when extrapolating in the X, Y and Z directions are given in Figure 4.8.

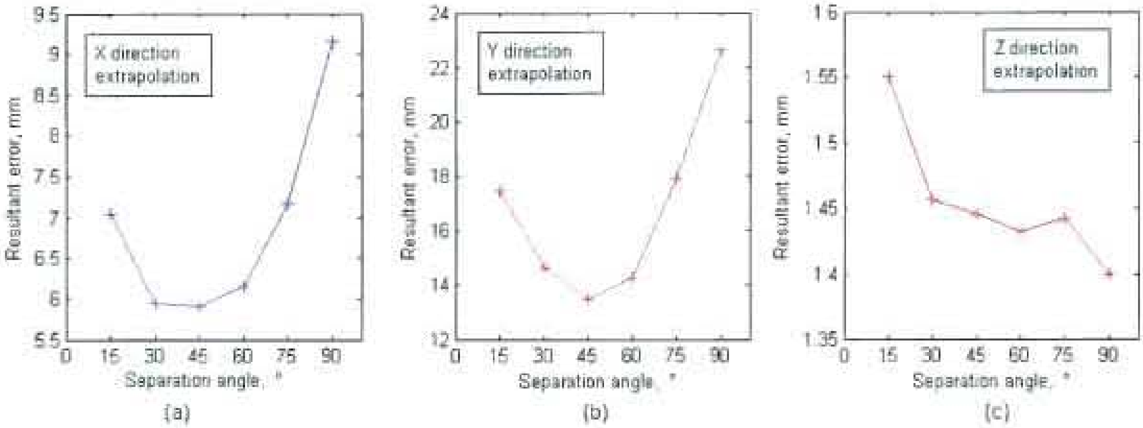

Figure 4.8 The resultant errors for the reconstruction of five test points when using extrapolation in the (a) X-, (b) Y- and (c) Z directions.

The results of a more detailed assessment of the effect of control marker configurations on the marker reconstruction accuracy when using extrapolation are included in Appendix E.

Like the effect of scanning angle on test point reconstruction (see Figure 4.6), the effect of the scanning angle on extrapolation results was assessed. To study this effect, the mean absolute X, Y and Z errors for reconstruction of the five test points were plotted using X-, Y- and Z-direction extrapolation (configuration 1 in each case) with six different stereo-images, each pair with a separation angle of 15° (see Figure 4.9). When extrapolating in the X-direction, the X and Y errors tended to increase with increasing scanning angles, whereas when extrapolating in the Y-direction, the X and Y errors were at a maximum at the 15°-30° scanning angles. The Z-extrapolation errors were fairly constant across the scanning angles.

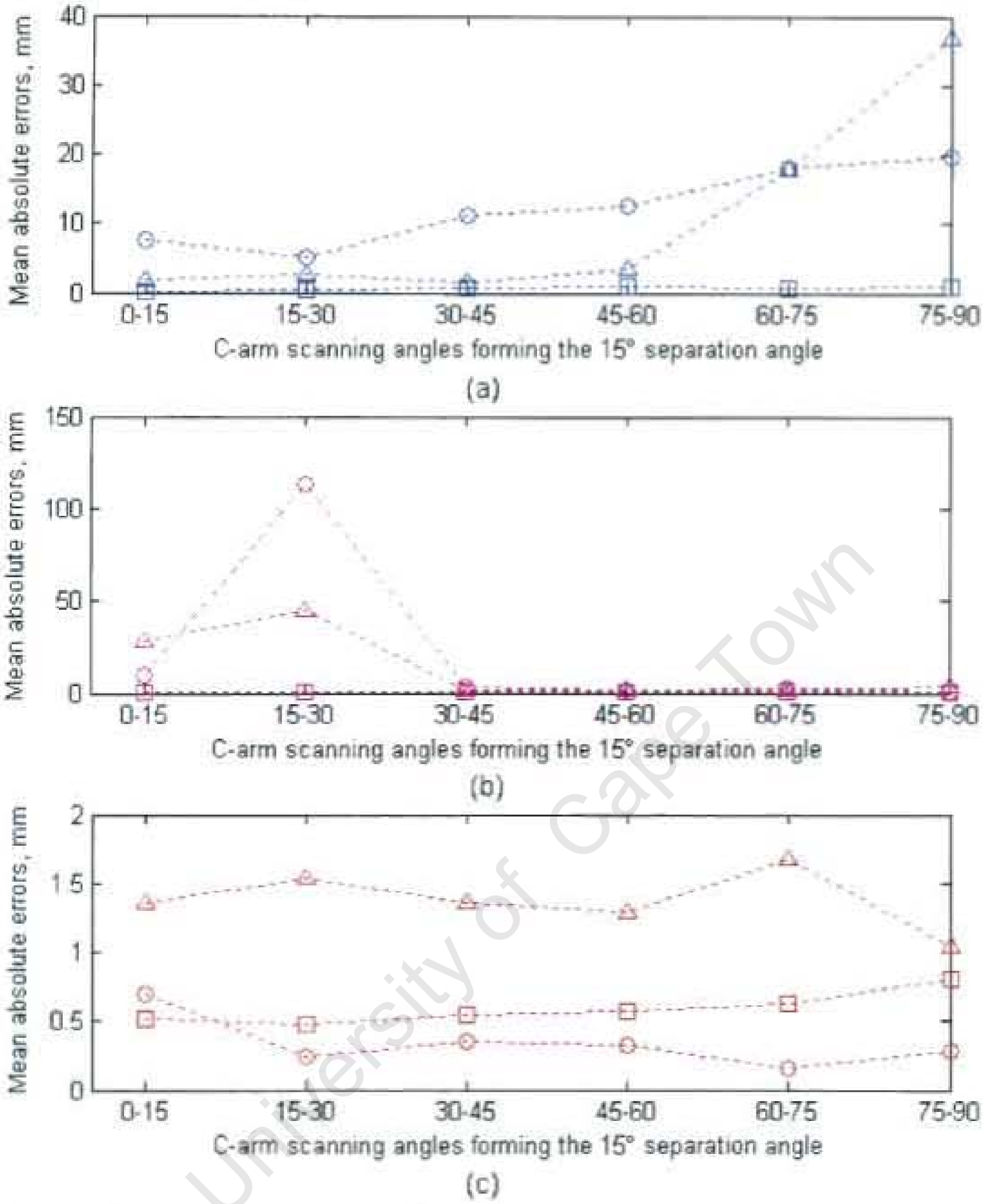

Figure 4.9 An illustration of the effect of C-arm scanning angles that form the separation angle of 15° on the X (o),Y (Δ) and Z (□) mean absolute errors when extrapolating in the (a) X- (b) Y- and (c) Z-directions

To summarise, the errors observed when reconstructing test points using extrapolation were much larger than when the test points are well-distributed around the control space. It was also shown that the extrapolation errors depended on separation angle, scanning angle and the configuration of control and test points.

4.5 Reconstruction of phantom points using interpolation

The purpose of this experiment is to assess the use of Statscan using interpolation (i.e. reconstruction of unknown points that lie within the volume delimited by the control points). A phantom with measured object marker positions (see Section 3.4.2) was imaged within the calibration frame (see Figure 4.10) using different source-detector assembly scanning angles with respect to the scanned object in intervals of 15° from 0° to 90° (Image-set B).

Figure 4.10 The phantom within the calibration frame on the patient table of the Statscan machine, Groote Schuur Hospital.

As in previous experiments, the X-ray images taken at seven different scanning angles (0°, 15°, 30°, 45°, 60°, 75°, 90°) were paired to form 21 combinations at six different separation angles. An example of a stereo-pair of Statscan images taken at scanning angles of 0° and 45° (45° separation angle) is given in Figure 4.11.

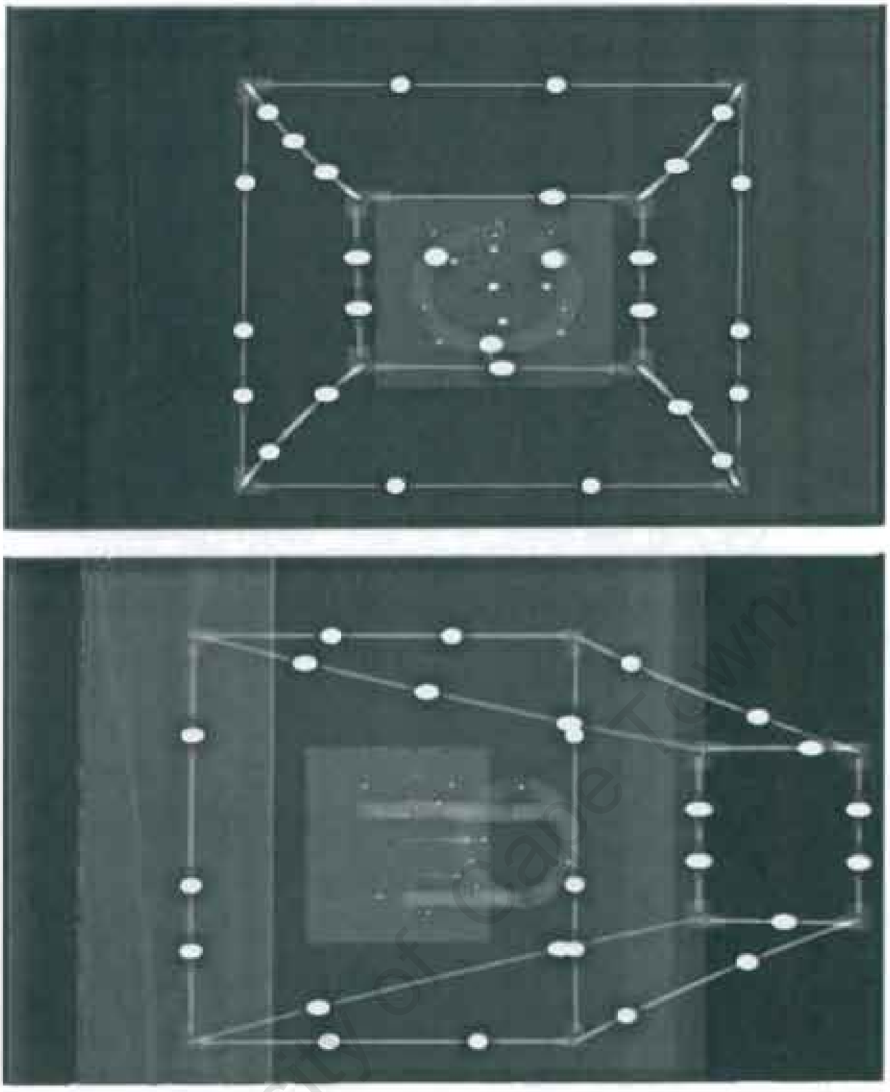

Figure 4.11 A pair of Statscan images where the phantom was radiographed within the calibration frame at 0° and 45° respectively.

The Matlab routines were used to identify the two-dimensional (x, y) coordinates of the calibration markers (see Section 3.4.1) and phantom markers (see Section 3.4.2) on each image. The manual correction of calibration frame markers for image-set B (see Table 4.1) applies here. Regarding the phantom markers, at certain C-arm angles it was difficult to be absolutely sure whether the marker label was identified correctly and also whether the centre was identified correctly by the Matlab program. In cases where the marker label identification was sure but the marker was overlapped by other markers or Perspex columns, the marker position was manually corrected (see Table 4.7). In cases where there was confusion of marker label identification or where the marker was completely occluded by some object (e.g. Perspex column), the marker was excluded. This study did not establish an identification routine for occluded markers, such as that presented by Kaptein *et al.*, 2005.

Table 4.7 The manually corrected and excluded phantom markers

C-Arm Angle	Corrected Phantom Markers	Excluded Phantom Markers
0°	10, 11, 12, 13	8
15°	7	6
30°	12, 13	3
45°	3	-
60°	-	8, 9
75°	10	-
90°	11, 12	1, 3, 4, 5

4.5.1 Description of the control point sets for phantom marker interpolation

Five phantom markers were chosen for the reconstruction based on ease of marker identification on the X-ray images (see Tables 4.7 and 4.8). The control point sets were the same 16, 11 and 7 control point sets as used in the reconstruction of test points using calibration frame markers (see Table 4.5 in Section 4.3).

Table 4.8 Marker sets used to assess the transformation for interpolation with a phantom

Control point configuration	Markers used as control points	Phantom test points
16	1,3,4,5,6,8,9,11,12,13,14,15,17,19,22,25	2,7,10,11,12
	1,2,4,5,7,9,10,11,13,14,16,17,18,19,22,25	2,7,10,11,12
	1,2,3,4,5,6,8,10,11,12,14,15,17,18,19,25	2,7,10,11,12
	1,2,3,4,5,7,9,11,12,13,14,16,17,18,19,22	2,7,10,11,12
11	1,3,4,6,9,12,13,14,15,22,25	2,7,10,11,12
	1,2,5,7,11,14,16,17,19,22,25	2,7,10,11,12
	2,4,6,8,10,14,15,17,18,19,25	2,7,10,11,12
	3,5,7,9,11,12,13,14,16,19,22	2,7,10,11,12
7	1,6,9,12,14,22,25	2,7,10,11,12
	1,5,7,11,16,22,25	2,7,10,11,12
	2,6,10,14,17,19,25	2,7,10,11,12
	3,5,7,12,16,19,22	2,7,10,11,12

4.5.2 Results of phantom marker interpolation

In order to compare the reconstructed marker positions with the measured positions, phantom marker number 2 was redefined as the origin in both the calibration frame and phantom coordinate systems (see Figure B.1 in Appendix B for the phantom axes definition). The errors were then taken as the difference between the measured phantom coordinates and the calculated coordinates using the origin (phantom marker 2) as the reference point. This comparison method can be likened to that of Adams and Constant (1988) where a comparison of measured and calculated distances was used find the accuracy of the reconstruction of bony landmarks of lumbar vertebrae. The resultant error was calculated as shown by equations 12 and 13 in Section 4.2.2.

The above approach provides information on how well the phantom points are reconstructed relative to another phantom point.

The results (see Figure 4.12) show that the resultant mean absolute errors decreased with increasing separation angles and this was true for all control point sets used. The lowest resultant error was found when the lowest number of control points were used (7 control points). The greatest resultant error was found when 11 control points were used.

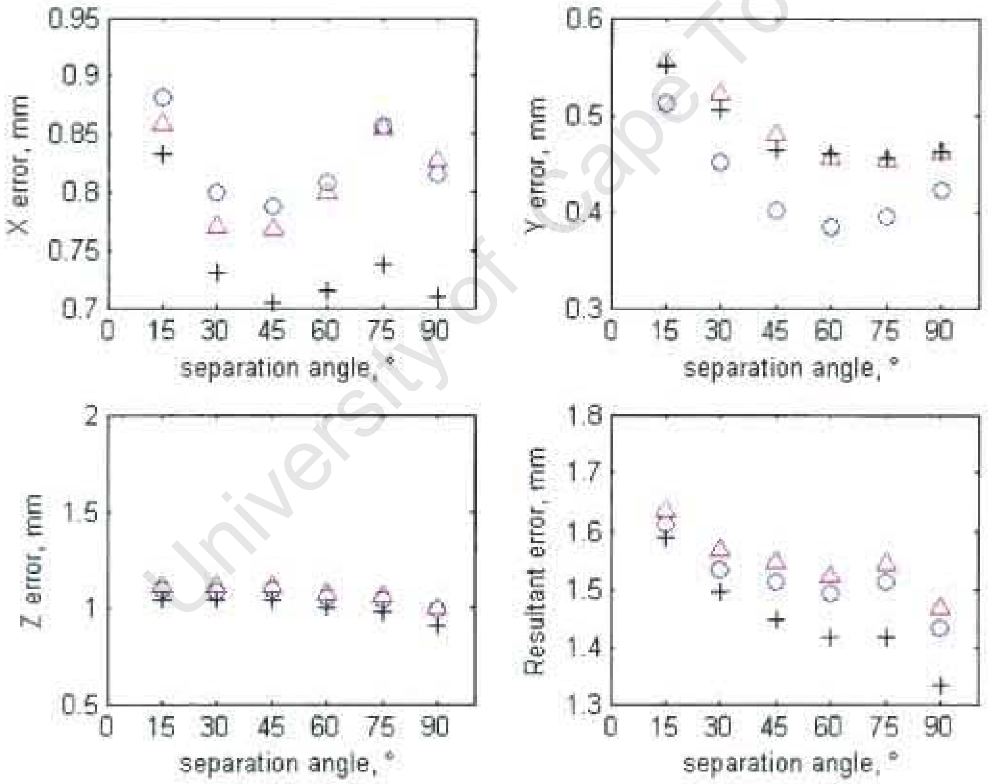

Figure 4.12 X-, Y-, Z- and resultant absolute mean errors for the reconstruction of five phantom points using different control point sets 16 (o); 11 (Δ); 7 (+) control points.

Although the resultant error showed an increase in accuracy (i.e. decrease in error) with increasing separation angles, the X-error showed an increase in error between 60° and 75° and then the error decreased again at the 90° separation angle. The Y-error showed a slight increase in error at 75° and 90° separation angles when 16 control points were used, however this increase in Y-error was not as pronounced when using 11 and 7 control points.

Another noteworthy observation is that the lowest X-, Z- and resultant errors were found when using 7 control points, however the lowest Y-error was found when using 16 control points.

While the mean absolute errors for the Z coordinates were higher than those seen in previous experiments, the error was constant across all separation angles and control point configurations. The three-dimensional reconstruction of five phantom points within the calibration frame is shown graphically in Figure 4.13.

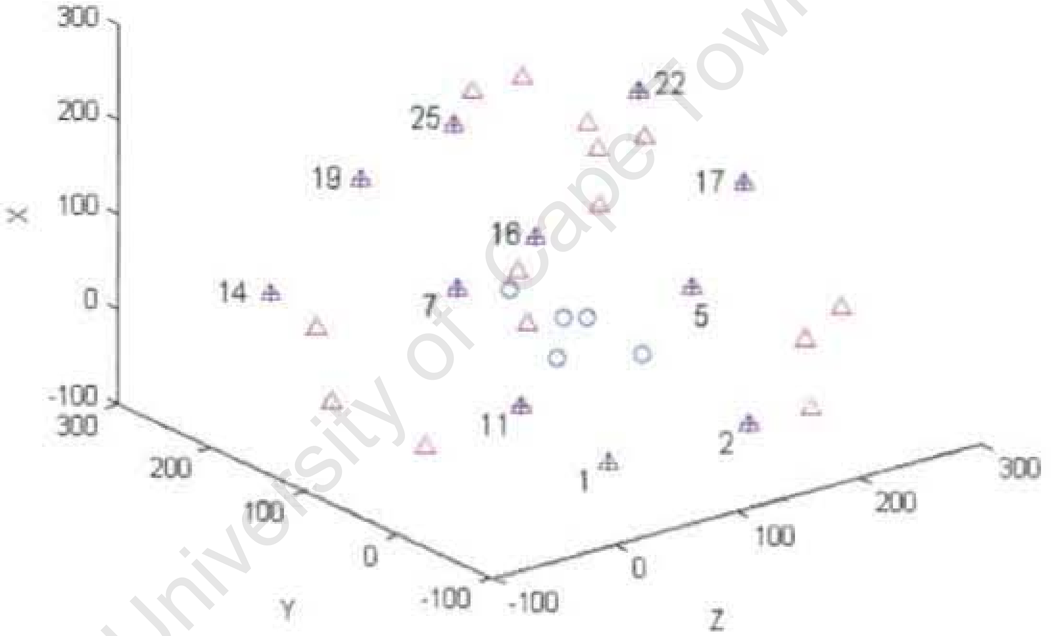

Figure 4.13 A three-dimensional plot of the 25 frame marker measured positions (Δ), 11 labelled control points (+) and the 5 interpolated points (o) within the calibration frame space.

To summarise, resultant mean absolute errors of between 1.33 mm and 1.64mm were observed when reconstructing unknown points using interpolation (points lie within the control point space). The errors were shown to depend on separation angle and number of control points.

Chapter 5 : Discussion

The results obtained from the experiments presented in Chapter 4 highlight differences in the three-dimensional reconstruction of discrete points when the reconstruction is performed under various conditions such as varying separation angles and numbers of control points. Point reconstruction errors when using interpolation and extrapolation marker configurations have also been established.

In this chapter, these results are compared with those of previous stereophotogrammetry studies where projective transformation techniques such as the DLT method were used. Some Roentgen Stereophotogrammetric Analysis (RSA) results are used for comparison where relevant. In addition, the results are compared to those of previous Statscan point localisation experiments (Douglas *et al.*, 2004).

While many of the findings agreed with the literature results, several noteworthy differences were observed. The differences between the results of this study and those in the literature are discussed in detail in this chapter and possible reasons for the differences are examined.

The material used in this study differs from that used in the literature and these differences may account for differences in results. The set-up of equipment used in this study is therefore compared to that of the literature to assess the impact the differences could have on reconstruction errors (see Section 5.1).

In addition, the effect of different calibration configurations on reconstruction accuracy has been compared to that described for previous studies. Despite the fact that the marker configurations and separation angles differ from those used in the literature, the comparison is useful since trends in reconstruction accuracy can be identified (see Section 5.2).

5.1 Equipment as a Possible Source of Error

5.1.1 The Calibration Frame

This section analyses the calibration frame as a possible source of reconstruction error.

While sturdy, the calibration frame was not completely rigid. If a force was applied to the frame, it tended to bend slightly before returning to its original shape. Any errors that may have been introduced through slight altering of the control frame were considered negligible. The maximum standard deviations for the measured marker coordinates were 0.10 mm, 0.12 mm and 0.06 mm, respectively in the X-, Y-, and Z-directions (Section 3.3.2) and this is in line with the measurement accuracies of previous studies e.g. 0.5 mm accuracy for measurement with a Theodolite, Chen *et al.* (1994).

The markers on the calibration frame were 10 mm in diameter, which is large in comparison to those used in other X-ray stereophotogrammetry studies (0.7 mm in the André *et al.* (1994) study; 1 mm in the Plamondon and Gagnon (1991) study and 3 mm in the Choo and Oxland (2003) study). However, in a conventional stereo-photogrammetry study, 3.18 cm markers were used (Chen *et al.*, 1994) and in a conventional cinematography study, 3 cm spherical markers were used (Hinrichs and McLean, 1995). The large markers could have introduced measurement errors, although the comparisons shown in this study are relative and thus the overall results of trends should not be affected.

As in the study of Chen *et al.* (1993), a limitation of this study was that the calibration frame markers were fixed. The marker positions could not be altered once they were glued in place, even when it was found that several calibration frame markers overlapped one another in the images. It would have been prudent to perform a test with the frame before the markers were finally glued into position.

In such cases where the calibration markers overlapped on the X-ray images, the marker centres were estimated manually using the Matlab pixel value and zoom functions. This is expected to have a minor impact on errors since the manual marker identification standard deviation was found to be 0.08 mm and 0.07 mm for x and y image coordinates respectively compared to 0.09 mm and 0.02 mm for x and y image coordinates respectively for marker correction using the Matlab program. Where markers could not be identified on the stereo images, these markers were completely excluded from the experiments.

Although the calibration frame was designed to avoid object truncation, (see Section 3.3.1) insufficient margin was included in the design geometry to take changes in patient table set-up into account. This lead to marker truncation in image-set B. Despite this, sufficient remaining calibration frame markers were available to perform the required experiments.

5.1.2 The Digital Imaging System

While the sources of error inherent to the process of Statscan digital X-ray image generation were not studied in detail, possible sources of error are mentioned based on observations when using the X-ray scanner.

The Statscan X-ray imaging system is different to those used in other studies because it is a fully digital system while many of the studies reviewed in the literature were based on film or digitised X-ray film.

The geometry of the Statscan machine is also different to the X-ray machines used in the literature. The Statscan machine has been designed for clinical use and therefore has a movable patient table. This table, which can be raised and lowered, had to be raised for the duration of the image pair acquisition so that the C-arm could be rotated. However, the table does not have a height measurement and so it was not possible to be confident that the experiments performed with image-set A and B were performed under exactly the same conditions.

The fact that it was not possible to position the calibration frame within the X-ray beam for all scanning angles in image-set B demonstrates that there were some set-up differences. This led to the exclusion of four markers (20, 21, 24 and 25) that could otherwise have been used in the study. Since these markers were unavailable, the experiments could not make use of the same control point sets as were used in the previous Statscan stereophotogrammetry study of Douglas *et al.* (2004).

The table and calibration frame positions were not altered in any way between X-ray scans to ensure that they remain as a rigid unit, otherwise, the transformation parameters would be invalidated (Adams, 1981). Therefore, no errors were introduced in this way.

The accuracy of the C-arm angle measurement is not known but errors in the scanning angle would not affect the trends reported. On the other hand, if it was necessary to calibrate the system prior to using the system for patient studies i.e. radiograph the patient without the calibration frame (Adams and Constant, 1988), the fact that the C-arm may not return to exactly the same point each time would probably lead to significant reconstruction errors.

The accuracy of the scanning start and end point settings is also not known. The start and finish positions should be the same for each image so that the image y-coordinates are not significantly offset from one image to another. The Z-coordinate was determined by taking the average from both stereo-images so the offset should not significantly affect the reconstructed Z-coordinate accuracy.

The limitation of the Statscan machine is that the C-arm has a limited 90° rotation. This limited the angles that were used in the experiments.

5.2 The effect of calibration variables on reconstruction accuracy

5.2.1 The reproducibility of two-dimensional marker identification

The identification of marker centroids plays an important role in the three-dimensional reconstruction of discrete points (Adams and Constant, 1988); therefore the reproducibility of marker identification was evaluated. The literature presents two main ways of assessing marker identification accuracy by either the comparison of the two-dimensional coordinates obtained by different methods (Wang *et al.*, 1996; Ostgaard *et al.*, 1997), or the comparison of reconstructed three-dimensional coordinates that were found using two-dimensional image coordinates obtained by different methods (Ostgaard *et al.*, 1997; Douglas *et al.*, 2004). As in Ostgaard *et al.* (1997), both of these methods were used in this study.

In the present study, the mean standard deviations for the eighteen sets of two dimensional coordinates (nine selections on each 0° and 90° image) using the marker centroid correction program were approximately 0.09 mm and 0.02 mm for x and y image coordinates respectively (estimating 0.2 mm per pixel). These errors are significantly larger than the errors reported in the literature, 0.007 mm to 0.008 mm (Ostgaard *et al.*, 1997) and 0.013 mm to 0.057 mm (Wang *et al.*, 1996). This can be attributed to the fact that the markers used in this study (10mm) were more than a factor of 10 bigger than those used in the referenced studies, 0.8 mm (Ostgaard *et al.*, 1997) and 1 mm (Wang *et al.*, 1996). It may be possible to identify a marker centroid on a smaller marker to greater accuracy. The fact that the error is greater in the image x direction could be attributed to the marker elongation in the x-direction, so there is a greater chance that the centre in the x-direction could be poorly identified.

While the reproducibility of the two-dimensional marker centroid identification is relatively low in this study, the marker centroid correction program results are comparable to the standard deviation for typical manual marker centre identification, 0.05 mm (Wang *et al.*, 1996). In addition, the results obtained for manual marker selection of the same markers (0.08 mm and 0.07 mm standard deviation for image coordinates x and y respectively, estimating 0.2 mm per pixel) are also similar in magnitude to the results reported by Wang *et al.* (1996).

The mean standard deviations for the reconstruction of the nine sets of 15 manually identified markers were 0.05 mm, 0.07 mm and 0.05 mm for X, Y and Z-coordinates respectively. When using the marker correction program, there was only a slight reduction in error (0.07 mm, 0.06 mm and 0.02 mm for X, Y and Z-coordinates respectively). The results were similar to those found by Douglas *et al.* (2004), where standard deviations of 0.14 mm, 0.06 mm and 0.05 mm were reported for the X, Y and Z directions respectively.

The three-dimensional reconstruction reproducibility was significantly lower than that found by Ostgaard *et al.* (1997) in an RSA study, where standard deviations of 0.005 mm to 0.006 mm were obtained. However the results were within the region of magnitude found by Gussekloo *et al.* (2000) where 0.12 mm standard deviation was obtained in each direction. In addition, the results are comparable to the reproducibility of the automated RSA procedure by Vrooman *et al.* (1998), where translation errors between 0.03 mm and 0.11 mm were reported.

Differences in two-dimensional marker coordinates between this and other studies could also be due to differences in image resolution.

While a lower error in locating the two-dimensional marker centroids is desirable since it reduces the magnitude of the reconstruction errors, it will not change the relative effects of the mathematical algorithm and marker distribution (Choo and Oxland, 2003). Therefore, the relative effects of separation angles and control point configurations on reconstruction accuracy can still be compared.

5.2.2 The effect of separation angle and scanning angle on reconstruction accuracy

The results from the reconstruction of control points (image-sets A and B), test points (image-set B) and independent phantom points found by interpolation (image-set B) showed that the resultant mean absolute errors decrease with increasing separation angles irrespective of the number of control points used (see Figures 4.2, 4.3, 4.4 and 4.12). This result agrees with previous stereophotogrammetry studies (Wood and Marshall, 1986; Adams and Constant, 1988; Plamondon and Gagnon, 1991; Douglas *et al.*, 2004).

The improvement in accuracy with an increase in separation angle can be attributed to the fact that more information is available about the object space when the stereo-pair is taken at large separation angles. Adams and Constant (1988) pointed out that small misidentifications on the two dimensional images will result in significant differences when small separation angles are used, but that these errors would be minimum in biplanar radiography, where a 90° separation angle is used. This explains why the biplane radiography method is popular in X-ray stereophotogrammetry.

Comparing the results with those from Douglas *et al.* (2004) where a similar study was performed with Statscan using different control point sets we notice that for control and test point reconstruction the maximum X and Y errors are found when using a 15° separation angle. In contrast, the results from the reconstruction of test points using extrapolation did not demonstrate an increase in accuracy that corresponds to an increase in separation angle. This will be discussed in Section 5.2.4.

In the reconstruction of control points, the mean absolute Z-error was fairly constant across all the separation angles: in the region of 0.5 mm for image-set A and 0.4 mm for image-set B. In the reconstruction of test points, the mean absolute Z-error was also found to be constant across all separation angles in the region of 0.5 mm. This can be attributed to the fact that the Z coordinate was found by the linear mapping of the image y coordinate. The results agree with those of Douglas *et al.* (2004), where the mean absolute error in the Z direction was constant between 0.4 mm and 0.5 mm, depending on the number of control points used.

The slight upward trend in mean absolute Z-error with increasing separation angle could be attributed to possible marker centre identification errors present in some markers that were used in the reconstruction. This is supported by the results in Figure 4.5 where the test point reconstruction was performed for four different marker configurations of 16 control points each. The graph shows an increase in Z-error in configurations 1 and 2, whereas the Z-error is fairly constant in the other two reconstructions.

The results from the different configurations cannot be compared to the different configurations of Challis and Kerwin (1992), since the calibration frame used in the present study has a different shape, and the markers are not arranged symmetrically.

The effect of the scanning angle orientation on test point reconstruction accuracy was assessed using a constant separation angle of 15°, as was used by Plamondon and Gagnon (1991). A significant difference in the Y-direction was found with large errors found at larger scanning angles. This can be explained by the fact that the calibration frame was not symmetrical and therefore despite the constant separation angle used, the information available for the generation of transformation parameters was different at different scanning angles. These results agree with Plamondon and Gagnon (1991), who observed similar significant differences (0.12 mm mean compared to 0.04 mm mean) in the x-direction (equivalent to our Y-direction) when a higher film angle (equivalent to our scanning angle) was used.

5.2.3 The effect of the number of control points on reconstruction accuracy

The results from the reconstruction of control points (image-sets A and B) show that the mean absolute error is highest when high numbers of control points are used (21 points) and the accuracy increases with decreasing numbers of control points. The lowest mean absolute errors were seen in the reconstruction of 7 control points. This result agrees with the findings of Challis and Kerwin (1992), Hinrichs and McLean (1995) and Douglas *et al.*, (2004). While the magnitude of the reconstruction errors are shown to be much lower than those of Hinrichs and McLean (1995), the results are comparable to the mean errors of Adams and Constant (1988) for the reconstruction of 21 control points (0.3 mm, 0.3 mm, 0.9 mm in the X, Y and Z directions respectively).

Like in the Statscan study, in the cinematography study of Hinrichs and McLean (1995), with a 90° separation angle, the highest accuracy was seen in the reconstruction of the lowest number of control points (16 control points in this case) and errors in reconstructing control points increased as numbers of control points were increased (16 to 60 control points).

In contrast, when the test points were reconstructed, the mean absolute error was highest when the smallest number of control points (7 control points) were reconstructed (see Figure 4.4). This is in agreement with the results of Challis and Kerwin (1992), Wood and Marshal (1986) and Hinrichs and McLean (1995). In a study for minimally invasive hepatic surgery, Stefansic *et al.* (2000) also observed high non-control marker localisation errors when the lowest number of control points (6 and 7) were used and this was attributed to the mathematical instability of the DLT when only a few points are available. This could explain some of the non-linearity in the Statscan Y- errors when reconstructing test points where there is a much greater error between using 7 control points and 11 control points compared to the errors between 11 and 16 control points (see Figure 4.4).

The phenomenon of high accuracy when reconstructing a few control points using the DLT can be explained by the "over-fitting" of the equations to the few control points, known as over-parameterisation (Hinrichs and McLean, 1995; Challis and Kerwin, 1992). It is clear that over-parameterisation occurred in this study since the reconstruction errors were high when non-control points (test points) were reconstructed using the same transformation parameters. The reconstruction of a few control points can therefore not be taken as a reflection of the true reconstruction accuracy for unknown point reconstruction.

To permit a direct comparison with the results of the DLT study by Hinrichs and McLean (1995), the relationship between control point and non-control (test) point reconstruction errors was plotted using various numbers of control points at a separation angle of 90° (see Figure 5.1).

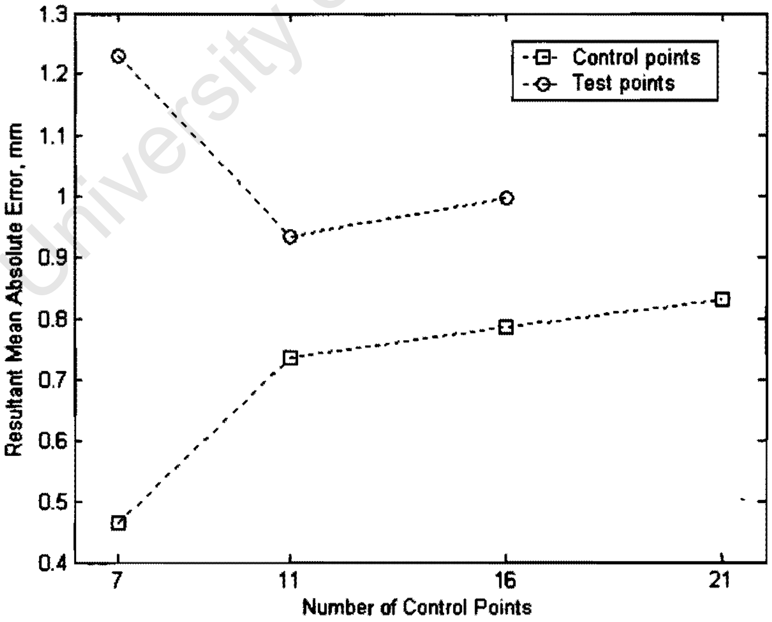

Figure 5.1 A graph of the resultant mean absolute errors for the reconstruction of control points (□, experiment 4.2) and test points (o, experiment 4.3) versus the number of control points used while using a 90° separation angle and image-set B in each case.

The trend is comparable to that of the DLT study by Hinrichs and McLean (1995) shown in Figure 5.2 even though the numbers of control points (7-21 compared to 16-60) and magnitudes of reconstruction errors (mm compared to cm) differ between the two studies.

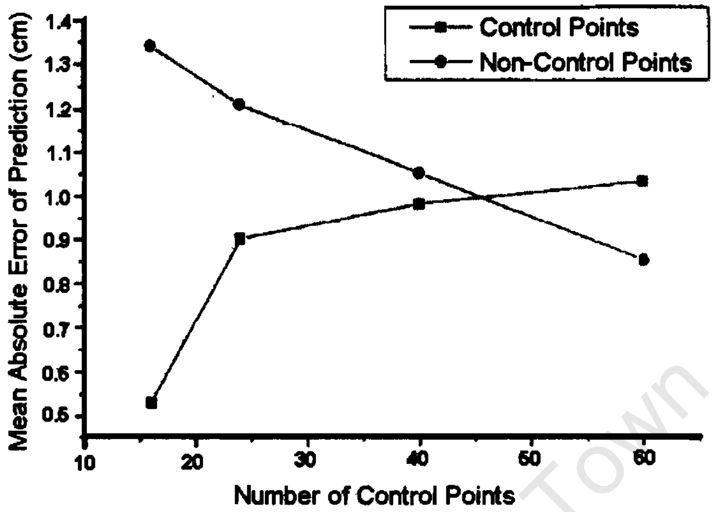

Figure 5.2 A plot of the results of a previous DLT study showing mean absolute errors for control points and non-control test points using various numbers of control points (Hinrichs and McLean, 1995)

The comparison shown in Figure 5.1 can also be compared to the DLT results of Stefansic *et al.* (2000) where similar curves were observed. Where control points were reconstructed, the median control point error was low (0.15 mm – 0.3 mm) when using a few control points for the transformation (6 – 8 control points). As control points were increased to 14, the error increased on a very gradual slope from 0.3 to 0.35 mm. This can be likened to the reconstruction error plateau observed in Figure 5.1 at approximately 0.75 mm between 11 and 21 control points.

Based on the over-parameterisation explanation and observations when using 7 control points, we expected the non-control (test) point reconstruction errors to decrease as the number of control points increased. However in this study, the 11 control point configuration yielded the most accurate results (lowest resultant mean absolute error) instead of the 16 control point configuration.

The results of Figure 4.4 for the reconstruction of test points show how the reconstruction X-errors for 11 and 16 points are very similar. In some cases, 16 control points yield the best accuracy whereas in other cases and in the Y-direction, 11 control points yield the best accuracy. The difference between resultant mean absolute errors for 16 control points and 11 control points when reconstructing test points is less than 0.1 mm, which may be within the random error region, thereby explaining the highest accuracy observed when using 11 control points.

An improvement of test point reconstruction accuracy with the use of an increased number of control points is also explained by Chen *et al.*, 1994 as being due to the likelihood of a more even distribution when an increased number of control points are used. The configuration of the control points could therefore also have an effect on the accuracy. This is illustrated in Figure 4.5 where different errors were observed when different configurations of the same number of control points (16 control points) are used to reconstruct the five different test points across different separation angles. One can clearly see the difference in error that is purely as a result of configuration. Chen *et al.* (1994) states that it is generally accepted that it is more important to have well-distributed control points than just to increase the number of control points. While every effort was made to ensure even distribution of control points in the experiments, the inherent uneven arrangement of control points on the calibration frame may have introduced errors.

In addition, the higher error that is seen when a minimum number of control points are used to reconstruct test points can be explained since the transformation parameters are more vulnerable to the individual random error of the control points (Chen *et al.*, 1994).

Chen *et al.* (1994) reported an increase in DLT accuracy as the number of control points increased from 8 to 16, but found that the accuracy did not continue to increase when numbers of control points exceeded 16. The results of Hinrichs and McLean (1995) dispute this since their results showed a continued increase in accuracy beyond 16 points to the maximum number available (60 control points). The reason given was that while Hinrichs and McLean (1995) reconstructed the same test points for each DLT assessment, Chen *et al.* (1994) did not.

Although the same test points were reconstructed for each of the 16, 11 and 7 control points, the present study did not include as many control points as Hinrichs and McLean (1995), where as many as 60 control points were available. It was therefore not possible to establish whether there would be a continued improvement in test point accuracy if more than 16 control points were used, as demonstrated by Hinrichs and McLean (1995), or whether the accuracy would reach a plateau if more than 16 control points were used.

5.2.4 The reconstruction accuracy when extrapolating

As expected, the errors resulting from discrete point reconstruction using extrapolation in the X and Y directions were found to be significantly larger than those for the reconstruction of well-distributed test points on the calibration frame. This is in line with the finding by Wood and Marshall (1986) and Hinrichs and McLean (1995) that unknown points should lie within the volume defined by the control points for optimum DLT reconstruction.

The highest errors were found when extrapolating in the Y-direction, where the X-error was highest at a 15° separation angle (13 mm), and the Y-error was highest at a 90° separation angle (22 mm). It was expected that the Y-error should be the greatest since the least spatial information is available in the direction of extrapolation. The same phenomenon was found when extrapolating in the X-direction, where the X-error was the greatest of the three coordinate errors (9 mm at 90° separation angle).

When examining the reconstruction of each individual control point configuration, it was shown that the error tended to be greatest when the test points were furthest away from the control point volume (see Figures E.2 and E.3 in Appendix E). This result agrees with that of Hinrichs and McLean (1995) and Choo and Oxland (2003), where the accuracies of different levels of extrapolation (distances from the control points) were assessed. Hinrichs and McLean (1995) found that at maximum extrapolation (expressed as 300%), the errors had increased nearly ten-fold compared to the 0% condition (6.01 cm compared to 0.61 cm). While Choo and Oxland (2003) found that accuracies were better if an initial DLT calibration was done followed by calibration frame removal compared to extrapolation accuracies. In addition, Wood and Marshal (1986) found that the errors were between 50% and 100% greater than reconstruction errors when using well-distributed control points.

On further examination of the reconstruction of each individual configuration, it was also observed that the extrapolation configuration played an important role in reconstruction accuracy. This is best illustrated by the mean absolute errors when extrapolating in the X-direction (see Figure E.1 in Appendix E). The errors for configuration 1, where the control points were grouped at the bottom of the frame and the test points were grouped at the top, were considerably larger than those for configuration 3, where the control points were grouped on the top of the frame and the test points were at the bottom (see Figures E.1 and E.2 in Appendix E). This could in part be due to the distance of the test points from the control points (they were further apart in configuration 1), but this could also be due to more information being available in the X-direction when using configuration 3.

The results of the extrapolation study are different to those of Douglas *et al.* (2004), and this is attributed to the fact that, while similar, the control and test configurations are not the same. Douglas *et al.* (2004) showed that the resultant X-direction extrapolation error first decreased from 48 mm to below 5 mm through separation angles of 15° to 60° and then increased to above 5 mm at a 90° separation angle. The present study results also showed an initial decrease in X-extrapolation resultant error followed by an increase (see Figure 4.8), however the error magnitudes differ somewhat (7 mm to 6 mm through separation angles of 15° to 45° followed by an increase to 9 mm at a 90° separation angle). The difference in error magnitudes has been shown to depend on control and test marker configuration; therefore it is assumed that this is the reason for the differences between the present study results and those of Douglas *et al.* (2004).

In the present study, the resultant mean absolute errors for Y-direction extrapolation were shown to first decrease from 18 mm to 13 mm through separation angles 15° to 45°, and then increase to a maximum at 23 mm at a 90° separation angle. In contrast, Douglas *et al.* (2004) found that the resultant Y- error decreased consistently from 14 mm to 6 mm as separation angles were increased from 15° to 90°.

These Y-direction extrapolation results can be further compared to those of the Wood and Marshall study (1986). Taking X-ray source and image orientations into account, we can equate the Statscan X, Y and Z coordinate system to the Wood and Marshall (1986) Z-, X-, and Y coordinates and so using the Statscan coordinate system we can say that the Wood and Marshal (1986) extrapolation was in the equivalent Y direction. It was found that the highest extrapolation reconstruction errors were also found in the Y direction, supporting the results of the present study. In addition, Wood and Marshal (1986) showed that the Y-errors were higher with increasing separation angles (13.1 mm with a 45° separation angle, 13.5 mm with a 90° separation angle). The mean resultant errors were also found to be higher when the larger separation angles were used.

The results from Y-direction extrapolation also showed an unexpected increase in Z-error with increasing separation angle. This was unexpected since the Z-error was merely a linear mapping of the y-image coordinate. The error is attributed to the cumulative effect of relatively poor two dimensional coordinate localisation in markers that were furthest away from the detector banks, as well as slight image distortion. This can be justified since the set of control points chosen in Y-direction extrapolation were either very close to the detector bank or far away from the detector bank. The resulting relatively poor two dimensional coordinate localisation of control points could have resulted in poor reconstruction of the test point Z-coordinate when large separation angles (which use laterally scanned images) were used. To reinforce this theory, we plotted the Z- mean absolute errors from Y-direction extrapolation when reconstructing five test points using 11 control points (configuration 1) and a 15° separation angle The Z-errors are plotted against the six pairs of scanning angles that were used to obtain the stereo-images (0° and 15°, 15° and 30°, 30° and 45°, 45° and 60°, 60° and 75°, 75° and 90°).

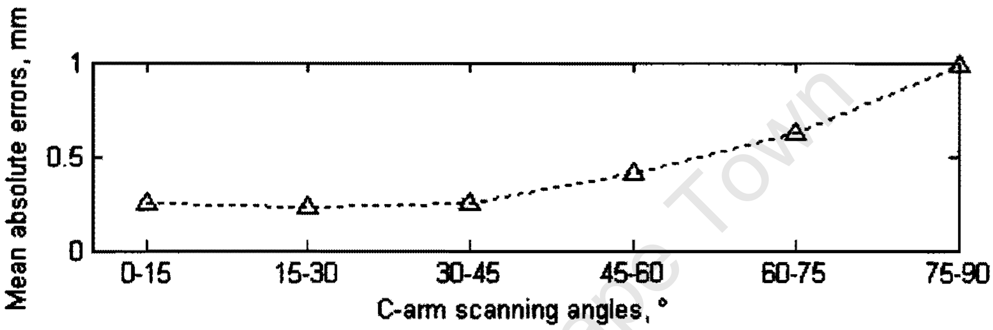

Figure 5.3 A plot of the mean absolute Z-errors from the reconstruction of five test points when extrapolating in the Y-direction using 11 control points (configuration 1) and a separation angle of 15° versus the pairs of C-arm scanning angles.

Figure 5.3 shows that the Y-extrapolation Z-error increased as the C-arm was turned into the more lateral scanning position, hence the control point sets would have been far away from the detector bank and thus elongated, which would have resulted in reduced two-dimensional marker identification. In addition, any slight image distortions, sometimes seen as the apparent bowing of the control frame struts on the images, would have added to the increased error when scanning in the more lateral positions (scanning angles between 45° and 90°). This slight image distortion was not assessed in full in this study.

The results for the resultant mean absolute errors for Z direction extrapolation agree with those of Douglas *et al.* (2004), where both studies showed a decrease in this error with increasing separation angles. In addition, both studies resulted in much lower errors when extrapolating in the Z direction compared to the X- and Y directions. The magnitudes of the Z-extrapolation errors are also comparable, e.g. the maximum resultant Z-extrapolation error in this study was 1.55 mm while the same error found by Douglas *et al.* (2004) was approximately 1.8 mm. This relatively good reconstruction in the Z-direction can be attributed to the linear mapping between the Z-axis image and frame coordinate systems.

From the comparison of mean absolute errors for the six different sets of stereo-images that each had a separation angle of 15° (Scanning angles of 0° and 15°, 15° and 30°, 30° and 45°, 45° and 60°, 60° and 75°, 75° and 90°) it was clear that not only did the separation angle play a role in determining reconstruction error, but the angles at which the two images were radiographed (scanning angle) also made a difference. The highest error when extrapolating in the X-direction was found in the Y-coordinate when the scanning angles of the stereo-pair were 75° and 90°. The highest error when extrapolating in the Y-direction was found in the X-coordinate when the scanning angles of the stereo-pair were 15° and 30°.

It is suggested that the accuracy depends on the scanning angle because the calibration frame is unsymmetrical, resulting in different reconstruction information available at different scanning angles. This dependence on scanning angle was also observed when reconstructing test points that lie on the outer limits of the volume of interest.

5.2.5 The reconstruction accuracy when interpolating

While the reconstruction of test points that lie on the limits of the volume of interest is often used as a measure of reconstruction accuracy in the literature, the reconstruction of completely independent points that lie within the volume of interest can be considered to be the final test of the reconstruction technique. Indeed, the reconstruction of independent object points using Statscan was the final objective of this study.

The minimum mean absolute coordinate errors for the reconstruction of five phantom points were 0.7 mm in the X-direction, 0.3 mm in the Y-direction and approximately 1 mm in the Z-direction, which is comparable to the findings of Adams and Constant (1988), in an interpolation study of lumbar vertebrae (average difference of distances between the measured and calculated coordinates was ± 0.8 mm). In their study, the vertebrae were radiographed within the calibration frame, just as the phantom is radiographed inside the Statscan calibration frame and so the points to be reconstructed were independent of the control frame.

As expected, the resultant mean absolute errors decreased with increased separation angles, and this was valid for all control point sets used (see Figure 4.12). However, the X-error and Y-errors increased slightly (about 0.05 mm) between 60° - 75°, and 75° - 90° separation angles respectively. This increase in error may be explained by the position of the phantom within the frame and the proximity to control points, since this increase in error was not observed when the same control points were used in the reconstruction of test points that were on the calibration frame (see Figure 4.4).

The mean absolute Z-error was constant across the separation angles (approximately 1 mm). Although the magnitude of the error was greater than that found in control and test point reconstruction, the consistent error across the separation angles was expected due to linear mapping of the image y coordinates to Statscan Z coordinates. If the Z-error could be reduced the resultant error would be reduced since the X and Y errors ranged between 0.7 – 0.9 mm and 0.38 – 0.55 mm respectively.

In the interpolation of phantom points, it can be said that the separation angle used to obtain the images is of more importance than the number of control points used and the best results would be achieved by using a large separation angle.

5.3 Applications for the use of Statscan Stereophotogrammetry

This section covers the suitability of the use of Statscan stereophotogrammetry for different medical applications by comparing the set-up and errors of this study to those found in the literature (see Section 2.6).

In some previous X-ray stereophotogrammetric studies, initial calibration of the volume of interest was done before the patient or object was radiographed so that the calibration frame did not impede patient set-up (van Geems *et al.*, 1995; Choo and Oxland, 2003). This approach was not assessed in this study, however it is postulated that to eliminate additional sources of error, the calibration of the volume of interest should be done simultaneously with patient or object radiography. This is because the C-arm positioning accuracy is not known. It is possible that the C-arm would not return to exactly the same starting positions and scanning angles, so there is a possibility that the transformation parameters would be invalidated by moving and then repositioning the C-arm. Using the calibration frame in the present study, only a small volume of interest could be radiographed e.g. ankle joint. In cases where larger volumes of interest need to be radiographed, a larger calibration frame will have to be constructed.

As with many literature studies, the greatest reconstruction errors were found when using extrapolation. It is therefore advised that this method be avoided unless very large errors in the region of 25 mm mean absolute errors are acceptable.

The resultant mean accuracy of locating unknown points using interpolation was found to be between 1.33 mm and 1.64 mm depending on the separation angle and number of control points used (see Figure 4.12). This error is above the acceptable limit for applications such as measuring the sub-millimetre micro-motion of orthopaedic implants such as the movements between prosthetic stems and the femur after total hip replacements (Djerf *et al.*, 1987; Kiss *et al.*, 1996; Önsten *et al.*, 1995; Alfaro-Adrian *et al.*, 1999) and the micromotion of knee joint prostheses (Ryd *et al.*, 1986; Kärrholm *et al.*, 1989). Typically, the maximum implant motion that results in stable long term fixation is between 0.15 mm and 0.2 mm (Nilsson and Kärrholm, 1996). To measure such distances the analysis method would require higher accuracy than that achieved in the present study. The literature has shown that the Roentgen Stereophotogrammetric Analysis (RSA) method is more suited to the assessment of micromotion (Valstar *et al.*, 2002).

Three-dimensional point reconstruction is often utilised in spine studies and the modelling of the human spine. X-ray stereophotogrammetry has also been used to evaluate the effectiveness of scoliosis treatment (André *et al.*, 1994; Aubin *et al.*, 1997). Andre *et al.* (1994) used the DLT algorithm for the three-dimensional reconstruction of the human spine and reported mean errors between 0.6 mm and 1.5 mm for the reconstruction of steel markers. The maximum error found when using the smallest separation angle was 4.5 mm. Where vertebral landmarks were used in the literature, errors as high as 5 mm were common due to the difficulty in identifying the points on the X-ray images (Andre *et al.*, 1994). Vertebral landmark reconstruction methods presented in the literature report varying errors; 0.7 mm (2D/3D method by Benameur *et al*, 2003); 1.4 mm for the NSCP method (Mitton *et al.*, 2000); 2.4 mm for the DLT (Mitulescu *et al.*, 2001) and 2.6 mm for the DLT (Aubin *et al.*, 1997).

The results presented in this study fall within the range of accuracies reported in the literature and therefore Statscan may be suitable for spinal stereophotogrammetric studies. However, it must be taken into consideration that scoliosis studies generally require the patient be in an upright position while radiographed and this would not be possible with the current Statscan machine set-up. Statscan stereophotogrammetry would be suitable for applications where the patient is required to be in the supine position.

Post-implant evaluation in brachytherapy is necessary to determine the error in placement of the implanted radioactive source and the dose impact to the target volume; such evaluation is ideally done using three-dimensional studies (Martel and Narayana, 1998). Source placement errors reported by Martel and Narayana (1988) were in the range of 0.2 mm - 5 mm. Other interstitial brachytherapy studies reported errors ranging from 1 mm to 5 mm for three dimensional source localisation using X-ray images (Li *et al.*, 1996; Cai *et al.*, 1997; Bice *et al.*, 1999). The results presented in the present study fall within the acceptable range for interstitial brachytherapy; therefore Statscan stereophotogrammetry may be suitable for post-implantation assessments.

In the field of cephalometry, the use of projective transformations and X-ray images to obtain three dimensional measurements of the cranium has yielded errors greater than 1 mm. These errors are considered acceptable in this field (Kusnoto *et al.*, 1999); therefore Statscan stereophotogrammetry may be suitable for cephalometry.

A major advantage of the use of Statscan is the relative low ionising radiation dose received by the patient; a mean surface dose of 6.2 µSv, which is approximately 3% of the standard conventional X-ray dose (Beningfield *et al.*, 1999). Scoliosis patients often require a number of X-ray examinations during the course of treatment; therefore it is very important that the radiation dose is as low as reasonably achievable (Kalmar *et al.*, 1994). This is especially important for children, who are more vulnerable to the effects of ionising radiation (Morin Doody *et al.*, 2000).

Chapter 6 : Conclusions

The main objective of this study was to assess the feasibility of using the Statscan low dose digital X-ray scanner for the localisation of discrete points using X-ray stereophotogrammetry.

To find a suitable stereophotogrammetric technique, traditional and newly developed methods were explored. The most suitable method for the calibration of Statscan was established to be the scan projection radiography (surview) method where the X- and Y-coordinates were found using information from the image x coordinates and the Z-coordinates were determined by linear mapping of the image y coordinates. Using information gathered from previous studies, a calibration frame with radio-opaque markers was constructed specifically for use with Statscan. The three dimensional marker positions were measured using a line-of-sight photogrammetric technique and a marker location routine was written in Matlab to locate the marker centroids on the X-ray images.

Experiments were performed to establish the reconstruction errors and characteristics of the Statscan set-up using different numbers of control points and various X-ray scanning angles. In addition, reconstruction accuracies when using both extrapolation and interpolation were assessed.

The following conclusions are drawn from the discussion of the results (see Chapter 5):

- The Statscan low dose X-ray scanner can be used to locate points in three dimensions using stereophotogrammetric techniques.
- The reconstruction errors differ depending on the number of control points used, their configuration, as well as the separation angle and scanning angle used.
- The optimum configuration for performing stereophotogrammetry to locate unknown points was when using interpolation with a large separation angle.
- The reconstruction errors when using extrapolation can be very large and this configuration should be avoided.

- Suitable applications for Statscan stereophotogrammetry depend on the required accuracy. The method is suitable for applications where errors above 1 mm and below 2 mm can be tolerated, such as cephalometry, brachytherapy planning and assessment of the spine.

By using the results of this study it may be possible to optimise the two-dimensional marker identification, calibration frame design and control marker configuration to obtain improved results using Statscan.

Chapter 7 : Recommendations

The reconstruction accuracy is greatly affected by the calibration of Statscan images, which could be optimised by an improvement in the calibration frame design. To avoid marker truncation, future Statscan calibration frames should not be as tall as the frame constructed for this study.

It is not necessary to round-off the two-dimensional marker coordinates to the nearest pixel value as was done in this study. Some noise may have been introduced by doing this, which could have affected the accuracy. This should be avoided in future studies. The identification of the marker centre could be optimised by using shape analysis of the markers rather than simple centroids to improve accuracy and robustness.

The designers of future calibration frames should also attempt to reduce or eliminate the overlapping markers when images are taken at different scanning angles. This is especially relevant when the frame is scanned laterally.

It is recommended that future studies establish how sensitive the results are to noise by perturbing the position of a marker and recording how the reconstructed position changes.

In cases where it would not be possible to radiograph the volume of interest within the calibration frame, it is necessary to calibrate the system prior to the patient study. In order to do this, it is recommended that the system be validated for the possible error source due to the C-arm not returning exactly to the same scanning position between calibration and patient study. It is recommended that future studies establish the influence of performing the calibration prior to the patient study.

It is recommended that the influence of patient movement between taking the two X-ray images is studied together with possible ways of compensating for patient movement.

In the application of scoliosis assessments and cephalometry, it may be useful to mount conventional cameras on the C-arm and to use conventional photogrammetry in conjunction with X-ray stereophotogrammetry so that surface as well as internal anatomy information can be obtained.

Appendix A: Measured Calibration Frame Marker Coordinates

Table A.1 The 3D coordinates of the 25 calibration frame markers as measured using the Australis Software (Geomatics Department, Melbourne University)

Marker number	X (mm)	Y (mm)	Z (mm)
1	54.9675	-21.9954	-68.7051
2	170.3936	-22.0499	-68.6406
3	220.3433	-21.9954	-68.7051
4	290.9364	75.1468	-67.8372
5	290.5157	197.3222	-66.8947
6	218.0902	289.1242	-67.4319
7	169.0128	289.1054	-68.2057
8	53.8497	289.3481	-68.9390
9	-21.5489	173.5313	-68.6066
10	-21.3486	75.0771	-68.6066
11	0	0	0
12	264.3730	4.1490	8.1095
13	270.2516	270.0469	-6.2904
14	-0.5260	267.4379	-2.8697
15	22.2243	22.4789	67.8178
16	46.4584	46.8392	141.0369
17	219.1059	47.9926	135.4750
18	228.8911	229.0072	113.8032
19	41.0746	225.0669	122.2146
20	112.9338	66.6352	200.4574
21	152.3277	67.3085	199.8355
22	198.8461	134.8890	201.0628
23	153.2557	199.9837	201.1605
24	112.5103	199.4511	201.1004
25	65.2881	157.5331	200.6699

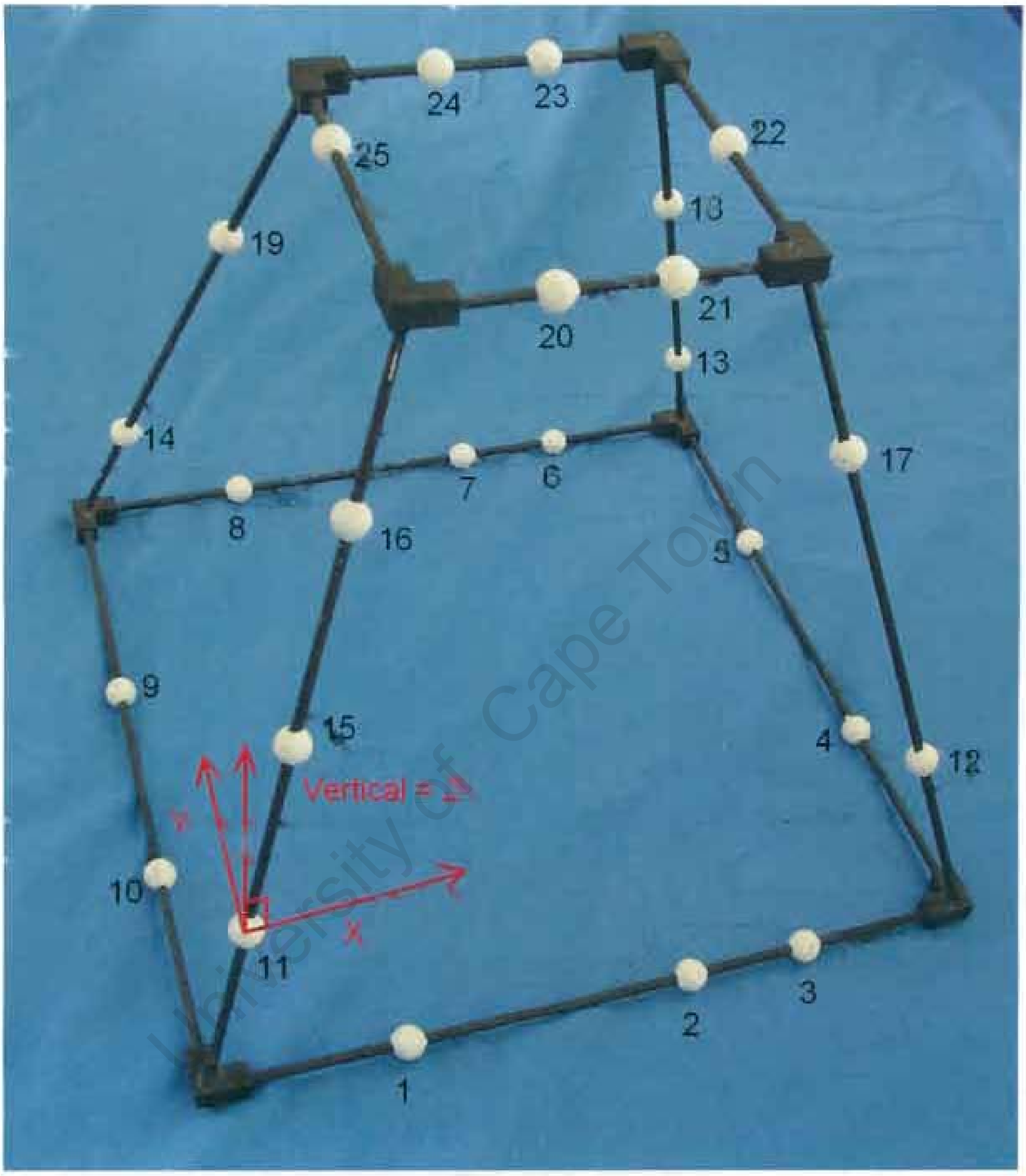

Figure A.1 Definition of the Axes for the Calibration Frame Marker Coordinates. Marker number 11 is the origin.

Appendix B: Measured Phantom Marker 3D Coordinates

Table B.1 The measured 3D coordinates of the 13 phantom frame markers.

Marker Number	X (mm)	Y (mm)	Z (mm)
1	-46.56	-20.24	-0.02
2	-6.6	36.6	0.02
3	33.26	-20.4	0.02
4	-43.41	39.24	-91.11
5	29.83	39.96	-92.43
6	-4.73	27.65	-66.06
7	-31.36	17.08	-68.92
8	-6.86	-2.48	-41.87
9	26.13	-2.52	-60.6
10	-0.85	-29.92	-56.29
11	-40.22	-45.76	-80.04
12	35.84	-38.72	-75.99
13	-10.43	-61.72	-74.7

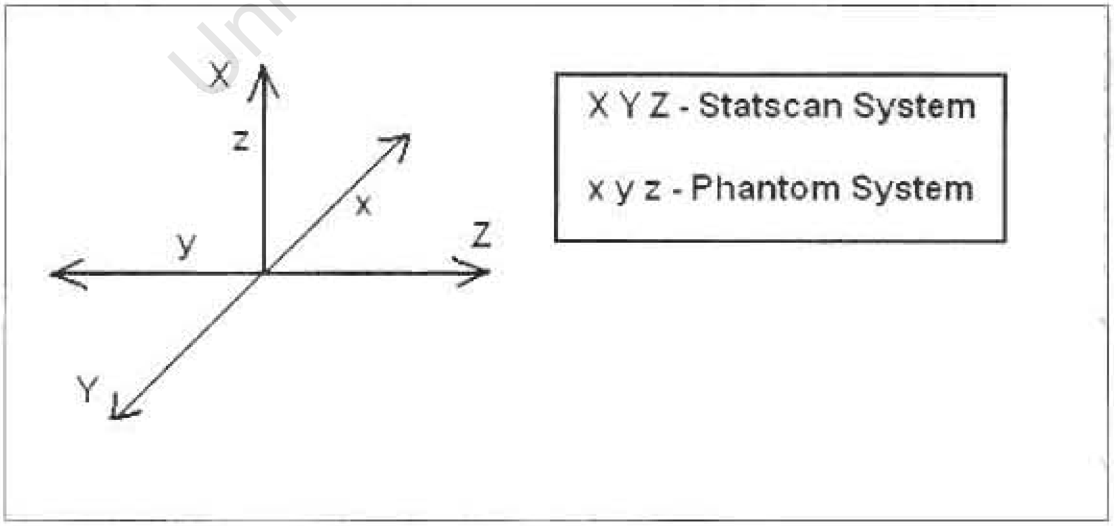

Figure B.1 A graphical illustration of the difference between the Statscan axes, and the phantom axes.

Appendix C: Matlab Software Code

This section provides an overview of the Matlab code used to perform the image processing and mathematical transformations for the three-dimensional reconstructions. The codes (m-files) will be stored on CD-ROM in the Department of Biomedical Engineering, University of Cape Town.

Three main codes were used in the experiments which were then modified to suit the specific experiments. Suffixes were added to the code names to identify the changes. First, the getmarks.m code is the marker correction program. The output of "getmarks.m" is used in the "Run.m" code, which calls "calcpoints.m" to perform the 3D reconstruction. The next code is "Evaluate.m", which uses the data saved by "Run.m" to plot the data.

Program to locate the marker centroids – "getmarks.m"

The input of this program is the X-ray image with markers, and the output is an array of the marker x and y coordinates. This code requires user input to select the markers in the correct sequence.

An X-ray image is read into the Matlab workspace and the user is then prompted to identify each marker by using the mouse and cursor. Each marker is labelled according to the user selection. A region of interest is then defined for each marker using the user defined points as a reference. The program identifies the centroid by using thresholding in the region of interest and the centroid coordinates are rounded off to the nearest pixel values.

The "getmarks_phantom.m" code differs from "getmarks.m" by using a smaller region of interest due to the smaller phantom markers compared to calibration markers. The program also uses a Matlab function to identify the centroid.

Program to define the control points and test points – "Run.m"

After gathering all the necessary 2D marker data from stereo-images, the 2D coordinates are then used in the Run.m code. This code first defines the known 3D marker coordinates and then loads the 2D stereo-image coordinates. Depending on the use, the lists (configurations) of control points and test points are defined here. This program uses a for-loop to perform the 3D reconstruction on the different X-ray stereo-pairs. The program calls another code, "calcpoints.m", which contains the algorithms to perform the 3D reconstruction. In turn, "calcpoints.m" uses programs called "make_A.m" and "BACKSUB.m" in the calculation. The outputs of "calcpoints.m" are the differences between the known 3D coordinates and the calculated 3D coordinates. These values are saved by "Run.m".

Program to organise and plot the results – "Evaluate.m"

This program loads the data files that were saved by "Run.m" and organises the results so that the data can be plotted as shown in Chapter 4. The program concatenates the results from like sets of data and calculates the mean absolute errors. The resultants and standard deviations are also performed here.

Appendix D: Experiment Data Tables

Table D.1 The standard deviations (SD) for nine sets of 2D calibration frame marker coordinates obtained using the marker correction program (0° scanning angle, image-set B).

Marker Number	SD x	SD y
1	0	0
2	0	0
3	0	0
6	0	0
7	0	0
8	0	0
12	0	0
13	0	0.5000
15	0.3333	0
16	0.7071	0
17	1.3333	0
18	1.1304	0.3333
19	0.7265	0
23	1.1667	0
24	0.8660	0.5000

Table D.2 Mean and maximum absolute errors of image-set A control point reconstruction using different separation angles and numbers of control points (CPS)

Separation Angle, °	Mean Absolute Error (mm)			Maximum Absolute Error (mm)		
	dX	dY	dZ	dX	dY	dZ
21 CPS						
15	0.5628	0.8272	0.5238	4.0515	5.4780	1.6227
30	0.4461	0.7610	0.5172	1.7254	3.2318	1.6267
45	0.4301	0.7364	0.5233	1.1124	2.0876	1.6284
60	0.4320	0.7432	0.5334	1.1396	1.8288	1.7268
75	0.3987	0.7472	0.5542	0.9909	1.7464	1.8529
90	0.3743	0.7257	0.5728	0.9066	1.5143	1.1837
16 CPS						
15	0.5009	0.7933	0.4964	3.4319	5.6041	1.7073
30	0.4290	0.7319	0.4910	1.4846	3.3969	1.7249
45	0.4185	0.7004	0.4956	1.1783	2.3023	1.7255
60	0.4280	0.7114	0.5068	1.3169	1.9631	1.8377
75	0.3971	0.7066	0.5300	1.1597	1.9921	1.9331
90	0.3834	0.7107	0.5604	0.8927	1.8129	1.2445
11 CPS						
15	0.4819	0.7451	0.5099	3.4930	5.2672	1.6101
30	0.3964	0.6657	0.5020	1.6329	3.2076	1.6004
45	0.3799	0.6368	0.5072	1.1878	1.9904	1.6128
60	0.3802	0.6391	0.5177	1.2297	1.7476	1.7021
75	0.3424	0.6344	0.5416	1.0386	1.8459	1.8609
90	0.3169	0.6359	0.5594	0.7699	1.3305	1.2714
7 CPS						
15	0.4225	0.4595	0.4576	3.3331	2.1536	1.4127
30	0.3894	0.3724	0.4464	2.0601	1.9498	1.4222
45	0.3630	0.3068	0.4481	1.6508	1.4394	1.4550
60	0.3289	0.2454	0.4642	1.3645	0.9912	1.5506
75	0.2637	0.1943	0.4931	0.9606	0.6151	1.6225
90	0.2476	0.2112	0.4895	0.6983	0.6435	1.2192

Table D.3 Mean and maximum absolute errors of image-set B control point reconstruction using different separation angles and numbers of control points (CPS)

Separation Angle, °	Mean Absolute Error (mm)			Maximum Absolute Error (mm)		
	dX	dY	dZ	dX	dY	dZ
21 CPS						
15	0.3211	0.6605	0.3976	1.6732	3.1704	1.2396
30	0.2405	0.6003	0.3953	1.0787	2.0299	1.2098
45	0.2417	0.5898	0.4027	1.0276	1.6710	1.2271
60	0.2347	0.5830	0.4025	0.6865	1.4713	0.9913
75	0.2364	0.5807	0.4207	0.7448	1.4408	1.0392
90	0.2371	0.5495	0.4413	0.5719	1.2294	0.9164
16 CPS						
15	0.3070	0.6286	0.3606	1.7175	3.3452	1.2505
30	0.2347	0.5901	0.3574	1.0993	2.3018	1.2128
45	0.2366	0.5738	0.3626	1.0728	1.9311	1.2143
60	0.2329	0.5670	0.3639	0.7831	1.7429	1.0062
75	0.2302	0.5639	0.3853	0.7657	1.6586	1.0495
90	0.2438	0.5405	0.4030	0.6177	1.4411	0.9484
11 CPS						
15	0.2774	0.5535	0.3918	1.5174	3.1212	1.2356
30	0.2139	0.5187	0.3889	0.8113	2.1611	1.1795
45	0.2098	0.5038	0.3913	0.7494	1.6059	1.1142
60	0.2043	0.4986	0.3896	0.6646	1.3923	0.9815
75	0.2013	0.4947	0.4071	0.7041	1.2831	0.9848
90	0.1982	0.4747	0.4238	0.5964	1.1001	0.8992
7 CPS						
15	0.2300	0.3031	0.3821	1.1924	3.4977	1.4355
30	0.1997	0.2618	0.3825	1.1413	2.0451	1.3525
45	0.1760	0.2311	0.3825	0.8435	1.3109	1.2629
60	0.1462	0.2040	0.3725	0.7561	0.9726	1.1767
75	0.1187	0.1770	0.3726	0.5505	0.5951	1.1376
90	0.0918	0.1485	0.3829	0.5387	0.5111	1.0117

Table D.4 Difference between the errors of image-set A and image-set B (Control Point Reconstruction) using different separation angles and numbers of control points (CPS)

Separation Angle, °	Difference between Image-set A and B Mean Absolute Error (mm)			Difference between Image-set A and B Maximum Absolute Error (mm)		
	dX	dY	dZ	dX	dY	dZ
21 CPS						
15	0.2417	0.1667	0.1262	2.3783	2.3076	0.3831
30	0.2056	0.1607	0.1219	0.6467	1.2019	0.4169
45	0.1884	0.1466	0.1206	0.0848	0.4166	0.4013
60	0.1973	0.1602	0.1309	0.4531	0.3575	0.7355
75	0.1623	0.1665	0.1335	0.2461	0.3056	0.8137
90	0.1372	0.1762	0.1315	0.3347	0.2849	0.2673
16 CPS						
15	0.1939	0.1647	0.1358	1.7144	2.2589	0.4568
30	0.1943	0.1418	0.1336	0.3853	1.0951	0.5121
45	0.1819	0.1266	0.133	0.1055	0.3712	0.5112
60	0.1951	0.1444	0.1429	0.5338	0.2202	0.8315
75	0.1669	0.1427	0.1447	0.394	0.3335	0.8836
90	0.1396	0.1702	0.1574	0.275	0.3718	0.2961
11 CPS						
15	0.2045	0.1916	0.1181	1.9756	2.146	0.3745
30	0.1825	0.147	0.1131	0.8216	1.0465	0.4209
45	0.1701	0.133	0.1159	0.4384	0.3845	0.4986
60	0.1759	0.1405	0.1281	0.5651	0.3553	0.7206
75	0.1411	0.1397	0.1345	0.3345	0.5628	0.8761
90	0.1187	0.1612	0.1356	0.1735	0.2304	0.3722
7 CPS						
15	0.1925	0.1564	0.0755	2.1407	-1.3441	-0.0228
30	0.1897	0.1106	0.0639	0.9188	-0.0953	0.0697
45	0.187	0.0757	0.0656	0.8073	0.1285	0.1921
60	0.1827	0.0414	0.0917	0.6084	0.0186	0.3739
75	0.145	0.0173	0.1205	0.4101	0.0200	0.4849
90	0.1558	0.0627	0.1066	0.1596	0.1324	0.2075

Table D.5 Mean and maximum absolute errors of image-set B test point reconstruction using different separation angles and numbers of control points (CPS)

Separation Angle, °	Mean Absolute Error (mm)			Maximum Absolute Error (mm)		
	dX	dY	dZ	dX	dY	dZ
16 CPS						
15	0.4498	0.8808	0.5090	2.2873	3.6556	1.3039
30	0.3386	0.7195	0.5087	1.4944	2.4529	1.2742
45	0.3339	0.6967	0.5145	1.4078	2.0991	1.2964
60	0.3173	0.6724	0.5098	0.9063	1.8995	1.0501
75	0.3132	0.6695	0.5255	0.8657	1.8985	1.1166
90	0.2979	0.6170	0.5563	0.6820	1.6548	0.9859
11 CPS						
15	0.4556	0.8365	0.5070	2.3979	3.4061	1.4830
30	0.3334	0.6477	0.5054	1.6688	2.1870	1.4527
45	0.3264	0.6177	0.5085	1.3550	2.0422	1.4565
60	0.3074	0.5875	0.4994	1.0442	1.7558	1.2056
75	0.3204	0.5757	0.5127	0.9742	1.7476	1.2468
90	0.2980	0.5393	0.5428	0.7376	1.4936	1.1003
7 CPS						
15	0.5134	1.0351	0.5332	2.6387	3.9607	1.7525
30	0.3952	0.9006	0.5299	1.7059	2.9861	1.6896
45	0.3665	0.8903	0.5351	1.2842	2.9700	1.7240
60	0.3344	0.8777	0.5268	1.0431	2.8676	1.3936
75	0.3239	0.8876	0.5470	0.9651	2.9422	1.4116
90	0.3366	0.8779	0.5914	0.6469	2.7687	1.2432

Appendix E: Additional Extrapolation Experiment Details

In order to gain more information about extrapolation, the mean absolute X-, Y-, Z- and resultant errors were plotted for each of the four control and test point configurations (defined in Table 4.6) in the three different extrapolation directions (see Figures E.1, E.4 and E.6).

When extrapolating in the X-direction, it was found that the errors were greatest when the test points were furthest away from the control point group such as in configuration X-extrapolation-1. Figures E.2 and E.3 show three-dimensional plots of reconstructed points for configurations 1 and 2 after extrapolation in the X-direction using a 15° separation angle. The large reconstruction errors are noticeable in test points 22 and 25, which are furthest away from the control points (Figure E.2).

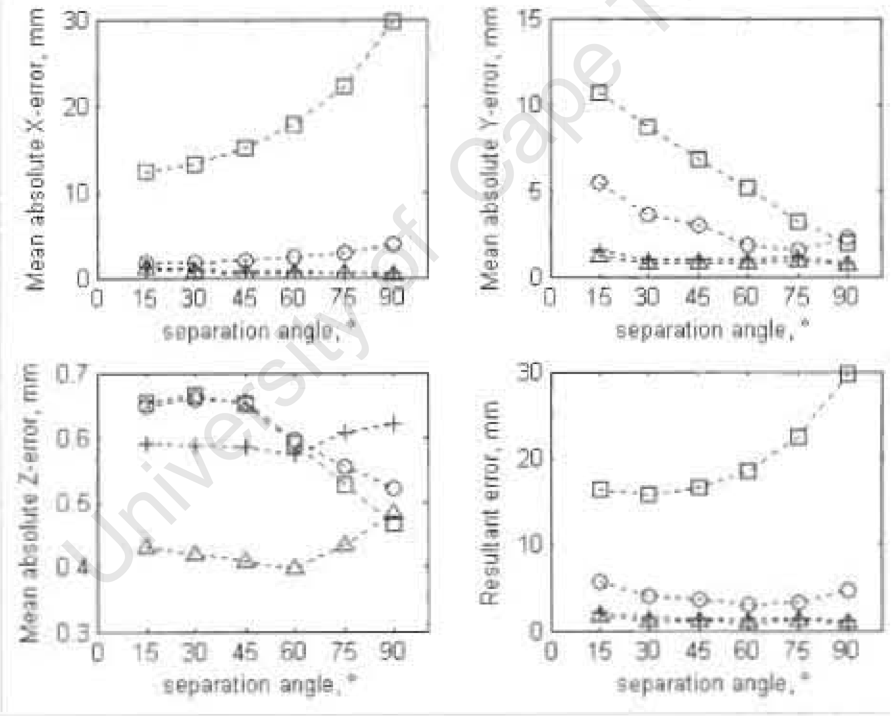

Figure E.1 The X-, Y-, Z- and resultant mean absolute errors for the reconstruction of five test points when extrapolating in the X direction. X-extrapolation-1 (□), X-extrapolation-2 (o), X-extrapolation-3 (Δ), X-extrapolation-4 (+).

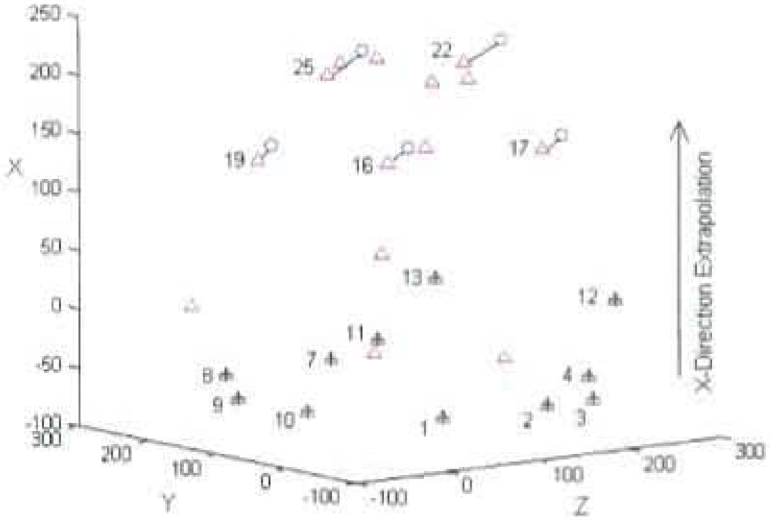

Figure E.2 A plot of the 25 points of the calibration frame (Δ), the 11 control points (+) and the 5 reconstructed test points (o) calculated by X-direction extrapolation (configuration-1) with a separation angle of 15° (images scanned at 75° and 90°). It is clear that the test points lie outside the control point group.

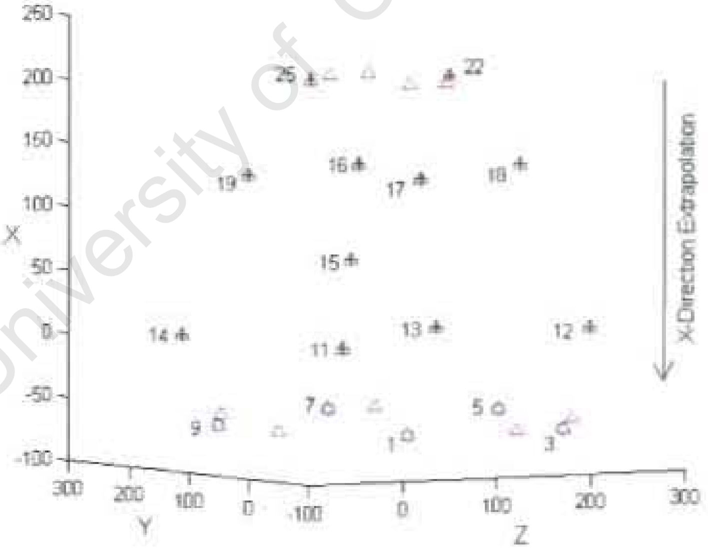

Figure E.3 A plot of the 25 points of the calibration frame (Δ), the 11 control points (+) and the 5 reconstructed test points (o) calculated by X-direction extrapolation (configuration-3) with a separation angle of 15° (images scanned at 75° and 90°).

When extrapolating in the Y-direction, it was found that the errors were greatest when the control points were in configurations Y-extrapolation-1 and Y-extrapolation-3 (see Figure E.4).

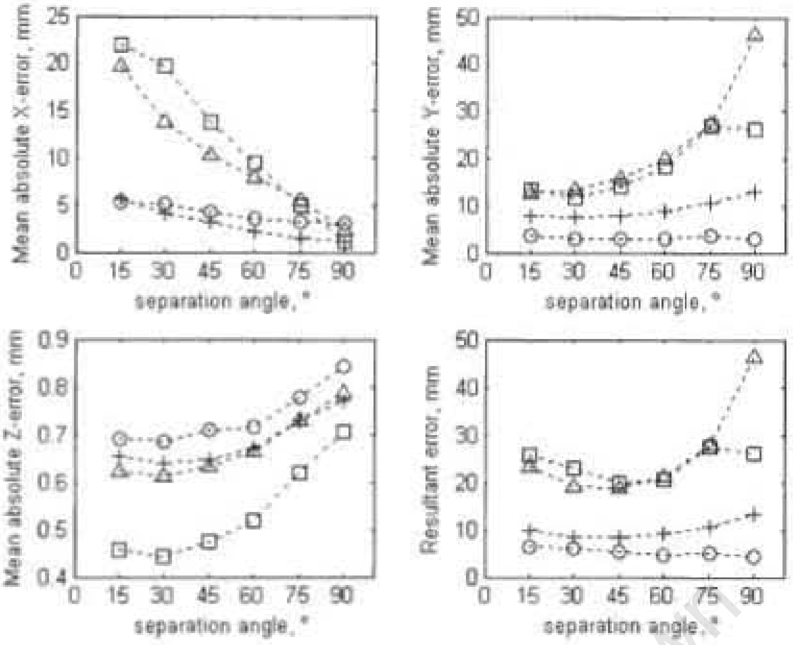

Figure E.4 The X-, Y-, Z- and resultant mean absolute errors for the reconstruction of five test points when extrapolating in the Y direction. Y-extrapolation-1 (□), Y-extrapolation-2 (o), Y-extrapolation-3 (Δ), Y-extrapolation-4 (+).

The results from Y-direction extrapolation also showed an increase in Z-error with increasing separation angle.

Figure E.5 shows an example of reconstruction using Y- extrapolation. Once again it is clear that test points 1 and 3, which are furthest away from the control points, yielded the greatest errors.

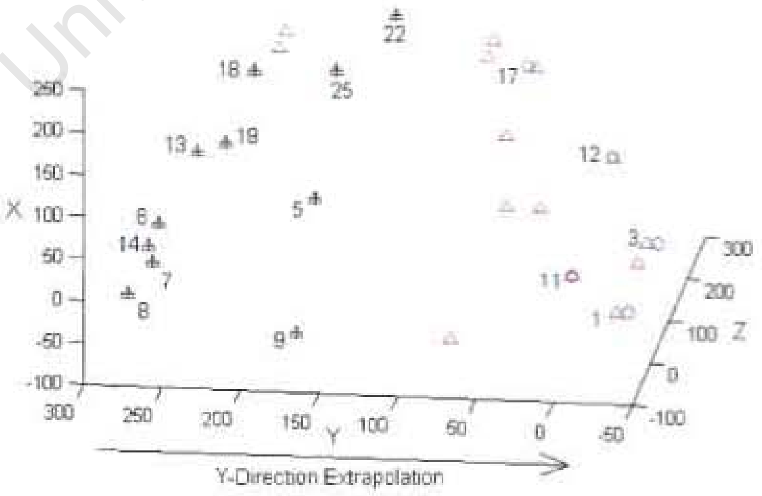

Figure E.5 A plot of the 25 points of the calibration frame (Δ), the 11 control points (+) and the 5 reconstructed test points (o) calculated by Y-direction extrapolation (configuration-1) with a separation angle of 15° (images scanned at 75° and 90°).

As with the extrapolation in the X and Y directions, the Z-direction extrapolation accuracy is shown to depend on the control and test point configuration (see Figure E.6). For the majority of configurations chosen, the X and Y mean absolute errors decrease with increasing separation angle and this can be attributed to there being more information available for the generation of these coordinates when the separation angle is large.

Figure E.7 shows an example of reconstruction using Z- extrapolation. The reconstruction is much more accurate than that of X and Y direction extrapolation and is similar to reconstruction without extrapolation.

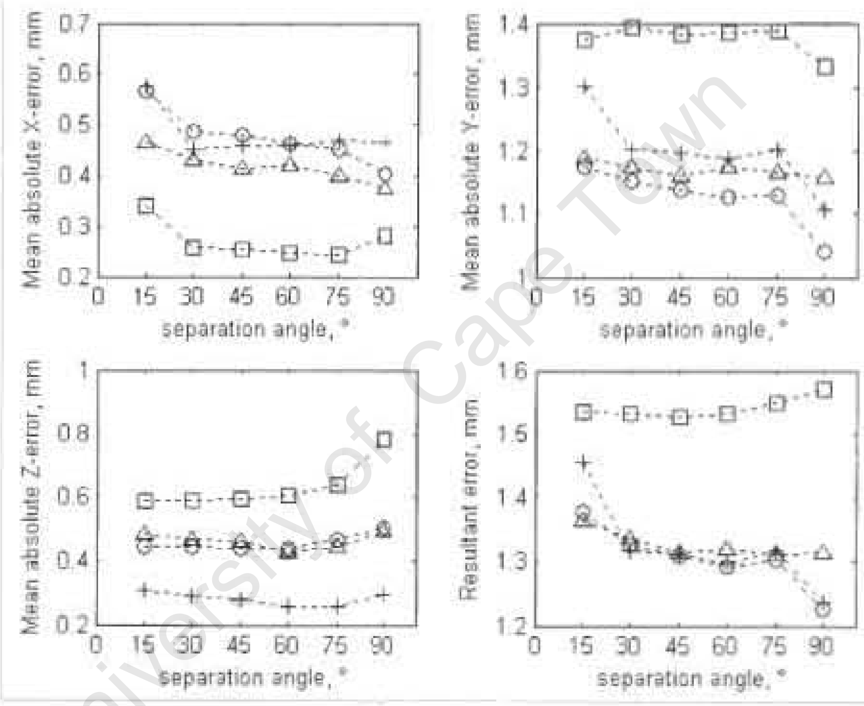

Figure E.6 The X-, Y-, Z- and resultant mean absolute errors for the reconstruction of five test points when extrapolating in the Z direction. Z-extrapolation-1 (□), Z-extrapolation-2 (o), Z-extrapolation-3 (Δ), Z-extrapolation-4 (+).

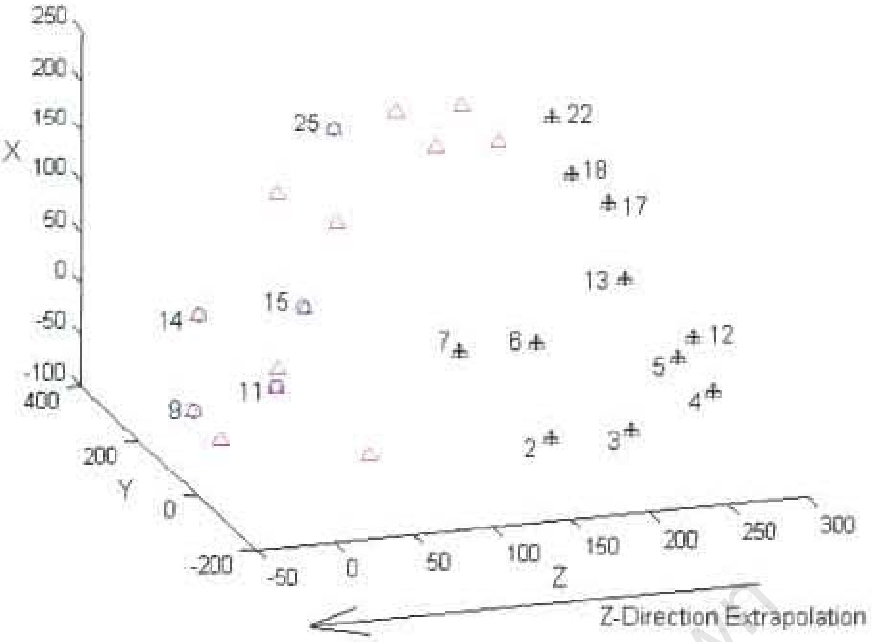

Figure E.7 A plot of the 25 points of the calibration frame (Δ), the 11 control points (+) and the 5 reconstructed test points (o) calculated by Z-direction extrapolation (configuration-3) with a separation angle of 15° (images scanned at 75° and 90°).

References

Abdel-Aziz YI, Karara HM (1971) Direct Linear transformation from comparator coordinates into object-space coordinates. In Proc. ASP/UI *Symposium on Close Range Photogrammetry*. American Society of Photogrammetry, Falls Church. pp. 1 – 18.

Adams LP (1981) X-ray stereo photogrammetry locating the precise, three dimensional position of image points. *Medical & Biological Engineering & Computing*, 19: 569 – 578.

Adams LP, Constant DA (1988) Biosteriometrics in the study of the morphology of the lumbar sacral spine. *Medical & Biological Engineering & Computing*, 26: 383 – 388.

Alberius P, Malmberg M, Persson S, Selvik G (1990) Variability of measurements of cranial growth in the rabbit. *American Journal of Anatomy*, 188: 393 – 400.

Alfaro-Adrian J, Gill HS, Murray DW (1999) Cement migration after THR: A comparison of Charnley Elite and Exeter Femoral Stems using RSA. *The Journal of Bone and Joint Surgery*, 81: 130 – 134.

André B, Dansereau J, Labelle H (1994) Optimized vertical stereo base radiographic setup for the clinical three-dimensional reconstruction of the human spine. *Journal of Biomechanics*, 27 (8): 1023 – 1035.

Aronson S, Jonsson N, Alberius P (1985) Tantalum markers in radiography: An assessment of tissue reactions. *Skeletal Radiology*, 14 (3): 207 – 211.

Aubin C-E, Dansereau J, Parent F, Labelle H, de Guise JA (1997) Morphometric evaluations of personalised 3D reconstructions and geometric models of the human spine. *Medical & Biological Engineering & Computing*, 35: 611 – 618.

Baumrind S, Moffit FH, Curry S (1983) The geometry of three dimensional measurement from coplanar x-ray images. *American Journal of Orthodontics*, 84: 313 - 322

Benameur S, Mignotte M, Parent S, Labelle H, Skalli W, de Guise J (2003) 3D / 2D registration and segmentation of scoliotic vertebrae using statistical models. *Computerized Medical Imaging and Graphics*, 27: 321 - 327

Benningfield SJ, Potgieter H, Nicol A, van As S, Bowie G, Hering G, Latti E (2003) Report on a new type of trauma full-body digital X-ray machine. *Emerging Radiology*, 10: 23 – 29.

Berg DC, Hill DL, Raso VJ, Lou E, Church T, Moreau MJ, Mahood JK (2002) Using three-dimensional difference maps to assess changes in scoliotic deformities. *Medical & Biological Engineering & Computing,* 40: 290 – 295.

Bice WS, Dubois DF, Prete JJ, Prestidge BR (1999) Source localisation from axial image sets by iterative relaxation of the nearest neighbour criterion. *Medical Physics,* 26: 1919 – 1924.

Börlin N (1997) High precision measurements in digital radiographs. Umeå University, Sweden.

Börlin N, Thien T, Kärrholm J (2002) The precision of radiostereometric measurements. Manual vs. digital measurements. *Journal of Biomechanics,* 35: 69 – 79.

Bragdon CR, Estok DM, Malchau H, Kärrholm J, Yuan X, Bourne R, Veldhoven J, Harris WH (2003) Comparison of two digital radiostereometric analysis methods in the determination of femoral head penetration in a total hip replacement phantom. *Journal of Orthopaedic Research,* 22 (3): 659 – 664.

Broadbent BH (1931) A new x-ray technique and its application to orthodontia. *Angle Orthodontist,* pp. 1-45.

Cai J, Chu JCH, Saxena VA, Lanzi LH (1997) A method for more efficient source localization of interstitial implants with biplane radiographs. *Medical Physics,* 24: 1229 – 1234.

Challis JH, Kerwin DG (1992) Accuracy assessment and control point configuration when using DLT for photogrammetry. *Journal of Biomechanics,* 25: 1053 – 1058.

Chen L, Armstrong CW, Raftopoulos DD (1994) An investigation on the accuracy of the direct linear transformation technique. *Journal of Biomechanics,* 27: 493 – 500.

Choo AMT, Oxland TR (2003) Improved RSA accuracy with DLT and balanced calibration marker distributions with an assessment of initial calibration. *Journal of Biomechanics,* 36: 259 – 264.

Dansereau J, Stokes IA (1988) Measurements of the three-dimensional shape of the rib cage. *Journal of Biomechanics,* 21 (11): 893 – 901.

De Lange A, Huiskes R, Kauer JMG (1990) Measurement errors in Roentgen-Stereophotogrammetric Joint Motion Analysis. *Journal of Biomechanics,* 23 (3): 259 – 269.

Djerf K, Edholm P, Hedbrant J (1987) A simplified Roentgen Stereo-photogrammetric Method: Analysis of small movements between the prosthetic stem and the femur after total hip replacement. *Acta Radiologica*, 28: 603 – 606.

Douglas TS, Meintjes EM, Vaughan CL, Viljoen D (2003) The role of depth in eye distance measurements: comparison of single and stereophotogrammetry. *American Journal of Human Biology*, 14: 573 – 578.

Douglas TS, Vaughan CL, Wynne SM (2004) Three-dimensional point localisation in low-dose X-ray images using stereophotogrammetry. *Medical & Biological Engineering & Computing*, 42: 37 – 43.

Gall K, Verhey L (1993) Computer-assisted positioning of radiotherapy patients using implanted radio-opaque fiducials. *Medical Physics*, 20 (4): 1153 – 1159.

Gazzani F (1993) Comparative assessment of two algorithms for calibrating stereophotogrammetric systems. *Journal of Biomechanics*, 26 (12): 1449 – 1454.

Gussekloo SWS, Janssen BAM, Vosselan MG, Bout RG (2000) A single camera roentgen stereophotogrammetry method for static displacement analysis. *Journal of Biomechanics*, 33: 759-763.

Hallert B (1960) Photogrammetry: Basic Principles and General Survey. *McGraw-Hill Book Company Inc*, New York.

Hatze H (1988) High precision 3D photogrammetric calibration and object space reconstruction using a modified DLT-approach. *Journal of Biomechanics*, 21(7): 533-538.

Hinrichs RN, McLean SP (1995) NLT and extrapolated DLT: 3D cinematography alternatives for enlarging the volume of calibration. *Journal of Biomechanics*, 28 (10): 1219 – 1223.

Jackson DD (1983) An automatic method for localizing radioactive seeds in implant dosimetry. *Medical Physics* 10 (3): 370 – 372.

Johnsson R, Axelsson P, Gunnarsson G, Stromqvist B (1999) Stability of Lumbar Fusion with Transpedicular Fixation determined by Roentgen Stereophotogrammetric Analysis. *Spine*, 24 (7): 687 – 690.

Judge AW (1926) Stereoscopic Photography: Its application to science, industry and education. *Chapman & Hall Ltd*, London, pp. 200 – 209.

Kalmar JA, Jones JP, Merritt CRB (1994) Low-dose radiography of scoliosis in children: A comparison of methods. *Spine*, 19: 818 – 823.

Kaptein BL, Valstar ER, Spoor CW, Soel BC, Rozing PM (2006) Model-based RSA of a femoral hip stem using surface and geometrical shape models. *Clinical Orthopaedics & Related Research.* 488: 92 – 97.

Kaptein BL, Valstar ER, Stoel BC, Rozing PM, Reiber JH (2003) A new model-based RSA method validating using CAD models and models from reversed engineering. *Journal of Biomechanics.* 36: 873 – 882.

Kaptein BL, Valstar ER, Stoel BC, Rozing PM, Reiber JH (2005) A new type of model-based Roentgen stereophotogrammetric analysis for solving the occluded marker problem. *Journal of Biomechanics.* 38: 2330 – 2334.

Kärrholm J, Elmqvist LG, Selvik G, Hansson LI (1989) Chronic Anterolateral instability of the knee – A roentgen stereophotogrammetric evaluation. *The American Journal of Sports Medicine,* 17 (4): 555 – 563.

Kiss J, Murray DW, Turner-smith AR, Bithell J, Bulstrode CJ (1996) Migration of cemented femoral components after THR. *The Journal of Bone & Joint Surgery*, pp 796 – 801.

Kofman J, Miller DI, Knopf GK, Zecevic A (1998) Calibration and measurement accuracy of a stereophotogrammetric system using the Direct Linear Transformation. *North American Congress on Biomechanics*, http://asb-biomech.org/NACOB98/107

Kreel, L (1981) Clark's Positioning in Radiography, Tenth Edition, Vol. 2. *William Heinemann Medical Books Ltd, London.* pp 704 – 707.

Kusnoto B, Evans CA, Begole EA, de Rijk W (1999) Assessment of 3-dimensional computer generated cephalometric measurements. *American Journal of Orthodontics and Dentofacial Orthopedics*, 166: 390 – 399.

Kwon Y-H, http://kwon3d.com/theory/dlt/dlt.html, Ball State University, Biomechanics Laboratory, United States of America. Last accessed January 2006.

Lam KL, Ten Haken RK (1991) Improvement of precision in spatial localisation of radio-opaque markers using the two-film technique. *Medical Physics,* 18 (6): 1126 – 1131.

Lam KL, Ten Haken RK, McShan DL, Thornton AF (1993) Automated determination of patient set-up errors in radiation therapy using spherical radio-opaque markers. *Medical Physics,* 20 (4): 1145 – 1152.

Li S, Chen GTY, Pelizzari CA, Reft C, Roeske JC, Lu Y (1996) A new source localization algorithm with no requirement of one-to-one source correspondence between biplane radiographs. *Medical Physics*, 23: 921 – 927.

Martel MK, Narayana V (1998) Brachytherapy for the Next Century: Use of Image Based Treatment Planning. *Radiation Research*, 150: S178 – S188.

Marzan GT, Karara HM (1975) A computer program for direct linear transformation solution of the collinearity condition, and some applications of it. *Symposium on Close Range Photogrammetric Systems, American Society of Photogrammetry, Falls Church*, pp. 420 – 476.

Medcyclopaedia, Last accessed October 2006.
http://www.medcyclopaedia.com/library/topics/volume_i/s/scanogram.aspx

Meintjes EM, Douglas TS, Martinez F, Vaughan CL, Adams LP, Stekhoven A, Viljoen D (2002) A stereophotogrammetric method to measure the facial dysmorphology of children in the diagnosis of Fetal Alcohol Syndrome. *Medical Engineering Physics*, 24: 683 – 689.

Mitchell HL, Newton I (2002) Medical photogrammetric measurement: overview and prospects. *ISPRS Journal of Photogrammetry & Remote Sensing*, 56: 286 – 294.

Mitton D, Landry C, Veron S, Skalli W, Lavaste F, De Guise J.A (2000) 3D reconstruction method from biplanar radiography using non-stereocorresponding points and elastic deformable meshes. *Medical & Biological Engineering & Computing*, 38: 133-139.

Mitulescu A, Semaan I, De Guise JA, Leborgne P, Adamsbaum C, Skalli A (2001) Validation of the non-stereo corresponding points stereoradiographic 3D reconstruction technique. *Medical & Biological Engineering & Computing*, 39: 152-158.

Moffit FH (1967) Photogrammetry, *International Textbook Company*, Pennsylvania, pp. 174 – 177.

Morin Doody M, Lonstein JE, Stovall M, Hacker DG, Luckyanov N, Land CE (2000) Breast cancer mortality after diagnostic radiography: Findings from the U.S. Scoliosis Cohort Study. *Spine*, 25 (16): 2052-2063.

Nelissen RGHH, Valstar ER, Rozing PM (1998) The effect of hydroxyapatite on the micromotion of total knee prostheses: A randomised, double-blind study. *Journal of Bone and Joint Surgery [Am]*, 80-A (11): 1665 – 1672.

Nilsson KG, Kärrholm J (1996) RSA in the assessment of aseptic loosening. *The Journal of Bone & Joint Surgery,* 78B (1): 1 – 3.

Nyström L, Soderkvist I, Wedin P (1994) Technical Note: A note on some identification problems arising in Roentgen Stereophotogrammetric Analysis. *Journal of Biomechanics,* 27 (10): 1291 – 1294.

Önsten I, Akesson K, Besjakov J, Obrant KJ (1995) Migration of the Charnley stem in Rheumatoid arthritis & osteoarthritis. *The Journal of Bone & Joint Surgery,* pp. 18 – 22.

Ostgaard SE, Gottlieb L, Toksvig-Larson S, Lebech A, Talbot A & Lund B (1997) Technical Note: Roentgen Stereophotogrammetric Analysis using computer-based image-analysis. *Journal of Biomechanics,* 30 (9): 993 – 995.

Papadopoulos MA, Christou PK, Athanasiou AE, Boettcher P, Zeilhofer HF, Sader R, Papadopoulos NA (2002) Three dimensional craniofacial reconstruction imaging. *Oral Surgery, Oral Medicine, Oral Pathology, Oral Radiol. Endod.,* 93: 382 – 393.

Petit Y, Dansereau J, Labelle H, de Guise JA (1998) Estimation of 3D location and orientation of human vertebral facet joints from standing digital radiographs. *Medical & Biological Engineering & Computing,* 36: 389 – 394.

Plamondon A, Gagonon M (1991) Effect of the configuration of data acquisition on the accuracy of a stereoradiographic system. *Medical & Biological Engineering & Computing,* 29: 620 – 622.

Ras F, Habets LLMH, van Ginkel FC, Prahl-Andersen B (1996) Quantification of facial morphology using stereophotogrammetry – demonstration of a new concept. *Journal of Dentistry,* 24: 369 – 374.

Rogus RD, Stern RL, Kubo HD (1999) Accuracy of a photogrammetry-based patient positioning and monitoring system for radiation therapy. *Medical Physics,* 26 (5): 721 – 728.

RSA Biomedical website, http://www.rsabiomedical.se, Last accessed September 2006.

Ryd L, Albrektsson BEJ, Herberts P, Lindstrand A, Selvik G (1986) Micromotion of non-cemented Freeman-Samuelson knee prostheses in Gonarthrosis. *Clinical Orthopaedics & Related Research.* pp: 205-212.

Ryd L, Yuan X, Lofgren H (2000) Methods for determining the accuracy of radiostereometric analysis (RSA). *Acta Orthopaedica Scandinavia,* 71 (4): 403-8.

Selvik G (1989) Roentgen Stereophotogrammetry, A method for the study of the kinematics of the skeletal system. *Acta Orthopaedica Scandinavia Supplement*, 232: 1-51

Selvik G, Alberius P & Aronson AS (1983) A Roentgen Stereophotogrammetric System. Construction, calibration and technical accuracy. *Acta Radiologica Diagnosis*, 24: 343-352.

Siddon RL, Chin LM (1985) Two-film Brachytherapy reconstruction algorithm. *Medical Physics*, 12: 77-83.

Slama CC, Theurer C, Henriksen SW (1980) Manual of Photogrammetry, Fourth Edition, *American Society of Photogrammetry*, pp. 846-857.

Stefansic JD, Herline AJ, Shyr Y, Chapman WC, Fitzmatrick JM, Dawant BM, Galloway RL (2000) Registration of Physical Space to Laparoscopic Image Space for Use in Minimally Invasive Hepatic Surgery. *IEEE Transactions on Medical Imaging*, 19 (10): 1012-1023.

Valstar ER, Botha CP, van der Glas M, Rozing PM, van der Helm FCT, Post FH, Vossepoel AM (2002) Towards computer-assisted surgery in shoulder joint replacement. *ISPRS Journal of Photogrammetry and Remote Sensing*, 56: 326 – 337.

Valstar ER, de Jong FW, Vrooman HA, Rozing PM, Reiber JHC (2001) Model based Roentgen Stereophotogrammetry of orthopaedic implants. *Journal of Biomechanics*, 34: 715 – 722.

Valstar ER, Gill R, Ryd L, Flivik G, Börlin N, Karholm J (2005) Guidelines for standardization of radiostereometery (RSA) of implants. *Acta Orthopaedica*, 76: 563 – 572.

Valstar ER, Nelissen RGHH, Reiber JHC, Rozing PM (2002) The use of Roentgen Stereophotogrammetry to study micromotion of orthopaedic implants. *ISPRS Journal of Photogrammetry and Remote Sensing, 56*: 376 – 389.

Van der Vlugt G (1991) The development of a real-time photogrammetric system for patient positioning in proton therapy. Dissertation, *University of Cape Town*.

Van Geems BA (1996) The use of multiple surviews of a computed tomography scanner to determine the 3D coordinates of external cranial markers. *International Archive of Photogrammetry and Remote Sensing*, 31: 576 – 580.

Van Geems BA (1997) The Development of a simple stereotatic device for neurosurgical applications. Dissertation, *University of Cape Town*, pp: 34 – 47; 192 – 199.

Van Geems BA, Adams LP, Hough J (1995) The use of a two dimensional projective transform to solve for the parameters for the anterior-posterior and lateral surviews of a CT scan. *International Archive of Photogrammetry and Remote Sensing*, 30, pp. 366 - 371.

Veress SA (1989) X-Ray Photogrammetry, Systems, and Applications. Non-Topographic Photogrammetry, Editor: Karara HM. *American Society for Photogrammetry and Remote Sensing*, Second Edition, pp. 167 – 186.

Vrooman HA, Valstar ER, Brand GJ, Admiraal DR, Rozing PM, Reiber JHC (1998) Fast and accurate automatic measurements in digitized stereophotogrammetric radiographs. *Journal of Biomechanics*, 31: 491 – 498.

Wang S, Jones NB, Richardson JB, Klaassens E (1996) Optimised method for locating reference markers in Roentgen stereophotogrammetric analysis of orthopaedic radiographs. *Medical & Biological Engineering & Computing*, 34: 88 – 92.

Weisz I, Jefferson RJ, Carr AJ, Turner-Smith AR, McInerney A, Houghton GR (1989) Back shape in brace treatment of idiopathic scoliosis. *Clinical Orthopaedics and Related Research*, 240: 157 – 163.

Wood GA, Marshall RN (1986) The accuracy of DLT extrapolation in three-dimensional film analysis. *Journal of Biomechanics*, 19: 781 – 785.

Yuan X, Ryd L (2000) Technical Note: Accuracy analysis for RSA: a computer simulation study on 3D marker reconstruction. *Journal of Biomechanics*, 33: 493 – 498.

Zill DG, Cullen MR (1992) Advanced Engineering Mathematics. *PWS publishing company*, Boston, pp. 465 – 468.